POWER REACTOR TECHNOLOGY

A Quarterly Technical Progress Review

Prepared for DIVISION OF TECHNICAL INFORMATION, USAEC, by
W. H. ZINN and J. R. DIETRICH, GENERAL NUCLEAR ENGINEERING CORPORATION

Winter 1963-1964

● VOLUME 7

● NUMBER 1

TECHNICAL PROGRESS REVIEWS

To meet the needs of industry for concise summaries of current atomic developments, the Atomic Energy Commission is publishing this series, Technical Progress Reviews. Issued quarterly, each of the reviews digests and evaluates the latest findings in a specific area of nuclear technology and science.

The five journals published in this series are:

Isotopes and Radiation Technology, P. S. Baker, A. F. Rupp, and associates, Oak Ridge National Laboratory

Nuclear Safety, Wm. B. Cottrell, W. H. Jordan, and associates, Oak Ridge National Laboratory

Power Reactor Technology, W. H. Zinn and J. R. Dietrich, General Nuclear Engineering Corporation

Reactor Fuel Processing, Stephen Lawroski and associates, Chemical Engineering Division, Argonne National Laboratory

Reactor Materials, R. W. Dayton, E. M. Simons, and associates, Battelle Memorial Institute

Each journal may be purchased from the Superintendent of Documents, U. S. Government Printing Office, Washington, D. C., 20402. *Isotopes and Radiation Technology* at $2.00 per year for subscription or $0.55 for individual issues; the other four journals at $2.50 per year and $0.70 per issue. See back cover for remittance instructions and foreign postage requirements.

Availability of Reports Cited in This Review

Unclassified AEC reports are available for inspection at AEC depository libraries and are sold by the Office of Technical Services, Department of Commerce, Washington, D. C., 20230. Some of the reports cited are not available owing to their preliminary nature; however, the information contained in them will eventually be made available in formal progress or topical reports.

Unclassified reports issued by other Government agencies or private organizations should be requested from the originator.

Unclassified British and Canadian reports may be inspected at AEC depository libraries. British reports are sold by the British Information Service, 45 Rockefeller Plaza, New York, N. Y.; Canadian reports (AECL series) are sold by the Scientific Document Distribution Office, Atomic Energy of Canada, Ltd., Chalk River, Ontario, Canada.

Classified U. S. and foreign reports identified in this journal as Classified may be purchased by properly cleared Access Permit Holders from the Division of Technical Information Extension, U. S. Atomic Energy Commission, P. O. Box 1001, Oak Ridge, Tenn., 37831. Such reports may be inspected at classified AEC depository libraries.

POWER REACTOR TECHNOLOGY

A REVIEW OF RECENT DEVELOPMENTS

Prepared for DIVISION OF TECHNICAL INFORMATION, USAEC,
by W. H. ZINN and J. R. DIETRICH,
GENERAL NUCLEAR ENGINEERING CORPORATION

WINTER 1963–1964

VOLUME 7

NUMBER 1

Foreword

This quarterly review of reactor development has been prepared at the request of the Division of Technical Information of the U. S. Atomic Energy Commission. Its purpose is to assist interested organizations in the task of keeping abreast of new results in reactor technology for civilian application.

Power Reactor Technology contains reviews of selected recently published reports that are judged noteworthy in the fields of power-reactor research and development, power-reactor applications, design practice, and operating experience. It is not meant to be a comprehensive abstract of all material published during the quarter, nor is it meant to be a treatise on any part of the subject. However, related reports from different sources are often treated together to yield reviews having some breadth of scope, and background material may be added to place recent developments in perspective. Occasionally the reviews are written by guest authors. Reviews having unusual breadth or significance are placed at the front of the issue as Feature Articles.

The intention is to cover the various areas of reactor development from the general viewpoint of the reactor designer rather than from the more detailed points of view of specialists in the individual areas. To whatever extent the coverage of *Power Reactor Technology* may occasionally overlap the fields of the other Technical Progress Reviews, the overlaps will be motivated by this objective of viewing current progress through the eyes of the reactor designer.

A degree of critical appraisal and some interpretation of results are often necessary to define the significance of reported work. Any such appraisal or interpretation represents only the opinion of the reviewer and (in the usual case, when the review is written by General Nuclear Engineering Corporation staff) the Editor. When the review is predominantly interpretive, the reviewer is named; unless identified as a guest author, he is a member of the General Nuclear Engineering Corporation staff. Readers are urged to consult the original references to obtain all the background of the work reported and to obtain the interpretation of the results given by the original authors.

For timely coverage, *Power Reactor Technology* must often review fragmentary material. The fixed subject headings listed below have been adopted in the hope of maintaining some continuity and order in the material from one issue to another: all reviews except Feature Articles will be arranged under these headings. A particular issue will not necessarily contain all the headings but only those under which material is reviewed.

Economics, Applications, Programs
Resources and Fuel Cycles
Physics
Fluid and Thermal Technology
Fuel Elements
Materials
Control and Dynamics
Containment, Radiation Control, and Siting
Systems Technology
Components
Design and Construction Practice
Operating Experience
Specific Reactor Types
Specific Applications
Unconventional Approaches

W. H. Zinn, President
J. R. Dietrich, Vice-President and Editor
General Nuclear Engineering Corporation

Contents

Issued quarterly by the U. S. Atomic Energy Commission. Use of funds for printing this publication approved by the Director of the Bureau of the Budget on October 14, 1963.

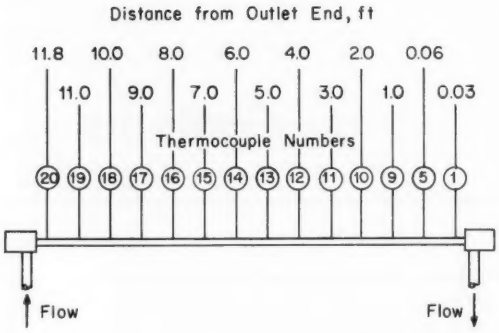

Fig. II-9 Test section thermocouple locations.[16]

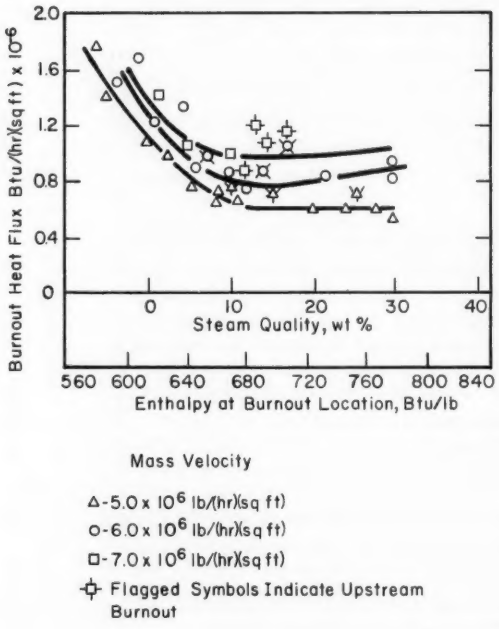

Fig. II-10 Experimental boiling-burnout data.[16]

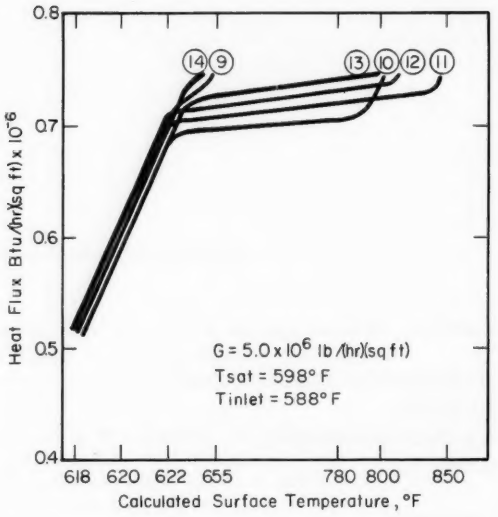

Fig. II-11 Test-section temperatures during a typical upstream burnout run.[16]

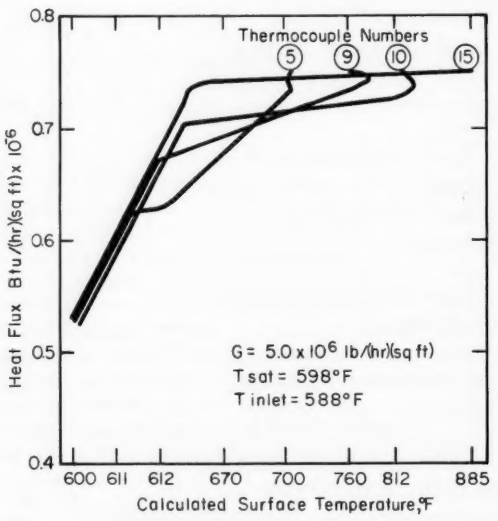

Fig. II-12 Magnitude of temperature excursions during a downstream boiling burnout.[16]

Note: In *Power Reactor Technology*, 6(4): 61, these figures were printed in the wrong order. The correct order is shown here.

Section

I

Power Reactor Technology

Economics, Applications, Programs

Solid-Fuel Gasification

A study of the economic feasibility of using nuclear energy to convert coal to synthesis gas for the manufacture of ammonia, methanol, synthetic pipeline gas, and liquid fuels is reported in Ref. 1. The analysis does not consider reactor design but proceeds on the assumption that the nuclear heat is supplied in the form of hot, nonradioactive helium at a pressure of about 435 psig and at temperatures in the 2000 to 2500°F range. The heat consumptions in the installations considered are in the range of 250 to 400 Mw(t). Two plants were evaluated; one produced 90 million standard cubic feet per day of 930 Btu/lb pipeline gas, and the other produced a variety of fuels and chemicals. The investments in the chemical plants considered (exclusive of the nuclear power source) range from $45 million to $133 million; therefore the nuclear plant does not represent the major portion of the total investment.

At present coal gasification, although technically feasible, has not been put into commercial practice in the United States because of cost disadvantages compared to processes utilizing naphtha or natural gas as sources of synthesis gas. A major contributor to the high cost of coal gasification using conventional

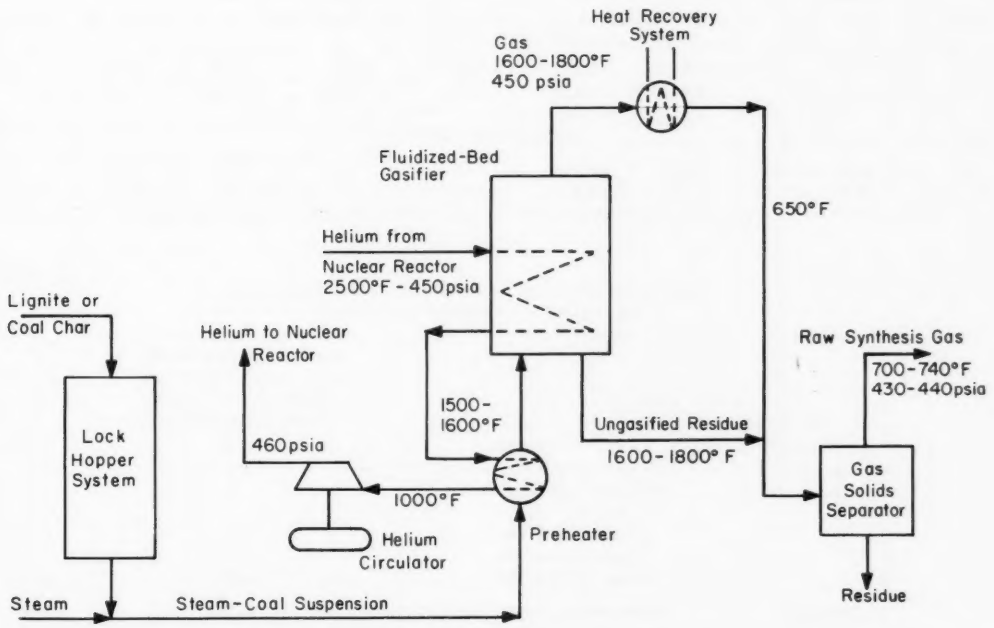

Fig. I-1 Schematic flow diagram of gasification section.[1]

fuels has been the cost of oxygen.[1] The reaction that takes place when coal is gasified is endothermic, and the oxygen is used to burn a portion of the coal to produce the necessary heat. Air cannot be used because the nitrogen thus introduced would end up as a major impurity in the product synthesis gas. The use of a nuclear reactor as a source of heat overcomes the problem of dilution of the product gas by nitrogen and by the CO_2 that is also produced by the combustion of coal. A schematic of the process is shown in Fig. I-1.

The results of the study with respect to the cost of pipeline gas are shown in Table I-1. The selling prices of pipeline gas that is produced from coal gasification by both conventional fuel and nuclear heat are compared in Table I-2.

Although the use of nuclear heat offers substantial cost advantages compared to processes using O_2, the range of $1.32 to $1.51 still is about a factor of 2 higher than natural-gas prices in the eastern portion of the United States.[1]

The lignite processing plant was assumed to be in North Dakota, whereas the bituminous coal processing plant was assumed to be in West Virginia. The reference concludes that the manufacture of pipeline gas with the use of nuclear heat should be studied further if a market could be developed for pipeline gas in North Dakota, since the present market is

Table I-1 EFFECT OF RAW MATERIAL COST, COST OF NUCLEAR HEAT, AND GROSS RETURN ON INVESTMENT ON THE SELLING PRICE OF PIPELINE GAS[1]

Cost of nucleat heat, $/million Btu	Selling price of pipeline gas, $/thousand standard cu ft					
	Lignite			Bituminous coal		
	$1.50/ton	$2.00/ton	$2.50/ton	$4.00/ton	$5.00/ton	$6.00/ton
	Gross Return = 12%					
0.50	0.71	0.75	0.79	1.08	1.13	1.18
0.80	0.78	0.82	0.86	1.19	1.24	1.29
	Gross Return = 20%					
0.50	0.83	0.87	0.91	1.27	1.32	1.37
0.80	0.90	0.94	0.98	1.38	1.43	1.48
	Gross Return = 30%					
0.50	0.98	1.02	1.06	1.51	1.56	1.61
0.80	1.05	1.09	1.13	1.62	1.67	1.72

Table I-2 COMPARISON OF PRICES OF PIPELINE GAS PREPARED BY VARIOUS PROCESSES[1]

Source of information	Process	Gas selling price at 20% gross return, 90% stream efficiency, $5/ton coal, $/thousand standard cu ft
Present study	Fluid-bed gasification, nuclear heat at	
	$0.50/million Btu	1.32
	$0.80/million Btu	1.43
	$1.00/million Btu	1.51
Kellogg[1]	Lurgi steam-oxygen gasification	1.70
	Suspension gasification with steam and oxygen	1.49
Bureau of Mines[2]	Suspension gasification with steam and oxygen	1.55

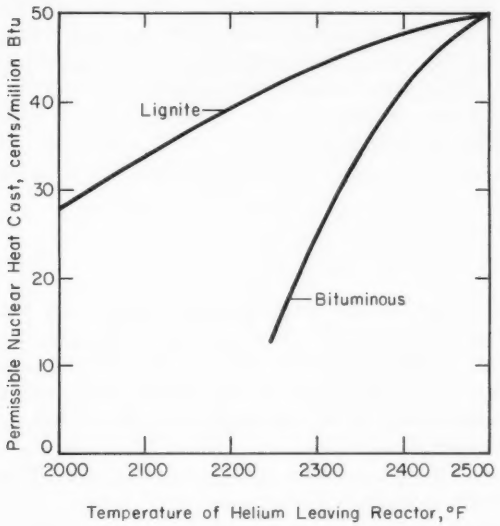

Fig. I-2 Permissible cost of heat to yield same pipeline gas selling price as 2500°F helium at $0.50 per million Btu. Cost of heat includes operating cost of reactor plant, return on investment (20%), and special costs associated with nuclear operation.[1]

limited. It is significant that the effect of the helium temperature is an important one (Fig. I-2). The helium temperature for gasifying bituminous coal[1] should be at least 2500°F, whereas the temperature requirement for gasifying lignite probably would be somewhat lower.

The manufacturing complex for producing a mixture of products consisting of gasoline, ammonia, methanol, hydrogen, and other chemicals from synthesis gas produced with nuclear heat looked unattractive economically. However, the economics of the ammonia and methanol components of the complex appeared quite favorable, and the reference suggests that plants producing these products alone would be fruitful areas for further study. The reference concludes with a general comment on this relation:

> It appears that the best applications for nuclear heat will be found in trying to improve an existing commercial process, not in trying to make a currently uneconomic process look attractive. For example, gasoline and pipeline gas are not produced from synthesis gas in the United States today, and the advent of cheap nuclear heat will not change the picture significantly. On the other hand, ammonia and methanol are manufactured from synthesis gas on a commercial scale, and the use of nuclear heat may furnish a significant cost advantage, whether the raw material used to make the synthesis gas be coal, oil, or natural gas. This would seem to be a fruitful area for further study.

References

1. L. J. Pieroni, R. P. Griffin, and W. H. Heffner, A Technical and Economic Evaluation of Solid-Fuel Gasification Using Nuclear Heat. Production of Pipeline Gas, Liquid Fuels, and Chemicals from Lignite and Bituminous Coal. Period Covered: May to October 1962, USAEC Report NYO-10301, The M. W. Kellogg Company, Nov. 30, 1962.
2. S. Katell, J. H. Faber, P. Wellman, W. C. Morel, and G. B. Taylor, 90 Million Std. Cubic Feet Per Day High-Btu Gas Plant, Report 61-7, U. S. Bureau of Mines, May 31, 1962.

Section

II

Power Reactor Technology

Physics

Critical and Exponential Experiments

A recent paper by Kaplan[1] gives a review of the use of subcritical and critical assemblies for the measurement of reactor parameters. It considers the various methods employing such assemblies from the points of view of their consistency with one another and of their accuracy and usefulness in measuring the basic characteristics of chain-reacting lattices for use in practical reactors. In addition to the conventional critical and exponential assemblies, the review considers three related methods that can utilize much smaller samples of the experimental lattice. These methods are the following:

1. Substitution, or two-region, critical experiments. In these experiments the critical buckling is first measured in a reference lattice; thereafter a central portion of the reference lattice is replaced by the experimental lattice, and the buckling of the experimental lattice is evaluated from the change in critical buckling produced by the substitution. This method has been applied extensively to heavy-water lattices at the Savannah River Laboratory, and it is particularly convenient when liquid moderators are used so that the change in buckling can be evaluated by the change in critical moderator level.

2. The flat-region technique, which has been used at Hanford in the Physical Constants Testing Reactor (PCTR). In this system a reference assembly is first made critical with an empty cavity at its center. The cavity is then filled with the experimental lattice, and some parameter of the experimental lattice is varied uniformly over its volume until the entire assembly is again critical. At this point the gross neutron-flux distribution in the experimental lattice is flat (as it was in the empty cavity), and the infinite multiplication factor (k_∞) for the experimental lattice is unity. Usually the adjustable parameter is an absorbing poison with an absorption cross section that varies with energy in a way that is easily handled by computation.*

3. The miniature-lattice technique. This method utilizes a suitable neutron source, usually a reactor, to irradiate a small assembly of the experimental lattice. No attempt is made to determine reactivity or buckling, but the basic lattice parameters such as thermal utilization and resonance escape probability are measured at points near the center of the assembly.

It is quite evident that a primary concern in any of the small-lattice techniques must be to assure that the quantity measured is characteristic of the neutron spectrum in the experimental lattice and is independent of the spectrum of the lattice that feeds neutrons to the experiment. Basically this involves the use of buffer regions between the two lattices, but the manner in which this technique is applied varies with the general method of the experiment and with the quantities being measured.

The reference[1] examines the mutual consistency of the results that have been obtained in the past by the several methods involving critical or subcritical lattices, with the comparison being organized about the several lattice types that have been subjects of extensive measurement programs: graphite-moderated, heavy-water-moderated, and light-water-moderated lattices. The review emphasizes the limitations of integral experiment techniques for investi-

*Recent investigations of this technique, for lattices having important fractions of epithermal fissions, have been carried out at the Babcock & Wilcox laboratory and are reviewed here in later paragraphs (see Fig. II-1).

gating the practical situations such as temperature, voiding, and fission-product poisoning, which occur in practical reactors. However, it necessarily confines its attention to the properties of more or less uniform lattices, since it is only in this area that extensive experimental information exists. Often the reactor designer finds that the major concern is not so much with the basic lattice parameters as with the complexity introduced by such local perturbations as water channels and control rods, the complex power distributions resulting from control-rod installations, temperature and void distributions, and burnup distributions. These questions are sometimes investigated by means of critical experiments of the mockup type. A recent experimental program of this type for a rather complex reactor, the Boiling Nuclear Superheat Reactor (BONUS) is described in Ref. 2.

Solution Assemblies

Power Reactor Technology, 6(1), contains a description of the Hanford 14-in.-diameter stainless-steel spherical critical assembly and of the experimental technique used there in measuring the worth of various solid reflector materials on critical plutonium nitrate solutions. The measurements covered a range of plutonium concentrations and acid molarities. In a continuation of this program, critical masses were determined[3] as functions of plutonium concentrations (33.5 to 70.4 g/liter) and acid molarities (~2.0 to 6.7) when the sphere was reflected by water and when the sphere was wrapped with a 0.030-in. layer of cadmium and water reflected. In addition, critical mass data were obtained for various thicknesses of the spherical stainless-steel wall to permit an evaluation of wall effects. The following conclu-

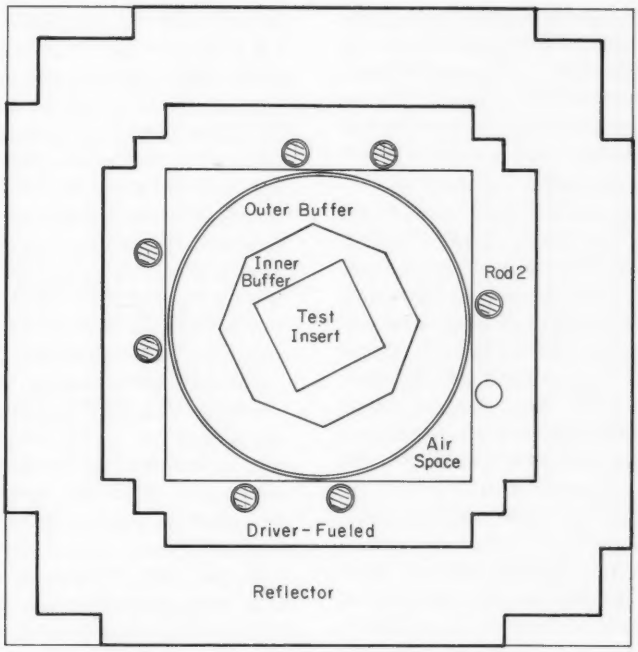

Fig. II-1 Small-lattice assembly plan (top view).[12] The test insert is a removable sublattice of 196 fuel rods. The insert itself is 6 ft long. The central 18 in. of the test insert contains the test region, the region that is poisoned and replaced by a void in the null reactivity measurements. The top and bottom 27-in. lengths form the axial parts of the inner buffer. The outer buffer is ThO_2-UO_2 fuel, and the driver region is graphite blocks containing U^{235} foils. The air space around the tank is not to be confused with the void region which is replaced by the test insert.

sion is drawn by the authors. Results obtained with the cadmium-wrapped vessel are of particular interest in nuclear safety applications where flooding is a possibility since, under the concentration range covered by the experiments, the data show that a vessel wrapped with cadmium would be only nominally reflected (reflector equivalent to 1 in. or less of water). The safe dimension could then be based on the condition of a nominal reflector, rather than on the more restrictive fully reflected condition with its consequent smaller size. After corrections are made for solution volumes and Pu^{240} concentrations, very good agreement is obtained between the present data and data obtained by Kruesi et al.[4] in the Hanford P-11 program.

Criticality measurements on plutonium nitrate solutions contained in an 11.5-in.-diameter stainless-steel sphere with water reflector are reported in Ref. 5. Plutonium concentrations ranged from 51 to 431 g of plutonium per liter. The plutonium contained 4.6 wt.% Pu^{240}. Criticality of the system was studied as a function of nitrate concentration. The results, which consisted of four criticality determinations, indicated a double value (about 150 and 295 g/liter) for the critical plutonium concentration at a nitrate concentration of 303 g/liter. All plutonium concentrations between these two values would be supercritical at the specified nitrate content. This behavior illustrates the sensitivity of the critical mass to neutron-spectrum effects in high-concentration high-leakage plutonium solutions, where the critical value of the thermal utilization is near unity. Analysis of the results indicated that the critical plutonium concentration for zero nitrate content (95.4% Pu^{239}, 4.6% Pu^{240}) would be 65.0 ± 5.0 g/liter for the water-reflected 11.5-in. sphere and 28.3 ± 0.7 g/liter for the water-reflected 14-in. sphere discussed above.

Pulsed neutron-source experiments also were performed along with the critical-mass measurements. The multiplication factor was determined as a function of plutonium concentration and solution volume in the sphere. One of the purposes of these experiments was to examine the feasibility of the pulsed-source technique for k_{eff} measurements on in-plant equipment; it is stated: "Whether k_{eff} measurements can be made on process vessels (which are well subcritical and located in fixed plant areas) with sufficient accuracy to establish nuclear safety limits remains to be demonstrated."[5]

A series of calculations of the critical configurations were performed, using the GAM-I code for fast group parameters and the TEMPEST code for thermal constants. These calculations give k_{eff} to about 0.6%.

Measurements were carried out at the PCTR on the limiting critical concentrations of U^{235} and Pu^{239} in aqueous solutions [*Power Reactor Technology*, 6(1)]; the measured values were 12.94 ± 0.03 g of uranium per liter and 8.4 ± 1.0 g of Pu^{239} per liter, respectively. The relatively large uncertainty in the Pu^{239} value was the result of uncertainties in the corrections for the worth of the stainless-steel containers. Subsequent measurements[6] on the limiting critical concentration of dilute uranyl fluoride in stainless-steel containers have provided more accurate data on the worth of the containers. It was also shown that, for stainless-steel containers, a container filled with helium was less reactive than an evacuated container, the measured reactivity difference being a function of the container wall thickness. Since previous measurements with Pu^{239} solutions used helium-filled containers as a reactivity base for normalization of the data, correction for this effect was necessary. After the corrections were applied, the limiting concentration of uranium (93.15% enriched) was found to be 13.0 ± 0.1 g of uranium per liter. This value is in good agreement with the previously accepted value of 12.94 ± 0.03 g of uranium per liter, which was obtained using aluminum containers. Application of the necessary corrections to the previously measured plutonium data, which also include corrections for the Pu^{240}, Pu^{241}, and nitrate content of the solutions, resulted in a value of 8.1 ± 0.3 g of Pu^{239} per liter as the limiting concentration of a Pu^{239}-water solution. This value is in better agreement with the Monte Carlo calculated value of 7.71 ± 0.46 g of Pu^{239} per liter.

Boiling-Superheating Reactors

The superheater region of the first-generation core for the Pathfinder reactor will contain fully enriched uranium dioxide fuel in stainless-steel cermet, clad with stainless steel, in the form of dual coaxial fuel tubes. An advanced superheater design for the second-generation core contains fuel elements of a seven-pin cluster type which utilize uranium oxide fuel of approximately 4% enrichment. Experiments that are described in Ref. 7 were directed toward

obtaining the information necessary for the computation of the thermal utilization and resonance escape probability for this type of fuel. The fuel pins used were 36½ in. long and were made up of 0.214-in. UO_2 pellets which had 95% of the theoretical density and which were in stainless-steel tubes of 0.010-in. wall thickness. The three enrichments studied were 3.5, 4.0, and 7.0% U^{235}, and three lattice spacings were studied for each enrichment. Results are also given for a six-pin cluster (center pin removed) for the 3.5 and 7.0% enrichments. The experiments were performed in the Pathfinder reactor core mockup. This mockup is approximately a right-circular cylinder 6 ft in diameter and 6 ft high, containing a central superheater region approximately 2.5 ft in diameter. The experimental data were taken at the radial geometric center of this superheater region, which was loaded with a sufficient number of the experimental assemblies (at least 25) to yield a typical spectrum at the center. Local flux distributions, disadvantage factors, cadmium ratios, and distributions of U^{238} activation are given for flooded and voided conditions.

A method of measuring the void distribution in an operating boiling reactor was proposed some time ago by S. Untermeyer. The local void content is inferred from the local ratio of epithermal-to-thermal neutron flux, which in turn is indicated by the measured local value of a cadmium ratio. Work on an exponential mockup of the BORAX-V reactor to explore the cadmium-ratio technique and to prepare a calibration curve for use of the technique in BORAX-V is described in Ref. 8. The known voids used in the mockup were made of sealed polyethylene tubes of the appropriate length and number. The void fractions simulated in this manner ranged from 0 to 0.4. The corresponding range of the measured cadmium ratio was 6.1 to 4.6. The radial flux distribution across a BORAX type fuel assembly and the flux details in and around fuel rods were also determined in the program. Nine of the BORAX-V subassemblies were mocked up in the exponential experiment. The neutron source for the experiment was provided by the TREAT reactor.

Heavy-Water Assemblies

A summary of experimental and theoretical results obtained in the Heavy-Water Lattice Project of the Massachusetts Institute of Technology during the period October 1961 to September 1962 is presented in Ref. 9. An initial study has been made in the main subcritical (exponential) assembly with 1-in.-diameter natural-uranium rods in triangular lattices of 4-, 5-, and 7.5-in. pitches. Material bucklings were measured and compared with results measured in both critical and exponential experiments at other laboratories. The ratios of fission rates in U^{238} relative to U^{235}, as well as the epicadmium-to-subcadmium fission ratios in U^{235}, were also measured. Experiments related to resonance capture in U^{238} included measurement of the average U^{238} cadmium ratio, average ratio of the U^{238} capture rate to the U^{235} fission rate, distribution of resonance neutrons in the moderator, and quantities related to the effective resonance integral of U^{238}. Data on intracellular thermal-neutron distribution were measured and compared with the predictions of the one-dimensional THERMOS code. In the relatively tight lattices (those in which the spacing between fuel rods was comparable to or less than the mean free path for thermal neutrons), the one-dimensional cylindrical representation of the unit cell did not predict the correct relative fluxes in the fuel and moderator regions. Two-dimensional THERMOS calculations, which approximated the hexagonal cell boundary more accurately, did provide better agreement with the experimental data. Measurements similar to those described above are being repeated for slightly enriched uranium fuel rods.

Also summarized[9] are the theoretical and experimental results from experiments on slightly enriched fuel rods that were moderated by D_2O and D_2O-H_2O mixtures in the small or miniature lattice studies. These measurements include the axial and radial flux traverses, the cadmium ratio of U^{238}, the U^{238}-to-U^{235} fission ratios, and the intracellular flux traverses with cadmium-covered gold foils.

Calculations reported in Ref. 10 relate to the uniform-lattice critical experiments performed in the ZPR-VII critical assembly with thoria-urania fuel and heavy-water moderator. The fuel consisted of pellets of thorium oxide and highly enriched uranium oxide, with atom ratios of thorium to U^{235} of 25:1 and 15:1. Experiments were carried out with both types of fuel in uniform triangular lattices having pitches of 1.905, 2.8575, 3.81, and 5.715 cm. The results of experiments for both uniform and clustered

lattices are given in Ref. 11. Group constants, material bucklings, and reflector savings were calculated for the various lattice pitches employed in the experiments. Analyses were performed, and these included measurements of cadmium ratios of U^{235} and thorium, water-worth experiments, and fuel-substitution experiments.

Spectral Shift

Previous experimental work under the Spectral Shift Control Reactor (SSCR) Basic Physics Program has been reviewed earlier [*Power Reactor Technology*, 5(4): 17; 6(2): 13; and 6(3): 81]. References 12 and 13 contain results of work performed under this program during the ninth and tenth contract quarters. Results from critical experiments with the 2.46%-enriched UO_2 fuel rods at a nonmoderator-to-moderator volume ratio of 0.65 are given. The two moderator compositions studied were 85.5 and 70.0 mole % D_2O (remainder H_2O). For each of these lattices the measurements include critical size, reactivity change with water height, critical buckling, reflector savings, thermal disadvantage factor, cadmium ratio of U^{238}, and the fission cadmium ratio of U^{235}. Also, perturbation experiments were performed at a nonmoderator-to-moderator volume ratio of 1.0 and a moderator composition of 72 mole % D_2O. Local flux distributions and the reactivity worth of various perturbations in the core were studied, including the effect of a boral blade inserted in the uniform lattice, the effect of a moderator gap in the uniform lattice, the effects of boral, cadmium, and aluminum blades, respectively, in a moderator gap, and the effects of boral and aluminum cruciforms, respectively, in a moderator gap.

The results of the first small-lattice experiment are of particular interest. The purpose of this experiment was to demonstrate, for systems having a high percentage of fissions occurring at epithermal energies, the validity of methods used previously for thermal systems in the Physical Constants Testing Reactor at Hanford. Reactor parameters susceptible to measurement by this technique include the infinite multiplication factor and all the intracellular lattice parameters normally measured in a critical experiment. In this first experiment in the SSCR program, a direct comparison of results obtained in the small lattice could be made with a corresponding critical experiment. The critical experiment utilized over 2000 fuel rods that were 6 ft long and 4% enriched, whereas the small test lattice required only about 200 rods which were of the same type but which were 18 in. long.

The source reactor for the small-lattice experiment was a graphite honeycomb mounted on a split-bed assembly (Fig. II-1). Suitable adjustment of graphite bars and highly enriched uranium-aluminum foils gave a critical system. A center cavity approximately 2 ft square houses a 2-ft-diameter aluminum tank that contains the test lattice and buffer regions. In this experiment the buffer region adjacent to the test lattice had the same composition as the test lattice. However, calculations indicate that a substantial part of the buffer might be replaced by dissimilar material without significant increase in the error caused by spectral mismatch. The nonmoderator-to-moderator volume ratio in the test lattice (and buffer region) was unity, and the moderator composition was approximately 70 mole % D_2O.

Table II-1 COMPARISON OF PARAMETER MEASUREMENTS IN THE SMALL-LATTICE AND CRITICAL EXPERIMENTS[12]

Parameter	Small-lattice experiment	Critical experiment
k_∞	1.131 ± 0.008	1.130 ± 0.006
ϕ_m/ϕ_f	1.159 ± 0.007	1.157 ± 0.009
C_{25}*	2.440 ± 0.006	2.434 ± 0.012
C_{28}*	1.086 ± 0.002	1.087 ± 0.004

*Cadmium ratios.

An extensive analysis of the errors introduced by spectral mismatch between the test and buffer region and the nonflatness of the spectral flux across the test region indicated that, at least for this experiment, these errors are small and, in fact, tend to cancel each other. A comparison of the final results obtained from the small-lattice experiment and the corresponding critical experiment is given in Table II-1.

Graphite-Moderated Assemblies

Results of a series of graphite-moderated uranium-metal-fueled critical experiments are given in Ref. 14. The graphite assembly is 8 ft

high and 12 ft in diameter. The fuel elements are hollow cylinders that are 1 in. in outside diameter and $\frac{3}{4}$ in. in inside diameter, and they contain uranium metal enriched to 2 wt.% U^{235}. The elements are assembled from individual, hollow cylindrical slugs of uranium metal clad with approximately 3 mils of nickel and stacked in 40-mil aluminum tubes to the desired height. The triangular lattice spacings studied ranged from 6.93 to 16.00 in., corresponding to moderator-to-fuel volume ratios from 25 to 140. An effectively infinite reflector was maintained radially for most of the assemblies, but there was no axial reflector.

In addition to critical-size measurements on the various fueled lattices, the thermal-diffusion length of the graphite was measured to determine the effective absorption cross section of the graphite.

The criticality experiments were analyzed by utilizing available IBM-7090 codes, and, in general, good agreement was obtained between calculation and experiment by means of a four-group scheme. The AIM-5 one-dimensional spatial code in four groups was used with fast constants from the FORM Fourier transform slowing-down code and thermal constants from a TEMPEST thermal-spectrum-S_4 spatial scheme. Neutron streaming through the air-filled centers of the fuel elements was accounted for by the method of Behrens. Some two-group calculations were performed, but the fit to experiments was not good. This is attributed to the inadequacy of the epithermal leakage terms and the failure of this scheme to give the proper balance between epithermal absorption and fission. However, the four-group scheme agreed with experiment to better than 1% on k_{eff} for all the lattices. It was also noted that some improvement was obtained in the agreement if the usual assumption of a Maxwell-Boltzmann thermal distribution was replaced by a calculated Wilkins spectrum.

Results of physics work performed under the BICEP program (British Industrial Collaborative Exponential Programme) were originally reported in 21 United Kingdom Atomic Energy Authority reports. A collection of these reports, along with the necessary editorial changes for the collection, is found in Refs. 15 to 17. The program was initiated to provide reactor physics data for the development of gas-cooled graphite-moderated reactor systems. Specifically, physics data were obtained for various fuel-element concepts under development in Britain. Exponential experiments were performed on graphite-moderated assemblies of rods and tubes of natural uranium metal, enriched-uranium metal rods, and clusters of uranium metal and uranium oxide rods. In addition, many fine-structure measurements were made.

The zero-energy reactor ZENITH has been used to measure[18] the temperature coefficients of reactivity of systems fueled with U^{235} and moderated and reflected by graphite. With ZENITH it is possible to investigate the effects of core plus end-reflector temperature up to 800°C and side-reflector temperature up to 400°C. Nitrogen circulates through a heater beneath the core and passes between the fuel elements; in the plenum above the core, the nitrogen may be mixed with cooler gas before passing down through the side reflector. A thermal barrier of lampblack between core and side reflector reduces heat transfer.

Temperature coefficient measurements were made in the fourth loading of ZENITH; this loading contained 7.72 kg of U^{235}, corresponding to a carbon-to-U^{235} atomic ratio of 7788. This core was the most dilute system in the projected experimental program on U^{235} systems. Reactivities were measured by the rod drop method and the critical-balance-point method. In the former method all measurements were made to the same shutdown configuration, whereas in the latter method a fine and a coarse control rod were calibrated by positive period techniques. Temperature coefficients were then evaluated from the change in critical positions of the calibrated rods. The rod oscillator technique was used to evaluate the prompt-neutron lifetime and to provide additional calibration data for the fine control rod. Axial and radial weighting factors for the temperature measurements were evaluated by measuring the worth of copper tubes at various positions in the core.

Core and end-reflector temperature coefficients, as well as side-reflector temperature coefficients, are given[18] for several temperature ranges and control-rod configurations. Apart from a possible insignificant increase in the lowest temperature interval, the temperature coefficient for the core plus end reflectors shows no evidence of temperature dependence. The mean temperature coefficient over the range 147 to 367°C is $-(15.6 \pm 1.6) \times 10^{-5}$ per degree centigrade. The side-reflector coeffi-

cient is positive and, as found for previous loadings, decreases as the number of inserted control rods increases. Calculated values of the temperature coefficient, except for the side-reflector values, agree well with experiment. The accuracy of the experimental measurements is somewhat impaired by a nonuniform core-temperature distribution.

In order to test theoretical calculations of buckling and reaction rates in plutonium-graphite assemblies using basic nuclear data, a series of near-homogeneous plutonium–graphite exponential lattices was studied in a program reported in Ref. 19. Measurements were made of the material bucklings, disadvantage factors, and relative fission rates of U^{235}, Pu^{239}, and U^{233}. The carbon-to-plutonium atom ratio covered the range 2420 to 14,520. Relative fission-rate measurements were made in one lattice at 200 and 370°C. One experiment was also performed on an enriched-uranium lattice similar to one of the plutonium experiments. Fuel for the experiments was in the form of plutonium-aluminum spikes that were 28 in. long, 1.2 in. wide, and 0.02 in. thick. Each spike, containing 6.5 g of plutonium, was sheathed in 0.02-in.-thick aluminum. Approximately 2.5 at.% of the plutonium consisted of the isotope Pu^{240}. The graphite was in the form of square prisms, which were 28 in. long and 1.73 in. in the other two dimensions.

STEWPOT, a 43-group slowing-down code for the Mercury computer, was used for theoretical calculations of the experiments. A comparison of the calculations with experiment indicated that for these systems the STEWPOT code will predict the material bucklings to ±3%. Calculations of the U^{233}-to-U^{235} fission ratios show good agreement with experiment. However, the calculated Pu^{239}-to-U^{235} fission ratios are consistently lower than the experiments by almost 6 to 9%. The reference points out that the energy group breakdown in STEWPOT was not intended for plutonium-fueled systems and is not optimum for them.

Measurements of thorium resonance-capture activations relative to those of Au^{197}, which were made in the Peach Bottom (HTGR) critical assembly, are analyzed in Ref. 20 and are compared with thorium resonance activations calculated from the tabulated values of the resonance parameters. Since some of the thorium activation measurements employed thorium oxide dispersed quasi-homogeneously in graphite, resonance captures in thorium were measured by the vanadium-subtraction technique rather than the cadmium-ratio technique. The former method measures the resonance capture rate of an unknown nuclide relative to that of a thin foil of Au^{197}, which is assumed to be known. The vanadium is employed to determine and subtract the $1/v$ cross-section component for the unknown nuclide. To check the technique and assure internal consistency, auxiliary measurements employing U^{238} and Mn^{55} were carried out. The cadmium-ratio technique was employed to obtain measurements of the resonance capture rates of vanadium, Mn^{55}, and Th^{232} foils placed in a void in the HTGR critical assembly. The measurements for the latter two elements were made for comparison with results obtained by the vanadium-subtraction technique.

Included in Ref. 20 is a review of the status of the knowledge of absorption cross sections and resonance parameters for thorium and gold. Two alternative sets of resonance parameters were selected for thorium and were employed in the calculations for comparison with the experimentally measured data on thorium resonance captures. The measurements show that the lowest several resonances of thorium capture less strongly than would be predicted by the listed parameters. This reduced capture is such that the thin-limit, epicadmium, $1/E$ spectrum resonance integral is about 84 barns instead of the 96 barns predicted by listed parameters.

BeO-Moderated Assemblies

The interaction effects of hafnium control rods in a near-homogeneous BeO-moderated oralloy-fueled system were measured[21] for two to five rods by the pulsed-neutron technique. The subcritical assembly used consisted of a matrix of BeO blocks and oralloy foils. One portion of the matrix was stacked on the platform of a hydraulic ram, and the second portion was supported directly above on a 0.019-in.-thick stainless-steel diaphragm. Seven horizontal slots, 1 by $\frac{1}{8}$ in., were built into the lower assembly. The delayed critical time constant for a burst of fast neutrons was determined by extrapolation of a curve of prompt decay constant vs. the inverse multiplication of the assembly. Two series of measurements were made with the hafnium control rods. These rods were hafnium strips, 24 by 0.5 by 0.065 in.

for the first series and 24 by 0.5 by 0.0325 in. for the second series. The thinner rods were used to reduce slightly the rod worth and permit the use of more rods. The relative worths of individual rods in the same slot, individual rods in different slots, and combinations of rods are given. Included for comparison purposes are predicted worths assuming no rod interaction. The assumption that the prompt-neutron lifetime remains constant is implicit in the interpretation of the changes of prompt decay constant in terms of reactivity changes. This assumption was validated by measuring the delayed critical decay constant with seven thick hafnium rods in the assembly; it was found to be unchanged within the 2% limit of uncertainty in the measurement of the time constant.

Fast-Neutron Assemblies

The inability to predict the critical masses of three fast dilute assemblies previously examined in the ZPR-III prompted a series of critical studies[22] to obtain data for use in evaluating the adequacy of the sodium and stainless-steel cross sections employed in multigroup calculations. The ZPR-III is a split-bed reactor with each half consisting of a matrix of square stainless-steel tubes. Drawers containing the appropriate materials for each region are inserted into the square tubes. The first assembly (No. 32) was designed for a study of a simple combination of stainless steel and enriched uranium. The second assembly (No. 33) was similar, except that part of the stainless steel in each drawer was replaced by sodium-filled stainless-steel cans. Both assemblies were completely reflected by a natural-uranium blanket. Fission ratios of various fissile materials (U^{233}, U^{234}, U^{236}, U^{238}, Pu^{239}, and Pu^{240}) were measured at the core centers using fission chambers of parallel-plate construction. Average prompt-neutron lifetimes were measured by the Rossi alpha method. The reactivity worths of common reactor materials were measured at the center of each core and, for a few selected materials, near the edge of each core. The latter data were taken for information on the transport properties of the materials. Radial fission rates of various fissile materials were measured with miniature cylindrical fission chambers in each core. A series of bunching experiments was carried out in a wedge section of one-half of core 32. These experiments provided data on the effect of fuel-plate thickness on reactivity. Distributed worths of stainless steel, sodium, and aluminum were determined by substitution of these materials over one octant of the core. A few preliminary measurements were made of the influence of the mass of sodium present on the reactivity worth of sodium and on its variation with radial position. The measurements on these and other ZPR assemblies have been summarized in Ref. 23.

The ZPR-III facility has also been used to study a mockup of the second loading (core B)[24] for the Enrico Fermi fast reactor. The core material for this reactor is UO_2–stainless-steel cermet clad in stainless steel, and the reactor is cooled by sodium. The volumetric composition of the core is 11.5% fully enriched UO_2, 51.8% stainless steel, and 33.2% sodium. The nominal fully loaded volume is 600 liters. The original mockup was too small for criticality, and alterations were necessary. The critical mass was found to be 505.4 kg of U^{235}, corresponding to a core volume of 664.6 liters. The core volume was then reduced to approximately the maximum allowable volume of 600 liters, and criticality was reached by the substitution of a nickel reflector for the radial blanket in an annulus about 2 in. thick adjacent to the core. Measurements of reactivity effects of the most important differences between the mockup and the actual Fermi reactor were necessary in order to establish the critical mass for the actual reactor. Some of these effects are end gaps, UO_2 axial blankets, a central gap, a source that occupies a subassembly at the radial edge of the actual core, and safety-rod and control-rod channels. The distributed reactivity worths of various materials were measured also in order to correct for discrepancies between the mockup and the core. A comparison of the reactivity effects of various radial reflectors was made. These included nickel, nickel oxide, iron oxide, beryllium, and beryllium oxide. Measurements were made of relative reaction rates as functions of both radial and axial position, and fission ratios of the various fissionable isotopes were measured at the center of the core.

Various features related to the dynamic behavior of the reactor were investigated. These included a measurement of the isothermal temperature coefficient, the reactivity effects of axial core expansion, and Rossi alpha measure-

ments at delayed critical. The reactivity effect of heterogeneity of the fuel was estimated by bunching the fuel plates in various arrangements; the final results give reactivity change as a function of effective fuel-plate thickness. This curve extrapolated to zero plate thickness gives the reactivity loss caused by homogenizing the fuel.

References

1. I. Kaplan, Measurements of Reactor Parameters in Subcritical and Critical Assemblies, USAEC Report MITNE-25, Massachusetts Institute of Technology, Aug. 15, 1962.
2. General Nuclear Engineering Corp., BONUS Zero Power Critical Experiments and Application to the Reactor Design, Terminal Report, USAEC Report GNEC-198, Feb. 10, 1962.
3. R. C. Lloyd, E. D. Clayton, and C. R. Richey, Critical Mass Experiments with Plutonium Nitrate Solutions, in Physics Research Quarterly Report, July, August, September 1962, USAEC Report HW-75228, pp. 33-39, Hanford Atomic Products Operation, Oct. 15, 1962.
4. F. E. Kruesi, J. O. Erkman, and D. D. Lanning, Critical Mass Studies of Plutonium Solutions, USAEC Report HW-24514(Del.), Hanford Atomic Products Operation, May 19, 1952.
5. R. C. Lloyd, E. D. Clayton, C. R. Richey, and S. R. Bierman, Critical Experiments with Plutonium Nitrate Solutions, in Physics Research Quarterly Report, January–March 1963, USAEC Report HW-77311, pp. 44-47, Hanford Atomic Products Operation, Apr. 15, 1963.
6. J. D. White, T. J. Powell, and R. H. Masterson, Limiting Critical Concentrations of U^{235} and Pu^{239} in Aqueous Solutions, in Physics Research Quarterly Report, July, August, September 1962, USAEC Report HW-75228, pp. 40-53, Hanford Atomic Products Operation, Oct. 15, 1962.
7. A. Selep, Pathfinder Atomic Power Plant. Clustered Pin Superheater Lattice Experiments, USAEC Report ACNP-63005, Allis-Chalmers Mfg. Co., Feb. 12, 1963.
8. F. S. Kirn and J. I. Hagen, BORAX-V Exponential Experiment, USAEC Report ANL-6707, Argonne National Laboratory, April 1963.
9. I. Kaplan, A. E. Profio, and T. J. Thompson, Heavy Water Lattice Project Annual Report, USAEC Report MITNE-26, Massachusetts Institute of Technology, Sept. 30, 1962.
10. E. M. Pennington, Calculations for ZPR-VII Uniform Lattice Critical Experiments with Thoria-Urania Fuel in Heavy Water, USAEC Report ANL-6661, Argonne National Laboratory, December 1962.
11. W. C. Redman, S. G. Kaufmann, K. E. Plumlee, and Q. L. Baird, Critical Experiments with Thoria-Urania Fuel in Heavy Water, USAEC Report ANL-6378, Argonne National Laboratory, December 1961.
12. The Babcock & Wilcox Co., Spectral Shift Control Reactor Basic Physics Program. Quarterly Technical Report No. 9, USAEC Report BAW-1266, October–December 1962.
13. The Babcock & Wilcox Co., Spectral Shift Control Reactor Basic Physics Program. Quarterly Technical Report No. 10, USAEC Report BAW-1271, January–March 1963.
14. R. W. Campbell, R. J. Doyas, H. C. Field, C. A. Guderjahn, R. L. Guenther, D. F. Hausknecht, M. S. Mayer, and H. A. Morewitz, Critical Experiments on Slightly Enriched Uranium Metal Fuel Elements in Graphite Lattices, USAEC Report NAA-SR-7541, Atomics International, June 30, 1963.
15. British Industries Collaborative Exponential Programme. Volume I. Introduction; Exponential Experiments on Rods and Tubes of Natural Uranium Metal, British Report AEEW-R-235 (Pt. I), March 1963.
16. British Industries Collaborative Exponential Programme. Volume II. Exponential Experiments on Enriched Uranium Metal Rods and on Clusters of Uranium Metal and Uranium Oxide Rods, British Report AEEW-R-235 (Pt. II), March 1963.
17. British Industries Collaborative Exponential Programme. Volume III. Fine Structure Experiments; Miscellaneous Exponential Experiments, British Report AEEW-R-235 (Pt. III), March 1963.
18. R. Caro Manso, R. G. Freemantle, and J. D. Rogers, Temperature Coefficients of Reactivity with Fourth Loading of ZENITH, British Report AEEW-R-208, October 1962.
19. D. H. Carter, W. G. Clarke, C. Hunt, J. Marshall, D. B. McCulloch, J. E. Sanders, and C. R. Symons, Measurements of Buckling and Relative Reaction Rates in Some Plutonium-Graphite Assemblies, British Report AEEW-R-201, January 1963.
20. J. B. Sampson, Analysis of Activation Measurements of Th^{232} Resonance Captures in the Peach Bottom (40-Mw(e) Prototype HTGR) Critical Assembly, USAEC Report GA-3069, General Atomic Division, General Dynamics Corp., Sept. 14, 1962.
21. J. M. Piowaty, J. R. Morton III, and L. L. Gardner, Coupling Effects of Hafnium Control Rods in a Near-Homogeneous, BeO-Moderated, Oralloy-Fueled System, USAEC Report UCRL-7262, University of California, Lawrence Radiation Laboratory, Feb. 27, 1963.
22. P. I. Amundson, W. Gemmell, J. K. Long, and R. L. McVean, Critical Studies of Uranium-Steel and Uranium-Steel-Sodium Fast Reactor Cores (ZPR-III Assemblies 32 and 33), USAEC Report ANL-6690, Argonne National Laboratory, February 1963.
23. J. K. Long, A. R. Baker, W. Gemmell, W. P. Keeney, R. L. McVean, and F. W. Thalgott, Ex-

perimental Results on Large Dilute Fast Critical Systems with Metallic and Ceramic Fuels, in *Physics of Fast and Intermediate Reactors*, Vol. I, International Atomic Energy Agency, Vienna, 1962.

24. T. A. Doyle and A. L. Hess, Critical Studies of Core B for the Enrico Fermi Atomic Power Plant (ZPR-III Assembly No. 35), USAEC Report ANL-6669, Argonne National Laboratory, February 1963.

Section

III

Power Reactor Technology

Fluid and Thermal Technology

Burnout Limits for Boiling-Water Reactors

By John S. Wiley

Heat-transfer burnout is one of the phenomena which determine the power capability of a water-cooled reactor. It is not the only one, nor is it necessarily the controlling one In oxide-fueled reactors the central temperature of the fuel elements often imposes a limitation that is more restrictive than the burnout limitation. Nevertheless, the burnout limitation is a highly important one. Its relative importance is likely to increase as reactor designs become more highly developed and as methods for extracting higher specific powers from oxide fuel elements are proved. Furthermore, rightly or wrongly, the burnout ratio is given serious consideration in safety evaluations of power reactors, and for this reason the question of burnout sometimes proves to be a more restrictive design consideration than might otherwise be supposed.

In recognition of the importance of burnout phenomena to the reactor designer, investigations and analyses related to burnout have been given considerable attention in past issues of *Power Reactor Technology*. Since these investigations are usually described in papers written for the heat-transfer specialist rather than for the reactor designer, it has seemed worthwhile to examine the question briefly from the point of view of the designer's interests. In this article advantage is taken of the opportunity offered by the presentation of two new burnout correlations[1,2] to present such a review. The discussion is limited to burnout under conditions of net boiling, because burnout tends to impose more severe restrictions on boiling reactors than on pressurized-water reactors, and because limitation of the discussion to a single burnout regime simplifies the problem of relating the phenomenon to questions of reactor design and analysis. In the course of the discussion, selected burnout data will be utilized to illustrate various points. Many of these data are taken from the extensive collection that has been assembled in Ref. 3.

To cover the range of practical interest in burnout, one must consider a relatively large number of variables and rather large ranges of these variables. The major variables, in addition to the heat flux, include the size, shape, and degree of interconnection of the coolant channels, the flow velocity of the coolant, its pressure, and the degree to which it is subcooled below the saturation temperature at the entrance to the coolant channel. Large ranges of variables have been covered by the many measurements of burnout which have been made, and the question naturally arises as to how to correlate all these experimental data.

Because the process of burnout is not understood in detail, it has not been possible to arrive at correlations that are based on the fundamental relations among the variables. In such a circumstance it is usually found that no single correlation will meet the needs of all users of the experimental data, and this proves to be the case for burnout. One approach is to attempt to find purely empirical equations that will relate the important variables with acceptable accuracy over the widest possible range. Such correlations are very useful and are widely used as methods of compressing the results of many experiments into a small volume. In arriving at such a correlation, the analyst must sometimes make compromises in the precision with which the correlation will cover the entire range of variables in order to arrive at an expression of reasonable length and complexity. When the

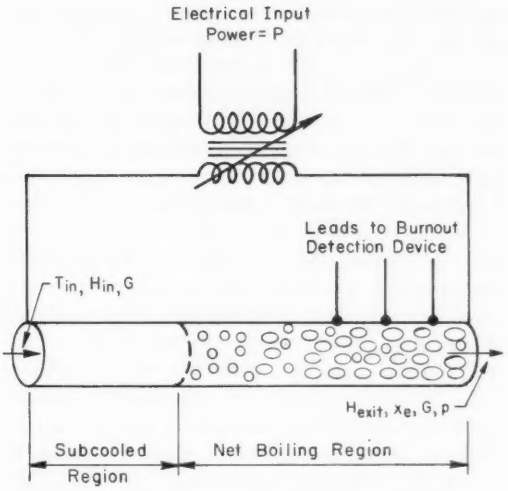

Fig. III-1 Diagram of representative burnout test. T = temperature, °F; H = enthalpy, Btu/lb; x = quality, lb/lb; G = mass flow, lb/(hr)(sq ft); p = pressure, psia.

fundamental relations among the variables are not known, arbitrary groupings and functional dependencies must be assumed. Once this is done the correlation can make no distinction between those deviations from its predictions resulting from true functional dependencies that have been neglected and those resulting from errors of measurement or perhaps from true fluctuations in the phenomenon under consideration. In this respect such a correlation falls short of the needs of the analyst who may desire to infer basic functional relations. Since it seeks to express the entire mass of accumulated data in terms of the fewest possible variables, the variables chosen for correlation are often not the independent variables of reactor design. In this respect the correlation may also fall short of the needs of the designer. It is not usually in a convenient form for illuminating the relations among the design variables.

It is instructive to consider how burnout experiments are run and how the data might be handled in the simple case in which the experimenter is provided with a heat-transfer apparatus of fixed dimensions. It will be assumed that the apparatus consists of a uniform round tube, electrically heated, as is usually the case in such experiments and as indicated in Fig. III-1. If it is assumed that the experimenter has chosen the pressure at which he is to operate (and to simplify later discussion it is here assumed that the pressure specified is that at the tube exit), then he has available only three further variables: the electric power input to the tube, the coolant flow velocity, and the inlet temperature of the coolant. If he fixes the inlet temperature (at, say, some value below the saturation temperature at the ambient pressure), he may choose to run the experiment in one of two ways: either he may fix the coolant flow velocity and gradually increase the power input to the test section until burnout occurs, or he may adjust the coolant flow to some value, fix the power input, and then gradually change the coolant flow until burnout occurs. Presumably, similar results may be obtained by both methods.

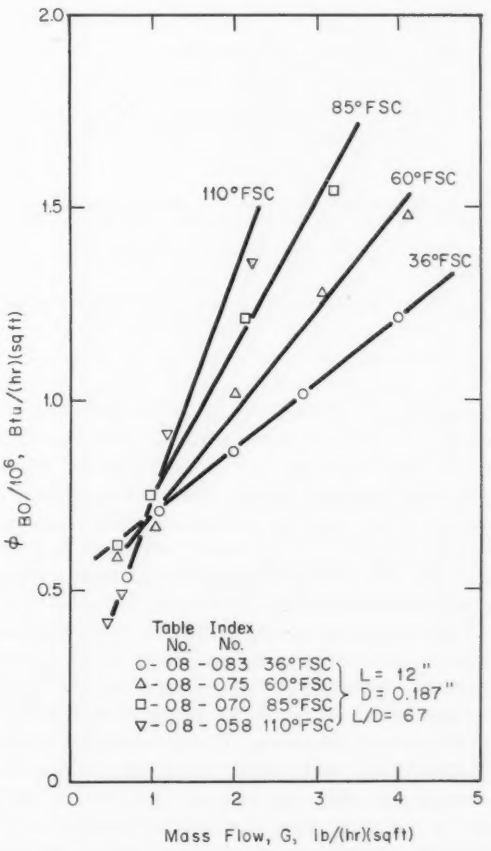

Fig. III-2 Plot of burnout data from Table 8 of Ref. 3. ϕ_{BO} vs. G; pressure = 2000 psia. The "Table No." and "Index No." refer to the method of organizing the data as used in Ref. 3.

If a number of such experiments are run, over a range of coolant flows and power inputs, the experimenter will accumulate a group of data and will be faced with the question of how to present it. A straightforward scheme is to plot the two directly controlled variables, coolant flow and power input (or the more general specification of the power input, the heat flux),

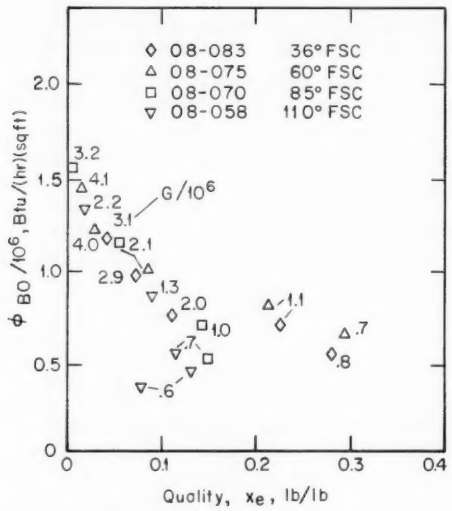

Fig. III-3 Plot of burnout data from Table 8 of Ref. 3. ϕ_{BO} vs. x_e; pressure = 2000 psia.

against one another. Figure III-2 shows the results of some experimental data of this kind (from Ref. 3), plotted in just such a way. There are four curves shown, each for a different value of inlet subcooling; as might be expected, the heat flux at which burnout occurs increases, for the tube of fixed length-to-diameter ratio, with inlet subcooling.

The question immediately arises as to whether there is some more general way of plotting (correlating) the data which might bring together all the curves for the different degrees of subcooling. This possibility seems particularly reasonable since all the experimental sections are actually observed to burn out at or very near the exit end and since, if burnout is determined purely by the local conditions of the coolant and heat flux (i.e., burnout is not affected by the past history of the coolant at points farther upstream in the tube), the condition of the coolant near the exit end of the tube can thus be completely specified simply by specifying its steam content. The obvious suggestion is to plot the burnout heat flux as a function of the steam quality at the tube exit, x_e. This has been done for the data of Fig. III-2 in Fig. III-3, and it is observed that, although the four sets of data are indeed integrated, there is a disappointing spread in the data points at the higher values of exit quality. This scatter is rather characteristic of burnout data at high exit quality if they are plotted in this way. Figure III-4 shows another set of data taken from the same reference.[3]

In considering the behavior of the data in Figs. III-3 and III-4, it is important to bear in mind that the exit steam quality is not a measured quantity but one that is computed from the measured values of mass flow and heat flux. The exit quality is computed from the heat balance, as follows:

$$4\phi L/D = G(H_{exit} - H_{in}) \qquad (1)$$

where* ϕ = uniform heat flux, Btu/(hr)(sq ft)
L = total length of test section, ft
D = diameter of test section, ft
H_{exit} = enthalpy of mixture leaving test section, Btu/lb
H_{in} = enthalpy of mixture entering test section, Btu/lb

If the definition of exit quality, x_e, in terms of enthalpy is used, Eq. 1 can be written as

$$\phi = GD/4L(x_e H_{fg} + H_f - H_{in}) \qquad (2)$$

The symbols H_{fg} and H_f have their conventional meanings. Equation 2 has been plotted on Fig. III-5 for two of the points of Fig. III-4 (runs 205 and 206 of Table 10, Ref. 3) where it is called the operating line, again following the nomenclature suggested in Fig. 74 of Ref. 3. The significance of this designation is that, if the burnout experiment was run by the first method described above—by setting the mass flow and the inlet subcooling and gradually increasing the input power until burnout oc-

*Equation 1 is valid over a range of ϕ from zero power to burnout. At burnout ϕ is termed ϕ_{BO} and the exit enthalpy is termed H_{BO}, following the nomenclature of Ref. 3. Thus the qualities plotted in Figs. III-3 and III-4 could be labeled $x_{e_{BO}}$; the last subscript was dropped, however, for simplicity in nomenclature.

curred—the exit quality would increase with heat flux during this process in the manner specified by the operating line.

As Eq. 2 shows, the slope of the operating line is proportional to the mass flow, and if, for example, there were in the experiment an uncertainty of ±10% in the mass flow, there would be a corresponding uncertainty in the slope of the operating line. If there were also an uncertainty of ±10% in the heat flux at which burnout occurred, either because of experimental imprecisions or because of real uncertainties in the burnout process, this uncertainty would combine with the uncertainty in mass flow to yield a net uncertainty of approximately ±20% in the value of the exit quality at burnout. These illustrative uncertainty ranges have been indicated for the two burnout points plotted in Fig. III-5. It is clear that the use of the derived exit quality as a plotted variable tends to emphasize whatever uncertainties may exist in the measurements, simply because x_e is given by the ratio of two measured quantities (the heat flux and the mass flow), and consequently its percentage range of uncertainty is approximately the sum of the ranges for the two measured quantities. One must be on the alert for such artificial changes in the apparent uncertainties of experimental determinations when considering the appropriateness and accuracy of correlation procedures.

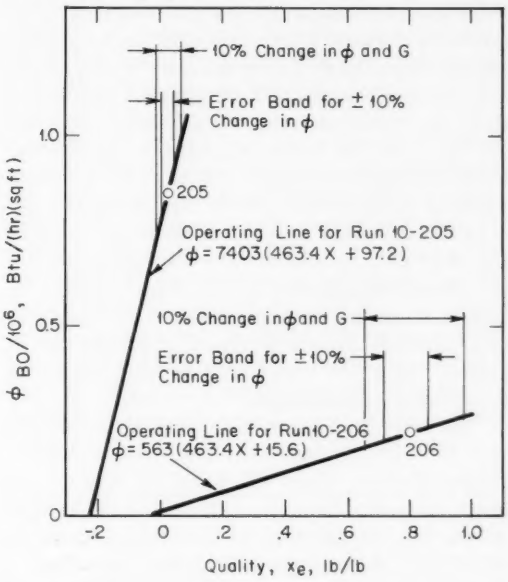

Fig. III-5 Plot of operating lines for runs 10-205 and 10-206 of Ref. 3. ϕ_{BO} vs. x_e; pressure = 2000 psia.

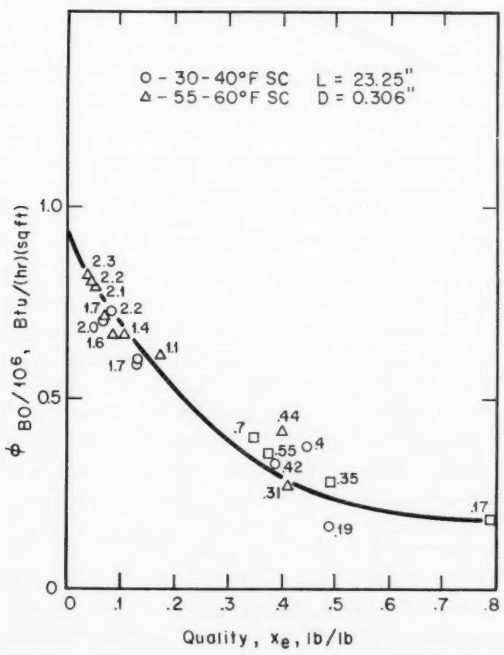

Fig. III-4 Plot of burnout data from Table 10 of Ref. 3. ϕ_{BO} vs. x_e; pressure = 2000 psia.

The plotting of burnout heat flux as a function of exit quality is an elementary correlation arrived at here through an intuitive judgment as to the burnout process, and it is fundamentally useful insofar as it gives some evaluation of that judgment. Although it does bring together data in which the only variables are heat flux, mass flow, and subcooling, it would be surprising if this single parameter alone could correlate the effects of many other variables. The correlations given in Ref. 2, which are discussed in later paragraphs, are expressed primarily in terms of the exit quality variable. They give a good indication of the usefulness of this parameter as a basis for correlation.

For the purposes of boiling reactor design, it is useful to treat the burnout data in a somewhat different manner that amounts to taking the mass flow, G, inside the parentheses in Eq. 2 and using the product Gx_eH_{fg} as the plotted variable

$$\phi = D/4L(Gx_eH_{fg} + GH_f - GH_{in}) \qquad (3)$$

This method of handling the data was first proposed by Levedahl,[4] who gave the name steam-energy flow (SEF) to the quantity Gx_eH_{fg}. When the burnout heat flux is plotted as a function of SEF, the curve presents to the reactor designer the effect of the burnout limit on the two important design quantities that specify the heat-removal characteristics for the boiling reactor core. The significance of the burnout value of the heat flux is well known; the significance of the steam-energy flow at the burnout point is that it tells the designer how much power can be removed, in the form of latent energy of steam, from the unit cross-sectional area of the coolant flow passage.

The data from Figs. III-3 and III-4 (Tables 8 and 10 of Ref. 3) have been replotted on steam-energy plots in Figs. III-6 and III-7. It can be seen that the data no longer fall on single curves but are again, as in Fig. III-2, separated according to mass flow, and each curve consists of two lines of opposite slope arbitrarily called DNB-1 and DNB-2. The scatter of the data about the line appropriate to them is small. In this method of plotting, the effects of compounded uncertainties are not accentuated in the region of low burnout heat flux, as is shown in Fig. III-8. The steam-energy flow plot can hardly be called a correlation, since it does not reduce the number of variables that must be taken into account, but it does have fundamental usefulness in addition to its usefulness to the designer, for it brings some order into the data and it suggests the existence of two quite different processes that may determine burnout (DNB-1 and DNB-2).

In setting the reactor power output, the designer never intentionally approaches near the burnout limit but always leaves a large safety factor that is usually expressed as the burnout ratio. This is the ratio of the burnout heat flux to the actual heat flux at the worst point in the reactor. Since it is the limitation of some specified burnout ratio that sets the permissible power output of the reactor, it is worthwhile to examine just what the ratio means in terms of a safety factor. The steam-energy flow plot is useful for this examination and is employed schematically in Fig. III-9. It shows a hypothetical DNB-1 line and an operating line, $\overline{AC}$, for the worst coolant channel of a hypothetical boiling reactor that has a uniform axial power-generation rate. It is assumed that the channel normally operates at point B, with a heat flux ϕ_1 and a steam-energy flow of SEF_1 at the channel exit. The burnout ratio is often defined as

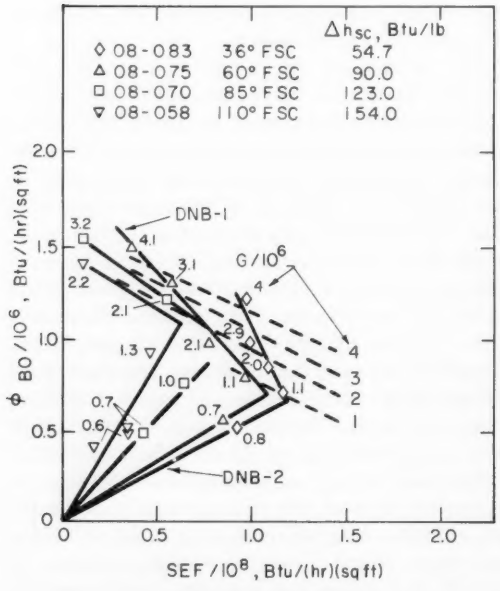

Fig. III-6 SEF plot of Table 8 data of Ref. 3. ϕ_{BO} vs. SEF; pressure = 2000 psia; L = 12.5 in.; D = 0.187 in., L/D = 67; A-nickel.

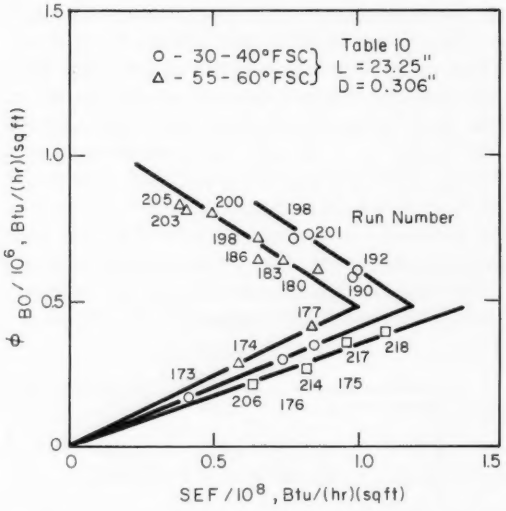

Fig. III-7 SEF plot of Table 10 data of Ref. 3. ϕ_{BO} vs. SEF; pressure = 2000 psia.

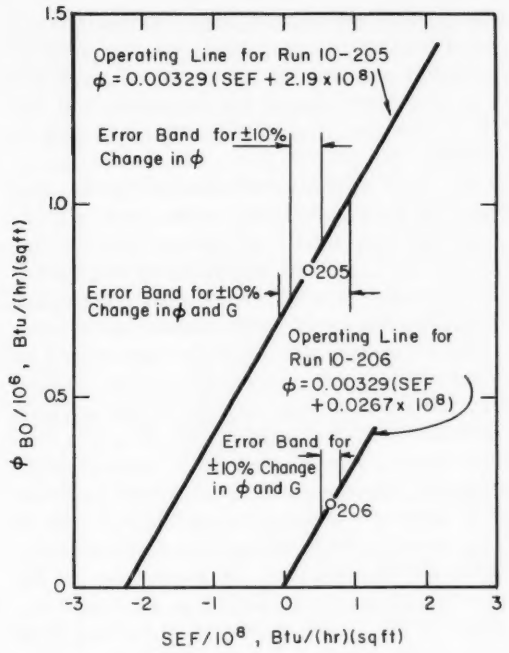

Fig. III-8 Operating lines for runs 10-205 and 10-206 of Ref. 3 on an SEF plot. Pressure = 2000 psia.

the ratio $\phi_3 : \phi_1$, but this ratio has little significance as a safety factor on reactor power, since heat flux and steam-energy flow must vary simultaneously, as specified by the operating line as reactor power is varied. If the reactor power were increased to burnout, the burnout in the coolant channel in question would occur at point C, corresponding to a heat flux ϕ_{BO} and a steam-energy flow SEF_{BO}. For normal operation at ϕ_1, the safety factor on reactor power is thus ϕ_{BO}/ϕ_1. These considerations have been pointed out in the past, notably by Ref. 3. In that paper the ratio $\phi_3 : \phi_1$ is called the heat-flux burnout ratio, whereas the ratio $\phi_{BO} : \phi_1$ is called the power burnout ratio. The ratio $\phi_3 : \phi_1$ has a physical significance only if it is postulated that the DNB-1 line is determined entirely by local conditions at the point of burnout. In such a case the ratio $\phi_3 : \phi_1$ in Fig. III-9 is the factor by which the heat flux would have to be increased in a very short section of the coolant channel, near the exit, to cause burnout.

As normally used, however, the burnout ratio is not so much a safety factor on reactor power as it is an uncertainty factor on the burnout prediction. Perhaps it is more precise to say that it is an uncertainty factor on the applicability, to the specific reactor situation in question, of the burnout data or burnout correlation used to predict the burnout limit. In this application it might be argued that the ratio $\phi_3 : \phi_1$ is as good a means of describing the uncertainty as the ratio $\phi_{BO} : \phi_1$. Actually the use of any single number is probably a poor way of expressing a safety factor on burnout, if it is recognized that the burnout correlation (exemplified by the DNB-1 line in Fig. III-9) may have an unexpected shape and that there will be uncertainties in the operating line for the reactor as well as in the burnout correlation. It is perhaps justified only because the burnout ratios actually

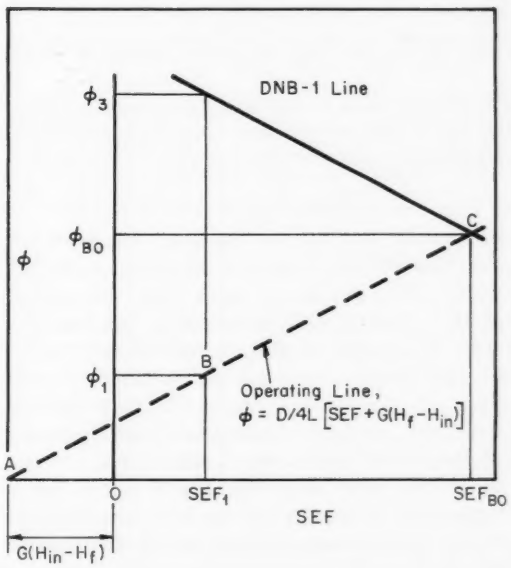

Fig. III-9 Steam-energy flow plot showing hypothetical DNB-1 and operating lines.

used in reactor design are large, and because other uncertainties, such as those arising from nonuniform heat generation and complex coolant-channel geometry, may affect the significance of the burnout ratio in a way that is poorly understood in any case.

The questions raised by axial nonuniformities in heat flux along the coolant channel are particularly significant because axial nonuniformity is the normal situation in reactor applications. This is the key question: Is burnout

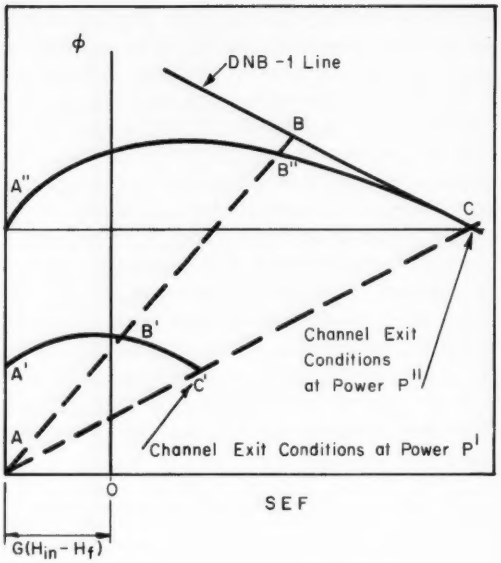

Fig. III-10 Steam-energy flow plot showing hypothetical DNB-1 line and operating lines corresponding to nonuniform axial power production.

determined entirely by the local value of the heat flux and the local time-averaged values of temperature, pressure, mass flow, and quality for the coolant? If the answer is yes, the effects of nonuniform heating should be reasonably predictable from burnout experiments on uniformly heated test sections. Experiments have been made to investigate this question, but they have been inconclusive, at least in the net boiling range. It is well known that in some cases burnout is induced by flow instabilities, and in these cases it would not be anticipated that local conditions will determine burnout.

If it is assumed that burnout is determined by only local factors in the DNB-1 range, the burnout relations along a single coolant channel in a reactor with nonuniform axial power distribution can be discussed in terms of Fig. III-10. In this figure the point values of ϕ and SEF at two powers, P' and P'', are schematically shown. Here there are an infinite number of burnout safety factors given by ratios such as $\overline{AB}:\overline{AB'}$ and $\overline{AC}:\overline{AC'}$. As power is increased (say from P' to P''), one of the ratios becomes unity and burnout ensues. Thus whether burnout occurs at the channel exit or somewhere upstream depends on the detailed shapes and relative positions of curves such as $A'B'C'$, $A''B''C$, and the DNB-1 line. If fairly rapid power transients are considered, the problem is further complicated by the fact that the flow rate may vary during the transient, and this affects the operating line position, as well as possibly the DNB-1 line. As shown in Fig. III-10, some nonuniformly heated test sections will still burn out at their exits. This is illustrated in Fig. III-10 by arbitrarily choosing curve $A''B''C$ so that it intersects the DNB-1 line at point C. A slight increase in the slope of the DNB-1 line could produce upstream burnout.

The preceding discussion is intended as an introduction to the examination of the burnout correlations presented in Refs. 1 and 2. Those presented in Ref. 1 also appear in a Westinghouse topical report[5] that deals with an AEC-sponsored research and development program for a large pressurized-water reactor that is to be built by Westinghouse for Southern California Edison Company. A correction to the material presented in Ref. 1 is contained in a Letter to the Editor published in the July 1963 issue of *Nucleonics*. The present discussion considers only the correlation for the quality region, which is given in Eq. 1 in Ref. 1:

$$\begin{aligned}\Delta H_{DNB} &= 0.529(H_f - H_{in}) \\ &\quad + (0.825 + 2.36e^{-204D_e})H_{fg}e^{-1.5G/10^6} \\ &\quad -0.41H_{fg}e^{-0.0048L/D_e} \\ &\quad -1.12H_{fg}\rho_g/\rho_f + 0.548H_{fg} \qquad (4)\end{aligned}$$

where

$$\Delta H_{DNB} = H_{DNB} - H_{in} = 4L_{DNB}/D_e \times \phi_{BO}/G \qquad (5)$$

and

D_e = equivalent diameter, ft = 4(cross-sectional area)/heated perimeter)
G = local mass velocity, lb/(hr)(sq ft)
H_{in} = inlet enthalpy, Btu/lb
H_f = saturated liquid enthalpy, Btu/lb
H_{fg} = heat of evaporation, Btu/lb
ΔH_{DNB} = $(H_{DNB} - H_{in})$, Btu/lb
L = length of heated channel, ft
ϕ_{BO} = heat flux at DNB, Btu/(hr)(sq ft)
ρ_f = density of saturated liquid, lb/cu ft
ρ_g = density of saturated vapor, lb/cu ft

The parameter ranges of the correlated experimental data are given as follows:[1]

Geometries: circular tube, rectangular channel, and rod bundle

Axial heat-flux distribution: uniform and non-uniform

Mass velocity = 0.2×10^6 to 4.0×10^6 lb/(hr)(sq ft)

Pressure = 800 to 2750 psia

L/D_e = 21 to 656

Inlet subcooling $H_{in} \geq 400$ Btu/lb

Local heat flux = 0.1×10^6 to 1.8×10^6 Btu/(hr)(sq ft)

Exit quality = 0 to 0.90 wt.%

Equivalent diameter = 0.1 to 0.54 in.

Heated-to-wetted perimeter ratio = 0.88 to 1.0

The terms H_{DNB} and L_{DNB} are presumably the enthalpy of the mixture at the point of departure from nucleate boiling and the length of the heated channel from inlet to the point of departure from nucleate boiling. In Ref. 1 ϕ_{BO} is termed q''_{DNB}; for uniformly heated test sections burning out at their exit $L_{DNB} = L$.

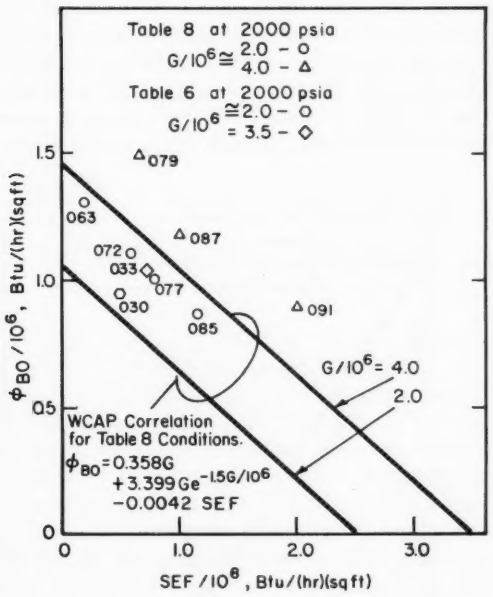

Fig. III-11 Comparison of WCAP correlation at 2000 psia with data from Tables 6 and 8 of Ref. 3.

Equation 4 can be stated in terms of the steam-energy flow if the geometry is fixed, so that the heat input can be specified in terms of the heat flux and the equivalent diameter, as required by the heat balance of Eq.2. The case of circular channels is considered, for which D, the equivalent diameter, is four times the heated perimeter divided by the cross-sectional flow area. Solving Eq. 2 for the quantity $(H_f - H_{in})$ gives

$$\frac{4\phi_{BO}L}{GD} - \frac{SEF_{BO}}{G} = H_f - H_{in} \qquad (6)$$

Substituting Eq. 6 into Eq. 4 yields

$$0.471\,\frac{4\phi_{BO}L}{GD} = -0.529\,\frac{SEF_{BO}}{G} + (0.825 + 2.36e^{-204D_e})H_{fg}e^{-1.5\,G/10^6} - 0.41H_{fg}e^{-0.0048L/D_e} - 1.12H_{fg}\rho_g/\rho_f + 0.548H_g \qquad (7)$$

Figure III-11 shows the Westinghouse Atomic Power Division (WCAP) correlation (in the form given by Eq. 7) as applied to conditions of Table 8, Ref. 3. The four data points of Table 8 for $G/10^6 = 2.0$ fall in a line parallel to the appropriate correlation line, as do the three higher mass-flow data points. The ratio of the experimental burnout heat flux, ϕ_{BO_e}, to the calculated heat flux, ϕ_{BO_c}, however, cannot be obtained directly from the figure. This is true because ϕ and SEF are related by means of the heat balance, and, if the correlation predicts ϕ_{BO}, it also predicts SEF_{BO}. An example will

Table III-1 COMPARISON OF CALCULATED AND EXPERIMENTAL DATA

Run No. (from Table 8 of Ref. 3)	Mass flow, G, lb/(hr)(sq ft) × 10^{-6}	ϕ_{BO_e}, Btu/(hr)(sq ft) × 10^{-6}	ϕ_{BO_c},* Btu/(hr)(sq ft) × 10^{-6}	$\frac{\phi_{BO_e}-\phi_{BO_c}}{\phi_{BO_e}}$	SEF_{BO_e}, Btu/(hr)(sq ft) × 10^{-8}	SEF_{BO_c}, Btu/(hr)(sq ft) × 10^{-8}	$\frac{SEF_{BO_e}-SEF_{BO_c}}{SEF_{BO_e}}$
08-076	1.08	0.75	0.71	5.3	1.08	0.96	11.1
08-077	2.11	0.99	0.86	13.0	0.82	0.48	41.5
08-078	3.14	1.27	1.11	12.6	0.63	0.26	58.5
08-079	4.12	1.48	1.41	4.7	0.36	0.22	38.9

*Calculated from $\phi_{BO} = 0.339G + 1.600Ge^{-1.5G/10^6}$. This is the equation shown on Fig. III-11 after substitution of Eq. 6 for SEF and using H_{in} = 585.2 Btu/lb.

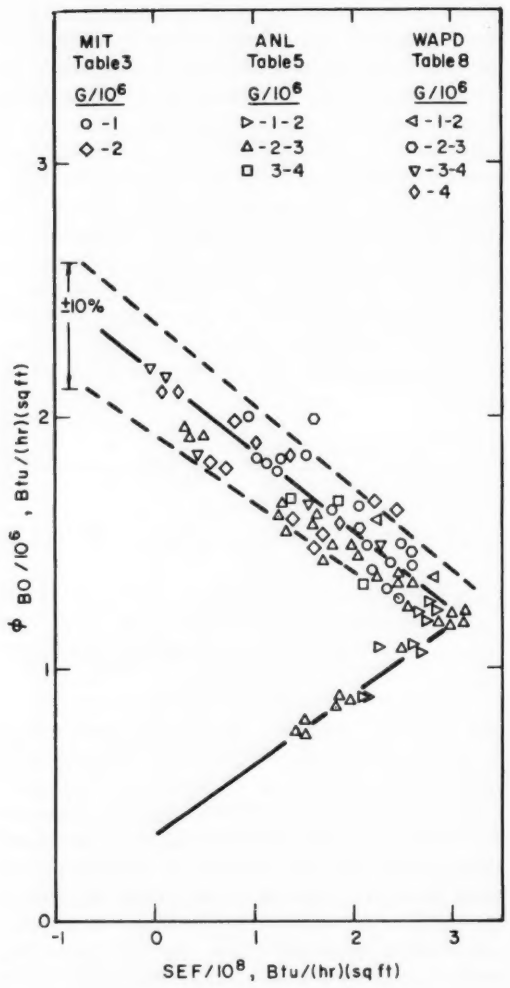

Fig. III-12 Steam-energy flow plot of data appearing in Tables 3, 5, and 8 of Ref. 3. Pressure = 1000 psia.

serve to illustrate the point. Table III-1 lists the experimental and calculated values of ϕ_{BO} and the exit steam-energy flow values at the burnout heat flux, SEF_{BO}, for runs 08-076, -077, -078, and -079. This table shows that the correlation does indeed predict the burnout heat flux within 20%, as stated.[1] The correlation also predicts an exit quality at burnout and the resulting SEF value at burnout; the accuracy of this prediction is quite poor. If nonuniformly heated test sections do burn out as is suggested in Fig. III-10, then the location of the DNB-1 line is important. If a correlation overpredicts ϕ_{BO}, it also overpredicts SEF_{BO}, which has the effect of moving the DNB-1 line both upward and to the right. The burnout safety factor given by the ratio $\overline{AC}:\overline{AC'}$ is thus also overpredicted, since the length of $\overline{AC}$ is given by a correlation and the length $\overline{AC'}$ is set by the designer.

Also plotted on Fig. III-11 are runs 030 and 033 from Table 6 of Ref. 3. This was done to show that there is still some unaccounted-for variable that prevents the Table 6 results from agreeing with the Table 8 results. That they should agree is suggested by the fact that the two test sections used to take the data of Tables 6 and 8 were almost identical in dimensions. This subject has been discussed in Ref. 6.

Figure III-12 contains 1000-psia burnout data contained in Tables 3, 5, and 8 of Ref. 3. Although the data all appear in a Westinghouse publication, they were actually taken at three different laboratories. It can be noted that at this pressure the steam-energy flow plot happens to bring the data for a wide range of mass flows very nearly together into a single curve.

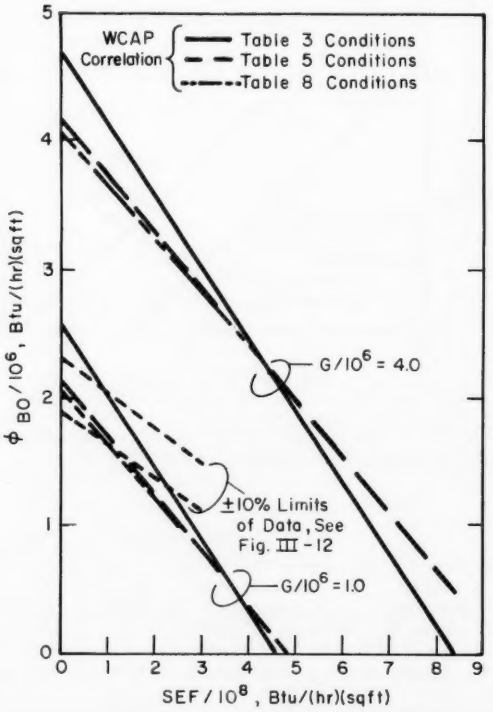

Fig. III-13 Comparison of WCAP correlation with data appearing in Tables 3, 5, and 8 of Ref. 3. Pressure = 1000 psia.

Table III-2 WCAP CORRELATION EQUATIONS PLOTTED ON FIG. III-13

(Pressure = 1000 psia)

Ref. 3 table No. wherein data appear	Test-section parameters		Burnout correlation equation
	Length, in.	Diameter, in.	
3	9.0	0.1805	$\phi_{BO} = 1.17G + 6.464Ge^{-1.5G/10^6} - 0.0056SEF$
5	11.625	0.180	$\phi_{BO} = 1.029G + 4.994Ge^{-1.5G/10^6} - 0.00435SEF$
8	12.5	0.187	$\phi_{BO} = 1.01G + 4.763Ge^{-1.5G/10^6} - 0.0042SEF$

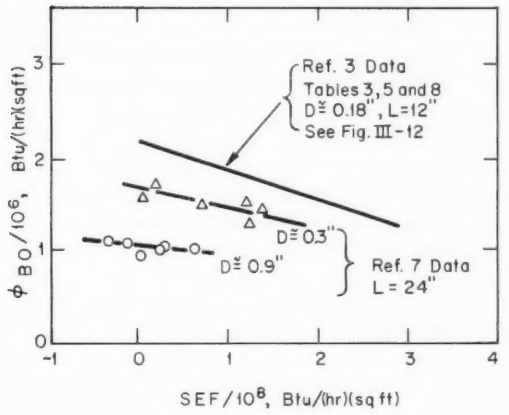

Fig. III-14 Steam-energy flow plot of burnout data from Refs. 7 and 3. Pressure = 1000 psia.

Whatever fundamental significance this may have is not readily apparent, but the practical significance—and possible importance—to the designer operating in this pressure range is obvious. Table 5 contains a few DNB-2 data, and these appear on the figure, although they will not be discussed. Figure III-13 compares the WCAP correlation with the data shown in Fig. III-12. The particular equations plotted are shown in Table III-2. It appears that the correlation does not recognize the insensitivity to mass flow in this pressure range.

An effect of the test-section diameter on ϕ_{BO} is shown in Fig. III-14, which plots data from Ref. 7. The data for $D = 0.3$ in. are replotted in Fig. III-15 along with some additional data from Table 10 of Ref. 3.* Again the data on Fig. III-15 point to a lack of effect of G on ϕ_{BO} on an SEF plot, although the Westinghouse (WCAP) correlation exhibits a rather strong effect.†

It can be noted that the coefficient of the SEF term in the WCAP correlation is pressure-independent, as can be seen from Eq. 7. This is substantiated in Fig. III-16, where data of Table 3 from Ref. 3 are plotted for three pressures. The lines are parallel, as they should be for a constant coefficient of the SEF term in Eq. 7.

The analyses contained in the report[2] by the Atomic Power Equipment Department (APED) of General Electric Company are intended to define lower limits of the burnout flux in practical situations. The analyses are based primarily on data taken at APED and appearing in Ref. 8. The approach can probably best be explained by the following quotation,[2] which explains that the set of burnout limit curves was constructed by:‡

> 1. Defining limit curves based upon extensive critical heat flux data obtained at General Electric Company in an internally heated annulus. The internally heated annulus geometry was selected because it simulates one of the three possible fuel cell geometries shown in [Fig. III-17]. It is not only representative of corner rod conditions, but it also has the highest ratio of unheated to heated surface area. As such, it gives the lowest critical heat flux value of the three possible fuel cells since the "burnout" point has been found to decrease with increased unheated surface area.[9]
>
> 2. Modifying the above limit curves to account for lower trends or special effects reported in some instances by other experimenters. This ensures that differences in test loops and experimental techniques or conditions are included in the recommended curves.

*The lines through the data, which were placed by eye, differ between Fig. III-14 and Fig. III-15, because of the modifying effect of the Ref. 3 data. However, the line shown in Fig. III-15 lies within ±10% of all points but three.

†The data in Ref. 7 have been greatly expanded by the appearance of Ref. 10. These latter data extend D to about 1.5 in., L to about 76 in., and $G/10^6$ to about 14 lb/(hr)(sq ft).

‡Figure numbers and reference notations have been changed to conform to the numbering used here.

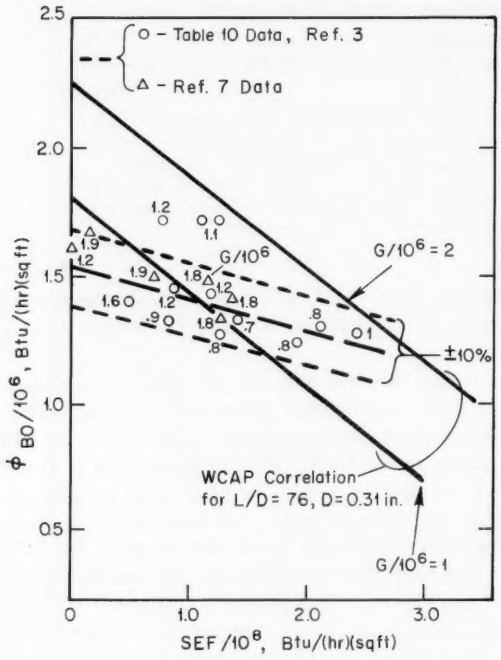

Fig. III-15 Comparison of WCAP correlation with data appearing in Refs. 3 and 7. Pressure = 1000 psia.

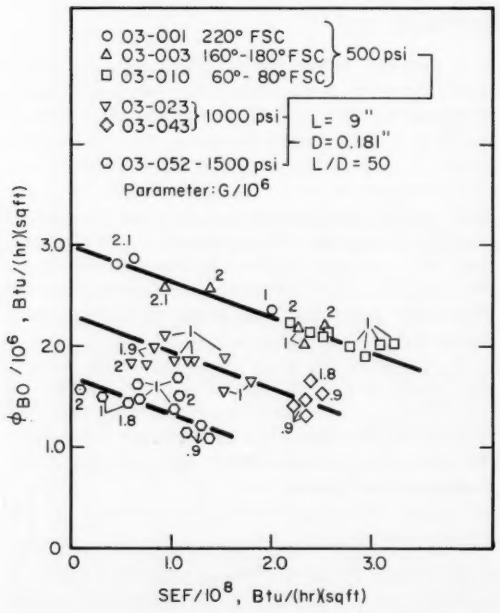

Fig. III-16 SEF plot comparing data at 500, 1000, and 1500 psia (from Table 3 of Ref. 3.)

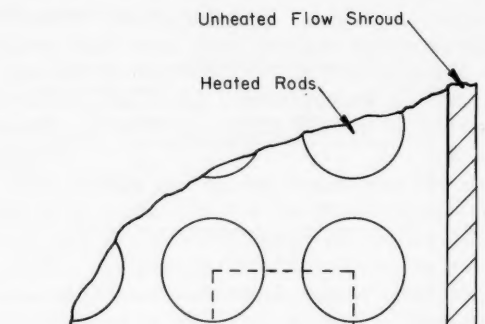

Fig. III-17 Multirod fuel assembly showing various kinds of cells.[2]

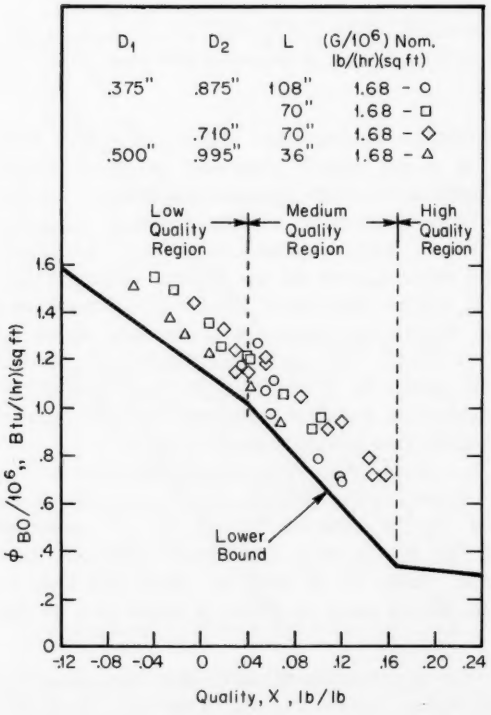

Fig. III-18 APED internally heated annulus data at high flows.[2] Pressure = 1000 psia.

3. Considering data obtained in multirod geometries or annular geometries modified to account for flow redistribution, presence of spacers and rough surface conditions. This step verifies that the limit curves developed for a normal annular geometry can be applied to reactor type multirod systems.

4. Comparing the recommended curves to other available data. This final check gives an overall perspective of how the proposed limit curves fair with respect to other test results.

Figure III-18 is typical of the plots of the APED data appearing in Ref. 2 and covers the high mass-flow range around 1.7×10^6 lb/(hr)(sq ft). Other plots are given which in total cover the mass-flow range from about 0.2 to 6×10^6 lb/(hr)(sq ft). The quality range was arbitrarily divided into three regions, and the burnout limit was described by three connected straight-line segments (see Fig. III-18). The whole range of qualities was not adequately covered by APED data for every value of mass flow. Accordingly, British and Italian data were used to establish the burnout limit curve in the high-quality region, and Ref. 3 data were used to establish the curve in the low-quality and subcooled regions. The complete set of burnout limit curves is shown in Fig. III-19. The reference also presents recipes for conversion of the curves to other pressures and to other hydraulic diameters. The pressure-adjustment recipe is as follows:

$$\phi_{BO_p} = \phi_{BO_{1000}} + 440\ (1000 - p) \qquad (8)$$

where ϕ_{BO_p} is the burnout heat flux at pressure p, Btu/(hr)(sq ft), $\phi_{BO_{1000}}$ is the burnout heat flux at $p = 1000$ psia, Btu/(hr)(sq ft), and p is the pressure, psia.

In conclusion, an attempt will be made to compare the WCAP and APED burnout correlations and recommendations. This is done in Fig. III-20; the APED limit lines shown thereon are merely a replot of the appropriate curves in Fig. III-19 for the middle quality range. The WCAP correlation is for a pressure of 1000 psia, an L/D of 100 and a D of 0.400 in. This comparison is believed to be a valid one, since the authors of both correlations state that their respective correlations are valid for rod bundles.

It is evident that the two correlations shown in Fig. III-20 are not in agreement. One reason for this is that, although the APED curves were

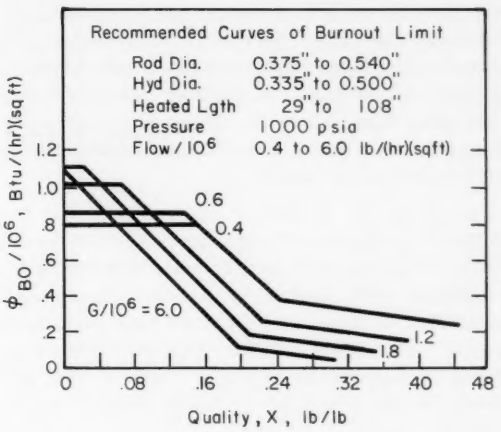

Fig. III-19 Modified burnout limit curve.[2]

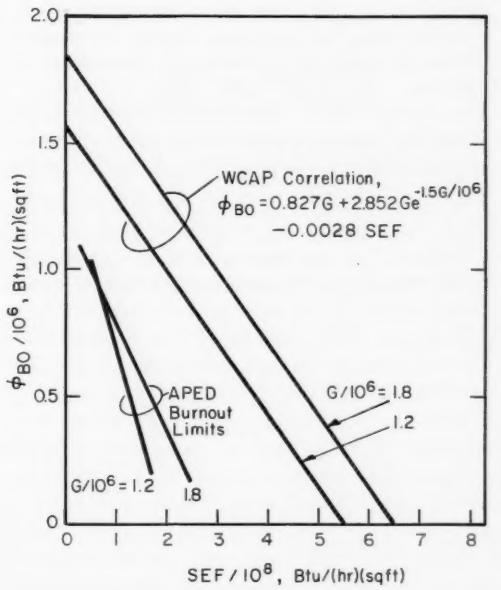

Fig. III-20 Comparison of WCAP correlation with APED burnout limit curves.

chosen on the low side of the data, the WCAP curves were chosen as best-fit curves. This does not explain the entire difference, however, since the WCAP correlation was stated to be within ±25% of the data. It is believed that the major difference between the WCAP and APED correlations can be explained by geometry. The former correlation was based primarily

on circular-tube and rectangular-channel data, whereas the latter correlation considered primarily data taken with internally heated annular-geometry test sections. Collier[11] states: "Burnout heat flux values for tubes and externally heated annuli are always higher than those for internally heated annuli . . . ."

If geometry is the primary reason for the differences shown between the two correlations, then it seems incorrect to state that both correlations will adequately predict the burnout heat flux of a bundle of heated rods such as is found in a power reactor. Further considerations of burnout in multirod clusters will appear in future issues of *Power Reactor Technology*.

References

1. L. S. Tong, H. B. Currin, and A. G. Thorp II, New Correlations Predict DNB Conditions, *Nucleonics*, 21(5): 43-47 (May 1963).
2. E. Janssen and S. Levy, Burnout Limit Curves for Boiling Water Reactors, Report APED-3892, General Electric Company, Atomic Power Equipment Department, Apr. 1, 1962.
3. R. A. DeBortoli, S. J. Green, B. W. LeTourneau, M. Troy, and A. Weiss, Forced-Convection Heat Transfer Burnout Studies for Water in Rectangular Channels and Round Tubes at Pressures Above 500 psia, USAEC Report WAPD-188, Westinghouse Electric Corp., Bettis Plant, October 1958.
4. W. J. Levedahl, Application of Steam Energy Flow to Reactor Design, *Trans. Am. Nucl. Soc.*, 5(1): 149 (June 1962).
5. L. S. Tong, H. B. Currin, and A. G. Thorp II, New DNB (Burnout) Correlations, USAEC Report WCAP-1997(Rev. 2), Westinghouse Electric Corp., Atomic Power Division, May 1963).
6. J. S. Wiley, Additional Comments on Statistical Burnout Correlations, *Nucleonics*, 22(2): (February 1964).
7. R. R. Hood and L. Isakoff (Comps.), Heavy Water Moderated Power Reactors. Progress Report, June 1962, USAEC Report DP-755, E. I. du Pont de Nemours & Co., Inc., July 1962.
8. E. Janssen and J. A. Kervinen, Burnout Conditions for Single Rod in Annular Geometry, Water at 600 to 1400 psia, USAEC Report GEAP-3899, General Electric Company, Atomic Power Equipment Department, February 1963.
9. M. Silvestri, Two-Phase (Steam and Water) Flow and Heat Transfer, Paper 39 in *International Developments in Heat Transfer*, Part II, pp. 341-353, American Society of Mechanical Engineers, 1962.
10. R. R. Hood and L. Isakoff, Heavy Water Moderated Power Reactors Progress Report, May-June 1963, USAEC Report DP-855, E. I. du Pont de Nemours & Co., Inc.
11. J. G. Collier, Heat Transfer and Fluid Dynamic Research As Applied to Fog Cooled Power Reactors, Canadian Report CRARE-1108 (AECL-1631), June 1962.

Section

IV

Power Reactor Technology

Fuel Elements

Programs at GE-APED Sponsored by USAEC and Euratom

Three government-sponsored research and development programs that include substantial efforts on oxide fuel elements are under way at the General Electric Atomic Power Equipment Department (APED). Two of these, the Fuel-Cycle Program and the High Power Density Development Project, are sponsored by the U. S. Atomic Energy Commission (AEC); the third, the High-Performance UO_2 Program, is sponsored jointly by AEC and Euratom. A large amount of literature has been produced under these programs in the form of quarterly and topical reports. It is the purpose of this review to summarize the work to date in the area of fuel-element development and to describe the objectives, the experimental approaches, and the existing complement of experimental samples in sufficient detail to form the background for more concise reviews of progress that may appear from time to time in future issues.

Fuel-Cycle Program [1–20]

This program was initiated early in 1959. The purpose of the program is to improve the technological limits of boiling-water reactors in several areas listed below[2] (of these, only Task A-1 is reviewed here):

Task A

1. Extend fuel life information on oxide fuel at high specific power operation and raise the performance limits of oxide fuels.
2. Study power stability and performance characteristics of an oxide fueled core under natural and forced circulation to improve design limits.

Task B

1. Out-of-pile experiments in heat transfer and fluid dynamics in the areas of burnout heat transfer, hydraulic instability, steam void observational studies, and two-phase pressure drop to support in-core work.

Task C

1. Study long-term reactivity characteristics of fuels having lattice characteristics of large power reactors.
2. Measure initial conversion ratio of a number of lattice configurations characteristic of large oxide fueled power reactors.

Task A-1 involves the fabrication of fuel assemblies and evaluation of results of irradiation in the Vallecitos Boiling-Water Reactor (VBWR). A total of 60 assemblies have been irradiated, although all 60 assemblies are not necessarily in the VBWR at the same time. These 60 assemblies are divided into 50 so-called "basic" assemblies and 10 "special" fuel assemblies. The design and fabrication of the basic fuel assemblies are detailed in Ref. 12; two different types were fabricated, one being a control-follower assembly and the other a stationary assembly. The follower assemblies, designated as type H, employ annealed type 304 stainless-steel cladding, whereas the stationary assemblies were fabricated from Zircaloy-2, Zircaloy-4, and cold-worked type 304 stainless-steel cladding. All cladding was designed to be freestanding. Additional details on the assemblies are given in Table IV-1. Figures IV-1 to IV-3 illustrate constructional details of the assemblies and their appearance in the VBWR.

The elements were fabricated in 1960 and 1961, and 25 stainless-steel-clad assemblies were loaded into the VBWR in September 1960. An instrumented stainless-steel assembly was loaded into the VBWR in October 1961, instrumented to provide data on in-core neutron flux,

Table IV-1 CHARACTERISTICS OF THE BASIC FUEL ASSEMBLIES IN THE FUEL-CYCLE PROGRAM[12]

	H	I	J
Type of assemblies			
Number of assemblies	10	16	24
Rods per assembly*	16	16	16
Removable rods per assembly	0	12	12
Rod center-to-center distance, in.	0.76	0.76	0.76
Cladding material	304 S.S.	304 S.S.	Zircaloy-2†
Nominal cladding thickness, in.	0.020	0.015	0.022
Nominal tube outside diameter, in.	0.420	0.410	0.424
Nominal tube inside diameter, in.	0.380	0.380	0.380
Maximum pellet diameter, in.	0.376	0.376	0.376
Average pellet density, % of theoretical density	95	95	95
UO_2 enrichment, %	2.7	3.2	‡
Water-to-fuel ratio	2.98	4.0	3.9
Active fuel length, in.	30	37	37
Total rod length, in.	$32\frac{5}{8}$	$39\frac{1}{4}$	$40\frac{1}{8}$
Plenum length, in.	$1\frac{7}{8}$	$1\frac{7}{8}$	$1\frac{7}{8}$
Wall thickness of plenum support tube, in.	0.020	0.020	0.020
Coolant-flow area, sq in.	5.25	7.13	6.98
Heat-transfer area, sq ft	4.37	5.28	5.47

*One I and two J assemblies are instrumented and contain only 14 fuel rods.
†One assembly contains three fuel rods clad with Zircaloy-4.
‡Enrichments of the J assemblies are as follows:

No. of assemblies	% enrichment
10	2.76
1	2.76 and 2.98 (8 rods each)
3	2.98
1	2.98 and 3.49 (8 rods each)
3	3.2
5	3.49
1	4.3
1	2.76 + PuO_2 segments

coolant temperature, pressure drop, and flow rates. The Zircaloy-clad assemblies, including two instrumented ones, were placed in the VBWR between June 1961 and January 1962. As of March 1963, the basic fuel assemblies had reached the burnups shown in Table IV-2; this table also illustrates the peak specific power and peak heat flux for the particular assembly operated at the highest power within its group. Table IV-3 compares the thermal performance of these basic fuel assemblies with the Dresden and Big Rock Point reactors.

In May of 1962, during a VBWR outage, four fuel-rod changes were made involving one type I assembly and three type J assemblies.[8] Hot-cell examination revealed that fretting corrosion had occurred on the Zircaloy cladding. Studies of four additional assemblies showed that fretting corrosion had occurred on some rods in each of the Zircaloy-clad assemblies (12J, 25J, and 7L, a special assembly), but not on the stainless-steel-clad assembly (8I). The observations are summarized in Ref. 8:

> The following observations were made ...: (1) lack of rod support at the upper tie plate caused general fretting corrosion at the middle spacer in the 7L assembly; (2) rods with large clearances at the upper tie plate showed the most penetration; (3) rods with tight support at the upper tie plate suffered comparatively light fretting corrosion even with large clearances at the middle spacer; (4) the corner rods which are rigidly supported at both top and bottom underwent no fretting corrosion.
>
> It appears that wire deformation as a result of fuel handling increases the clearance between the fuel rods and supporting spacer and upper tie plate wires .... The clearance subsequently allows the rods to vibrate freely as reeds and fret against the stainless steel wires. It is expected that the fretting corrosion can be reduced or eliminated by spring clips at the upper tie plate which will provide improved rod support. The spring clips can be in-

stalled on the assemblies in the VBWR storage pool without disassembly of the fuel bundle. Fabrication of trial clips is in progress.

The method of retaining the rods in the assembly is shown in Fig. IV-1. A new, undamaged fuel rod was placed into assembly 12J, and spring clips were fabricated to bear against the rod and damp vibration. This assembly was inserted in the VBWR and operated for about a month until the reactor was shut down because of a leak in the recirculation piping. Subsequent examination revealed no fretting damage to the clipped fuel rod, and spring clips were installed on all but two of the Zircaloy-clad type J assemblies.

No significant cladding deterioration other than fretting was exhibited by the Zircaloy-2- and Zircaloy-4-clad fuel rods. The stainless-steel-clad fuel rods also were sound. An intentionally defected Zircaloy-2-clad rod, an intentionally defected Zircaloy-4-clad rod, and a sound Zircaloy-2-clad rod were sectioned and examined remotely. The defect was a 20-mil hole in the cladding near the peak heat flux region. The results are summarized as follows in Ref. 9:

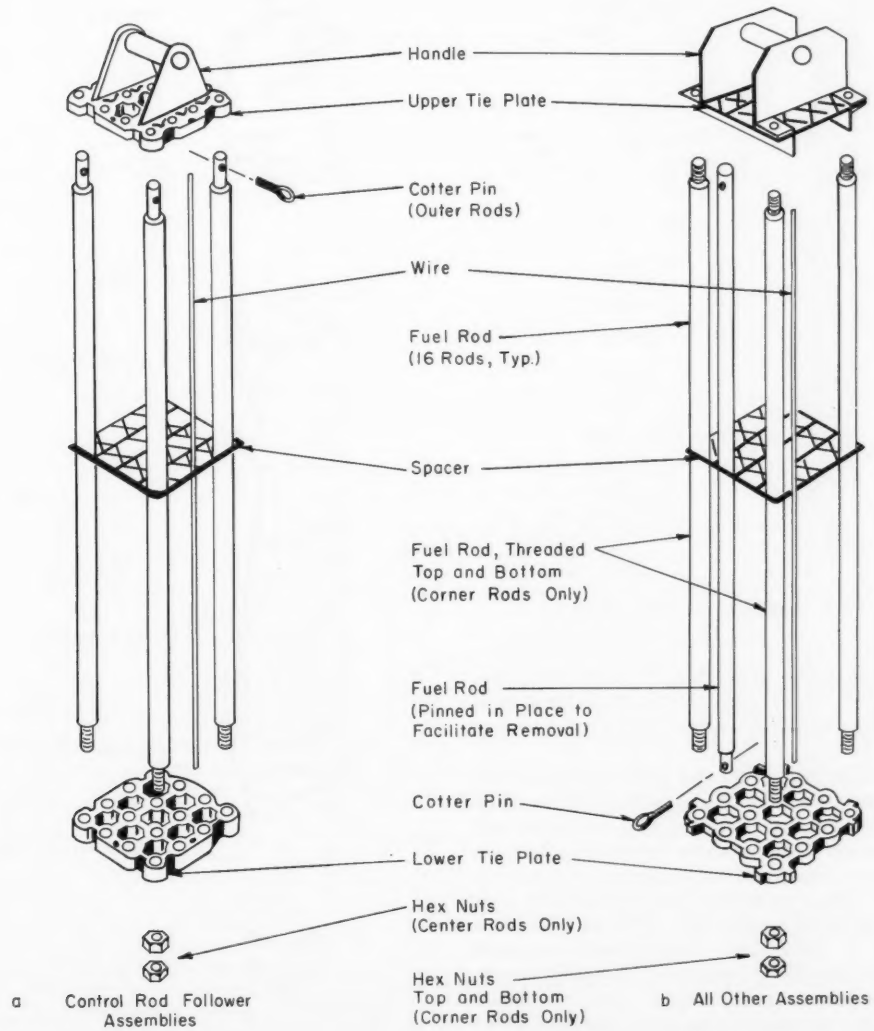

Fig. IV-1 Exploded view of fuel assemblies.[12]

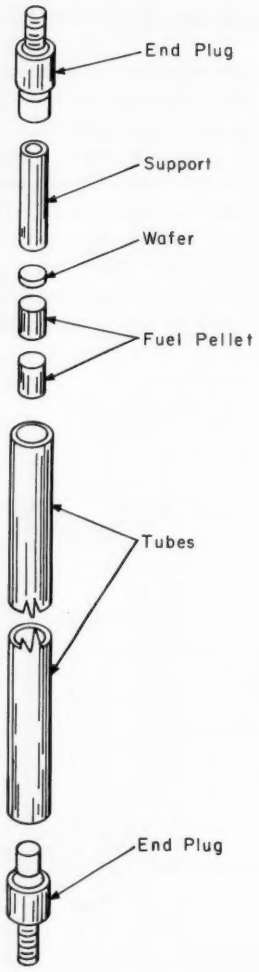

Fig. IV-2 Exploded view of fuel rod.[12]

a. In non-defect areas, the Zircaloy-4 corroded at a slightly faster rate than the Zircaloy-2 when tested under identical conditions in a boiling water reactor.

b. There is little difference in the corrosion rate on the inside surface of the clad in the Zr-2 and Zr-4 defected rods. However, the corrosion rate of both materials on the inside surface of a defected rod is more than twice that on the outside surface.

c. The higher corrosion rate on the inside surface of the defect rods seems consistent with rates expected at inside clad temperatures estimated from heat transfer calculations. Continued operation of intentionally defected Zr rods to evaluate performance at longer exposures may provide information on the effect of other potential factors, such as a reduction in the corrosion resistance of the clad resulting from the impregnation of the clad with fission fragments.

Also included in the VBWR irradiations under the Fuel-Cycle Program are 10 special fuel assemblies, whose status as of March 1963 is summarized in Table IV-4. Assembly 1L was designed to study the lifetime performance of a UO_2 fuel element operated near the melting point of UO_2 at the center line. The maximum heat flux of 1L was 530,000 Btu/(hr)(sq ft) during irradiation, and the assembly contained one purposely defected rod; the cladding of all rods in

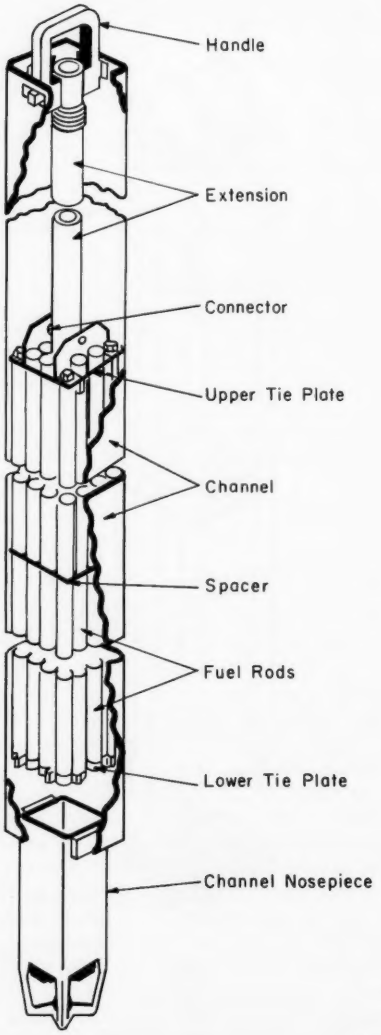

Fig. IV-3 Cutaway view of fuel assembly in VBWR channel.[12]

Table IV-2 STATUS OF THE BASIC FUEL ASSEMBLIES IN THE FUEL-CYCLE PROGRAM[11]

Assembly designation and cladding	Number	Burnup, Mwd/ton*		Peak specific power,‡ kw/kg	Peak heat flux,‡ Btu/(hr)(sq ft)
		Average of group	Average for lead assembly†		
H, annealed S.S. (control-rod follower)	10	5,191	6,231	34.4	367,000
I, cold-worked S.S.	16	4,564	5,803	36.6	405,000
J, Zircaloy	24	3,849	6,176	37.5	382,000

*Burnup that existed at the end of run 155 which was completed on Mar. 24, 1963.
†Peak exposure is about 1.65 times this value.
‡These values were attained in the quarter starting January 1963.

Table IV-3 COMPARISON OF THE BASIC FUEL ASSEMBLIES WITH FUEL CONDITIONS IN OTHER REACTORS[10]

	Average overall fuel			Peak location		
	Specific power, kw/kg	Power density, kw/liter	Heat flux, Btu/(hr)(sq ft) $\times 10^{-3}$	Specific power, kw/kg	Power density, kw/liter	Heat flux, Btu/(hr)(sq ft) $\times 10^{-3}$
Fuel-cycle program (run 153)						
H, S.S.-clad control-rod followers	38.5	53.4	238	78.5	163	377
I, S.S. cladding	30.0	51.4	184	65.0	112	420
J, Zircaloy cladding	31.2	53.1	204	73.7	126	448
Dresden, first core	12.4	31.2	99	35.6	90	285
Big Rock Point, 50 Mw(e), first core	16.5	45.0	110	52.6	144	352

Table IV-4 STATUS OF SPECIAL FUEL ASSEMBLIES[11]

Assembly	Concept	Specific power,* kw/kg	Heat flux,* Btu/(hr)(sq ft) $\times 10^{-3}$		Accumulated† exposure, Mwd/ton
			Average	Peak	
1L	Centermelt	‡	‡	‡	4075
4L	Low-temperature sintered pellets	‡	‡	‡	234
5L	Coextruded UO_2 and S.S. cladding	33.9	223	364	4592
6L	Zircaloy-4 cladding	16.8	145	287	1075
7L	S.S.-lined Zircaloy-2	35.6	224	383	4303
8L	0.005-in. S.S.-clad pellets	‡	‡	‡	2553
9L	Thermal-conductivity improver	30.9	233	385	907
10L	0.005-in. S.S. cladding over powder	19.2	116	211	396
11L	Extruded UO_2	‡	‡	‡	180
12L	Burnable poison	15.4	110	191	307
2L	Undefined§				
3L	Undefined§				

*Peak condition during VBWR run 155.
†Exposures are through VBWR run 155, which was completed on Mar. 24, 1963.
‡Not irradiated during VBWR run 155.
§Held in reserve for future use.

the assembly was stainless steel with an outside diameter of 0.515 in. Destructive examination of one of the rods revealed that center melting of the UO_2 did not occur, and large columnar grains were observed in the region from the center of the pellet to a distance of about one-half the radius. A narrow band of fine grains occurred at midradius and separated the as-sintered structure from the grain-growth region. This was interpreted to mean that recrystallization of the UO_2 occurs prior to grain growth.

Assembly 4L has had a varied history. It originally contained three rods made by hot-gas isostatic pressing of UO_2 in stainless-steel cladding, a specially designed rod known as the "centermelt" calibration test rod and other rods of conventional fabrication.

The gas-pressure-bonding technique was developed in a $2\frac{1}{2}$-year study done at Battelle Memorial Institute and is described in Refs. 13 to 15. Briefly, the process consisted of fabricating UO_2 pellets by cold-pressing the oxide powder and a binder at 50 tsi. The pellets were loaded into type 304L stainless-steel tubing, and end caps were added; the assembly was then heated and cooled, evacuated to 5 μ, and sealed. The rod was then subjected to 10,000 psi for 3 hr at 2100°F, swaged from 0.404 to 0.400 in. in outside diameter, and pressure bonded for 2 hr at 10,000 psi and 2100°F. This produced an average UO_2 density of 96.3% of theoretical. The rods produced in this manner were irradiated to an exposure of 693 Mwd/ton with a peak heat flux at 370,000 Btu/(hr)(sq ft). After irradiation the 4L assembly was damaged, and it was stored in the VBWR pool for about five months. In the process of handling the isostatically pressed rods, all three of them broke into a total of about 15 pieces. The evaluation of the failed isostatically pressed fuel rods is reported on in Ref. 16, and the conclusion is that inadequate removal of the binder from the UO_2 resulted in a very high carbon content of the cladding. In the resulting sigma phase, carbides and ferrite formation at the grain boundaries led to intergranular corrosion and cracking.

The centermelt calibration rod irradiated in assembly 4L was an oxide rod which was $1\frac{3}{8}$ in. in outside diameter and which contained 1.235-in.-diameter pellets; the peak heat flux was 535,000 Btu/(hr)(sq ft). The rod was examined remotely after irradiation. The oxide fuel had been molten, and it was established that fuel ran from the upper part of the rod to the lower part. Plastic deformation of the cladding was evident, and it is suggested[7] that this was caused by the relatively greater expansion of the hot UO_2 compared to the cladding. It was also concluded that "... A sintered uranium dioxide body may initially operate with a molten central portion which subsequently totally or partially solidifies during operation because of the increased thermal conductivity due to the growth of columnar grains."[7] This mechanism was discussed in *Power Reactor Technology*, 6(2): 36-37.

After the failure of the isostatically pressed fuel rods, the 4L assembly was rebuilt with three rods containing low-temperature sintered pellets produced by United Nuclear Corporation, three rods (including one intentionally defected) of UO_2 coextruded with the stainless-steel cladding, one intentionally defected rod containing UO_2 pellets clad with stainless-steel-lined Zircaloy-2, and nine standard rods. As indicated in Table IV-4, the assembly had received relatively modest burnups up to March 1963. The low-temperature sintered pellets involve sintering at 1100 to 1300°C, rather than the more customary 1600 to 1700°C. The design and fabrication of the fuel rods containing low-temperature sintered pellets are covered in Ref. 17.

Assembly 5L contains 12 rods fabricated by high-temperature coextrusion. The irradiation cycle for this assembly started in August 1961, whereas irradiation of the three coextruded rods in assembly 4L started in July 1962. The design and fabrication of the coextruded rods are covered in Refs. 18 and 19. The process consists in coextruding UO_2 and type 304 stainless-steel cladding. As of March 1963 assembly 5L had reached a modest burnup and apparently was operating satisfactorily.

Assembly 6L consists of rods containing UO_2 pellets clad with Zircaloy-4. An intentionally defected rod was included in assembly 6L but has been replaced with a sound rod. Assembly 7L contains fuel rods clad with Zircaloy-2 coextruded with approximately a 1-mil stainless-steel lining. This lining is present to prevent corrosion of the Zircaloy-2 by steam that would be formed if any water should leak into the element. Both assemblies are reported to be in satisfactory condition, although fretting corrosion was noticed on assembly 7L, and the rods had to be transferred to another fuel-rod bundle

frame owing to damage to the upper tie plate. Spring clips were then added to reduce the possibility of fretting.

Assemblies 8L and 10L test the concept of thin, collapsed cladding. The former assembly contains 0.370-in.-OD UO_2 pellets, whereas the latter assembly contains UO_2 powder compacted by vibratory techniques. Assembly 8L was inserted in the VBWR in November 1961; since the thin cladding prohibits high internal gas pressures, a plenum length of 7.0 in. is provided. To prevent collapse of the gas plenum, it was necessary to provide support to the cladding in the plenum area, and this was done by using an external plenum support with a wall thickness of 0.017 in. on six of the rods and by using an internal plenum support with a wall thickness of 0.016 in. on the remaining six rods. The four corner rods of assembly 8L are constructed of noncollapsed 20-mil cladding and are arranged as shown in part *b* of Fig. IV-1. One collapsed-cladding rod was intentionally defected with a 10-mil hole in the plenum area. The type 304 stainless-steel cladding was cold worked, with a room-temperature yield strength of about 110,000 psi (nonirradiated). The defected rod was installed in the assembly in February 1962, and the activity release from the defected rod was stated to be[7] less than 5 μc/sec. In August 1962 the assembly was transferred to a hot cell for visual examination. Reference 9 states:

> (1) At least two fuel rods were cracked, one in the area of maximum heat flux, the other in a wrinkled plenum area.
>
> (2) Three rods were wrinkled in the plenum area. The wrinkling occurred in rods containing internal plenum supports.

Four of the damaged or failed fuel rods were destructively examined, and the details are given in Ref. 11. The following comments pertain to the fuel rod exhibiting a crack in the peak heat flux region:[11]

> The cause of cracking of this rod is apparently strain cycling fatigue. The differential thermal expansion of the UO_2 and clad during operation of the fuel rod at the peak heat flux condition, about 500,000 Btu/hr-ft^2, would have caused a calculated plastic diametral deformation in the clad of 0.002 inch. When power is reduced after plastic strain of the clad, the contraction of the UO_2 leaves an equivalent gap between the clad and UO_2. If the gap is as large as these calculations indicate, there is high probability that collapse under the 1000-psig coolant pressure would have caused a wrinkle. Repeating cycling of this wrinkle after formation probably led to fatigue cracking. Metallurgical examination of the clad crack supports this conclusion .... The clad in the failure region appears to be slightly harder than the clad in the non-failure region. This increase in hardness may be caused by work hardening during the cycling.

The four rods destructively examined were replaced with four rods that had 5-mil annealed collapsed cladding.

Assembly 10L was placed in-pile in February 1963. The assembly contains rods utilizing both cold-worked and annealed tubing and arc-fused and Dynapak UO_2 powders. The latter process, developed at Hanford Atomic Products Operation (HAPO), involves the densification of the powder by drop forging. Six fuel rods are filled with the Dynapak powder with as-packed densities of about 84%. Ten rods are filled with arc-fused powder with as-packed densities of 84.3 to 84.9%. Additional data on assembly 10L are given in Table IV-5.

Table IV-5 ASSEMBLY 10L DESIGN[7] WITH THIN STAINLESS-STEEL CLADDING OVER UO_2 POWDER

UO_2 enrichment	6% U^{235}
Cladding material	Type 304 S.S.
Cladding thickness, in.	0.005
Number of rods	16
Rod outside diameter, in.	0.385
Rod spacing, in.	0.76, center to center

Irradiation of assembly 9L began in August 1962. The purpose of the irradiation is to evaluate an attempt to improve the thermal conductivity of UO_2 by the dispersion of molybdenum through the oxide. Two methods of dispersion were used to prepare a total of six rods for incorporation in the 9L assembly. One approach was to mix molybdenum fibers with the oxide powder before the pressing of the pellets; in the second approach the individual oxide particles were coated with molybdenum metal prior to pressing. Three rods were fabricated using the fiber process, and three others were fabricated using the coating process. The remaining rods in the assembly are of conventional construction. Whether the molybdenum will improve the thermal conductivity of the fuel is yet to be determined. Table IV-6 gives design data on assembly 9L.

Assembly 11L consists of fuel rods filled with UO_2 extrusions. The extrusions were supplied

Table IV-6 ASSEMBLY 9L DESIGN[7] THAT MAY IMPROVE THERMAL CONDUCTIVITY

Cladding material	Type 304 S.S.
Cladding thickness, in.	0.020
Fuel-rod outside diameter, in.	0.515
Fuel-pellet outside diameter, in.	0.471
Number of rods	8
Two rods contain 6.4% enriched UO_2 pellets (controls)	
Three rods contain 24 in. of 8.0% enriched UO_2 pellets containing 20 vol.% molybdenum fibers and 12 in. of 6.4% enriched UO_2 pellets	
Three rods contain 24 in. of 8.0% enriched molybdenum-coated UO_2 pellets and 12 in. of 6.4% enriched UO_2 pellets	
Rod spacing, in.	1.03, center to center
UO_2 density	95% of theoretical density for UO_2 pellets
	95% of theoretical density for UO_2-Mo pellets

by Allis-Chalmers Mfg. Co. and Compagnie Industrielle des Combustibles Atomiques Frittés (CICAF) of France. The extrusions were to be about 6 in. long, although the extrusions prepared by CICAF ranged in length from 0.3 to 6.06 in. One each of the rods containing the two extrusion types was purposely defected by means of a 13-mil hole through the cladding in the plenum region. The assembly has been irradiated for only a short burnup, and little information is available as to the usefulness of the fabrication technique in producing acceptable fuel material. Data on the 11L design are given in Table IV-7.

Assembly 12L, the last special assembly, was inserted in the VBWR in February 1963. The basic purpose of the element is to study the behavior of boron burnable poison when the boron is alloyed into the stainless-steel cladding and when the boron is intimately mixed with the fuel. Table IV-8 illustrates the fabrication details of each rod in assembly 12L. It is evident from Table IV-8 that the assembly also is intended to give information on the relative merits of annealed and cold-worked cladding material. The assembly had received only modest burnup by March 1963.

Table IV-7 ASSEMBLY 11L DESIGN WITH EXTRUDED UO_2

UO_2 enrichment, %	5.5
Cladding material	Type 304 S.S.
Cladding thickness, in.	0.022
Rod outside diameter, in.	0.539
Number of rods	16
Six rods are filled with extrusions from CICAF	
Six rods are filled with extrusions from Allis-Chalmers	
Four rods are filled with pellets	
Fuel outside diameter, in.	0.485 ± 0.002
Fuel density, %	97% of theoretical density

High-Power-Density (HPD) Development Project[20–34,45]

The HPD research and development program was begun in February of 1960 and is a program in support of the Consumers Power Company boiling-water reactor plant at Big Rock Point, Mich. References 20 to 26 are selected quarterly progress reports dealing with the project. The HPD program is divided into four tasks as follows:[21]

1. Task IA — High Power Density Fuel Development. This task will evaluate the feasibility and the performance of a partial reactor core operating in the VBWR at high power density and utilizing fuel elements manufactured from available fabricating processes.

2. Task IB — Fuel Fabrication Development. Design, fabrication, irradiation and examination of high power density fuel elements with potentially low fabrication costs is the objective of this task.

3. Task II — Stability and Heat Transfer Development. This task will evaluate analytically and by

Table IV-8 DESCRIPTION† OF BURNABLE-POISON ASSEMBLY 12L

Rod No.	Fuel data	U^{235} enrichment	Cladding data
	Controls (No Poison)		
A-1	Vibratory-compacted arc-fused powder, 85% of theoretical density	5.5%	Type 304 S.S. annealed, ~40,000-psi 2% yield strength, 0.485-in. outside diameter by 0.011-in. wall
B-1	Pellets, 95% of theoretical density	5.5%	
	Borated Cladding but No Poison in Fuel		
C-1	All rods vibratory-compacted arc-fused powder, 85% of theoretical density	6.6%	C-1 Annealed, ~45,000-psi 0.2% yield strength
C-2			C-2 Cold worked, ~70,000-psi 0.2% yield strength
C-1, C-2			500 ppm B^N + type 304 S.S., 0.485-in. outside diameter by 0.011-in. wall
C-3			C-3 Annealed, ~45,000-psi 0.2% yield strength
C-4			C-4 Cold worked, ~70,000-psi 0.2% yield strength
C-3, C-4			750 ppm B^N + type 304 S.S., 0.485-in. outside diameter by 0.011-in. wall
D-1	All rods pellets, 95% of theoretical density	6.6%	D-1 Annealed, ~45,000-psi 0.2% yield strength
D-2			D-2 Cold worked, ~70,000-psi 0.2% yield strength
D-1, D-2			500 ppm B^N + type 304 S.S., 0.485-in. outside diameter by 0.011-in. wall
D-3			D-3 Annealed, ~45,000-psi 0.2% yield strength
D-4			D-4 Cold worked, ~70,000-psi 0.2% yield strength
D-3, D-4			750 ppm B^N + type 304 S.S., 0.485-in. outside diameter by 0.011-in. wall
	Poison in Fuel but No Poison in Cladding		
E-1	Vibratory-compacted arc-fused powder, 85% of theoretical density, poisoned with 50 ppm B^N as BeO-coated ZrB_2 particles	6.6%/5.5%	E-1 Type 304 S.S. annealed, ~40,000-psi yield strength, 0.485 in. by 0.011-in. wall
E-2	Vibratory-compacted and swaged arc-fused powder, 92% of theoretical density, poisoned with 50 ppm B^N as BeO-coated ZrB_2 particles	6.6%/5.5%	E-2 Type 304 S.S. swaged, ~135,000-psi yield strength, 0.485 in. by 0.017-in. wall
	Poison in Fuel but No Poison in Cladding		
F-1	Vibratory compacted arc-fused powder, 85% of theoretical density, poisoned with 50 ppm B^N as molybdenum-coated ZrB_2 particles		F-1 Type 304 S.S. annealed, 40,000-psi yield strength, 0.485 in. by 0.011-in. wall
F-2	Vibratory compacted and swaged arc-fused powder, 92% of theoretical density, poisoned with 50 ppm B^N as molybdenum-coated ZrB_2 particles		F-2 Type 304 S.S. swaged, 135,000-psi yield strength, 0.485 in. by 0.017-in. wall
G-1	Vibratory compacted arc-fused powder, 85% of theoretical density, poisoned with 50 ppm B^N as ZrB_2 particles		G-1 Type 304 S.S. annealed, 40,000-psi yield strength, 0.485 in. by 0.017-in. wall
G-2	Vibratory compacted and swaged arc-fused powder, 92% of theoretical density, poisoned with 50 ppm B^N as ZrB_2		G-2 Type 304 S.S. swaged, 135,000-psi yield strength, 0.485 in. by 0.017-in. wall

test the transient behavior and stability characteristics of the HPD reactor, and will determine by test the heat transfer and fluid flow characteristics of the core, using elements simulating core characteristics.

4. Task III—Physics Development. This task involves the physics evaluation of control requirements and hot spot reduction; the physics and engineering conceptual design of a 300 Mwe high power density reactor; and the physics and engineering required to design, procure and put into operation a computer for scheduling control.

5. Task IV—Operational Planning and Test Coordination. The coordination of the R & D program between tasks, with Design Engineering, and with the AEC and Consumers is a major function of this

Table IV-9 DESCRIPTION OF FUEL ASSEMBLIES IN THE HPD PROJECT[27]

Assemblies	Nominal pellet diameter, in.		Cladding thickness, in.				Cladding condition*		Diametral gap, in. nominal				Enrichment, %			No. of fuel rods†			Swaged	Prototypes	Instrumented	Single-layer spacer	Prototype spacer	Requested heat flux, Btu/(hr)(sq ft)
	0.375	0.330	0.020	0.017	0.012	0.014	CW	Ann.	0.005	0.003	0.002	0.000	4.5	3.5	2.7	25	24	16						
1A	X		X					X	X						X			X				X		420,000
2A	X		X					X	X						X			X				X		420,000
1B	X		X					X	X						X			X				X		414,000
2B	X		X					X	X						X			X				X		414,000
1C	X			X				X	X					X			X					X		401,000
2C	X			X			X		X					X			X					X		379,000
3C	‡			X			X			X				X			X		X			X		401,000
4C	X			X			X				X			X			X		X			X		401,000
1D	X				X			X				X		X			X		X			X		409,000
2D	X				X		X					X		X			X		X			X		409,000
3D	X				X			X			X			X			X		X			X		379,000
4D	X				X		X				X			X			X		X			X		401,000
1E to 5E		X				X	X		X				X			X				X			X	422,000
6E		X				X	X		X				X				X				X	X		465,000
1F		X				X	X		X				X			X				X		X	X	465,000
2F		X				X	X		X				X				X				X	X		422,000
1G		X				X	X					X	X			X			X			X		422,000
2G		X				X		X				X	X			X			X			X		385,000
3G		X				X	X				X		X			X			X			X		385,000
4G		X				X		X			X		X			X			X			X		385,000

*CW = cold worked; Ann. = annealed.

†Fuel length, 37 in.

‡Unground pellets (simulated by grinding in 0.001-in. increments from 0.368 to 0.378 in.).

task, as is the design of tests and the procurement of instrumentation.

This review considers only Tasks IA and IB.

Under the HPD program (Task IA) 24 fuel assemblies have been fabricated and irradiated in the VBWR. These consisted of four 16-rod fuel-follower assemblies and twenty 25-rod test assemblies. The fabrication of these assemblies is detailed in Ref. 27, and the constructional details of the assemblies are given in Table IV-9. Groups A and B assemblies are control-rod follower assemblies. The Group C assemblies duplicate the Consumers Power Company reactor first core fuel assemblies with respect to cladding stress and diametral gap, but a single-layer spacer is used. The spacer designs and the fuel bundle itself are shown in Fig. IV-4. Bundle 3C contains fuel pellets that have been ground to several different diameters to simulate the variability of unground pellets. Group D includes variations in diametral gap, pellet tolerance, cladding thickness (the 12-mil cladding will be collapsed owing to reactor pressure), and the metallurgical condition of the cladding (cold worked or annealed). Group E assemblies are designed to duplicate the first core fuel in the Big Rock Point Reactor as closely as possible; one fuel element is instrumented for inlet and exit coolant flow rates, pressures, and temperatures and contains a flux monitor tube in place of the center fuel rod. Group F assemblies were built of fuel rods having lengths of about 5 ft rather than the normal length of slightly over 3 ft. Group G assemblies incorporated variations in diametral gap and cladding conditions. The fuel rods were swaged to produce a controlled pellet-cladding gap; the process reduced the pellet-cladding gap an average of about 5 mils.

Twenty-two of the 24 fuel assemblies were placed in the VBWR in September of 1960; the remaining two assemblies, the instrumented ones, were placed in the core during June 1961. A difficulty was experienced with the spacers

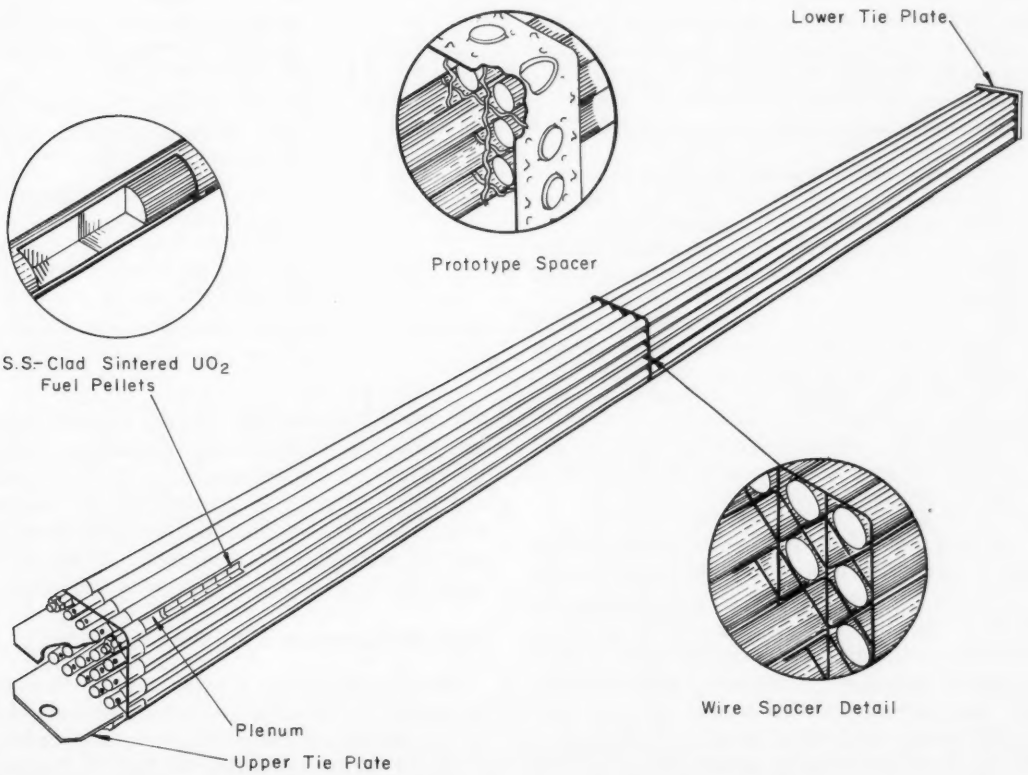

Fig. IV-4 Typical high-power-density VBWR fuel bundle.[27]

on E and F assemblies. The F bundles, with their 5-ft rods, have two spacers between the upper and lower tie plates, whereas the E assemblies, with 3-ft rods, have one spacer. These assemblies employed prototype spacers that were held in position by wires running between the spacers to the upper and lower tie plates. Quoting from Ref. 22: "It appears that the problem of breaking axial tie wires and skidding the spacers on bundles 1E-5E and 1F is one that will plague us through the remaining period of irradiation. Though it is a problem and certainly points to the elimination of this method for axial spacer location, it is not expected that this will affect the performance of the fuel or the information available from it, after irradiation." From the references it is not clear what the difference was between the method of locating the single-layer spacers and the prototype spacers or why the latter method would be giving trouble and the former method would not.

As of June 1963 some of the assemblies had reached peak burnups above 10,000 Mwd/ton. A total of 15 assemblies had been removed from the VBWR because of failed fuel rods. The irradiation exposure data on the sound assemblies are given in Table IV-10, and data on the fuel-rod failures are given in Table IV-11. Preliminary observations are quoted as follows:[26]

1. The cracks are predominately intergranular in nature, starting at the fuel rod outer diameter and eventually penetrating the clad thickness.
2. No grain boundary precipitates have been observed which may account for the intergranular cracking.
3. All of the failed fuel rods were clad with 304 stainless steel tubing purchased with an initial room temperature yield strength of 90–95,000 psi.
4. All of the cracks have occurred in the peak heat flux region of the fuel rods.
5. All of the cracks occurred in rods which had operated at peak surface heat fluxes in excess of 380,000 Btu/hr-ft^2.

In addition to the HPD project fuel elements listed in Table IV-9, a total of seven special elements (Task IB) have been irradiated in the VBWR. The fabrication details of these elements are given in Table IV-12, and their irradiation exposure data through December 1962 are listed in Table IV-13. The fabrication of these elements comes under Task IB of the HPD project, and it is evident from a consideration of Table IV-12 that the Task has studied a number of advanced methods for the fabrication of fuel rods. These include tandem rolling, electromagnetic vibratory compaction, pneumatic vibratory compaction, swaging employing powder fuel, and swaging employing pelletized fuel. The vibrational compaction of oxide is covered in greater detail in Ref. 28, and Refs. 29 to 31 report on fabrication of fuel elements by swaging.

Also included in Task IB is the preparation of eight developmental fuel assemblies for irradiation in the Consumers reactor. Each assembly contains 121 fuel rods of 6-ft length. The bundle is shown in Fig. IV-5.[22,32] Four of the assemblies contain rods prepared by the swaged-pellet process, whereas the other four assemblies contain swaged powder fuel rods. A functional description of the components shown in Fig. IV-5 is as follows:[22]

Spacer	Laterally positions fuel rods with respect to each other and the channel Adds stiffness to the corner angles and ties them together
Corner angle	Transmits force Positions the spacers axially Provides protection to the fuel rods during insertion and removal from channels by being the outermost part of the fuel bundle
Support	Supports the weight of all fuel rods and transmits this force to the corner angles
Weldment	Provides a handle without obstructing fuel-rod removal Transmits the weight of the fuel bundle from the corner angles to the lifting device
Retainer	Prevents withdrawal of fuel rods Adds stiffness to the weldment

The special assemblies 8S, 9S, and 10S which are being irradiated in the VBWR, as well as assembly 4S, are prototypical of the Consumers development fuel, or they contain mechanical design features representative of the research and development fuel assembly. Table IV-14 lists the Task IB failure data as of June 1963.

High-Performance UO_2 Program[35–44,46]

This program is a joint USAEC-Euratom program "... to obtain a better understanding of the maximum achievable operating characteristics of UO_2 as a reactor fuel."[35] The program is divided into three major tasks, as follows:

Table IV-10 DESIGN AND OPERATIONAL DATA[45] OF TASK IA

Task IA fuel assembly	Enrichment, %	Nominal rod diameter, in.	No. of rods and cladding thickness, in.	Nominal cladding-to-pellet gap, in.	Initial tubing condition	Fabrication process	Fabricated yield strength, psi	Average bundle exposure,* Mwd/ton of U	Peak bundle exposure, Mwd/ton of U	Peak heat flux, Btu/(hr)(sq ft)	Maximum average power density to date, kw/liter
1A	2.7	0.420	16, 0.020	0.005	Ann.†	Not swaged	40,000	6,330	10,129	361,000	80
2A	2.7	0.420	16, 0.020	0.005	Ann.	Not swaged	40,000	6,350	10,160	358,000	79
1B	2.7	0.420	16, 0.020	0.005	Ann.	Not swaged	40,000	6,464	10,342	333,000	88.9
2B	2.7	0.420	16, 0.020	0.005	Ann.	Not swaged	40,000	6,724	10,758	317,000	92.9
1C	3.5	0.415	25, 0.017	0.005	Ann.	Not swaged	40,000	4,832	7,731	377,000	109.7
2C	3.5	0.415	25, 0.017	0.005	CW‡	Not swaged	90,000	5,517	8,827	400,000	108.2
3C§	3.5	0.415	25, 0.017	0.003	CW	Swaged		4,686	7,498	400,000	103.9
4C	3.5	0.415	25, 0.017	0.002	CW	Swaged		5,308	8,493	393,000	109.3
1D	3.5	0.398	25, 0.012	0	CW	Swaged	100,000	4,948	7,916	400,000	110.4
2D	3.5	0.398	25, 0.012	0	CW	Swaged	100,000	4,030	6,448	399,000	111.3
3D	3.5	0.398	25, 0.012	0.002	CW	Swaged	100,000	4,288	6,860	440,000	109.2
4D	3.5	0.398	25, 0.012	0.002	CW	Swaged	100,000	1,769	2,830	360,000	113.8
1E	4.5	0.360	25, 0.014	0.005	6 Ann. 19 CW	Not swaged	40,000 90,000	6,247	9,995	470,000	116.3
2E	4.5	0.360	25, 0.014	0.005	5 Ann. 20 CW	Not swaged	40,000 90,000	7,920	12,672	470,000	113.9
3E	4.5	0.360	25, 0.014	0.005	2 Ann. 23 CW	Not swaged	40,000 90,000	8,715	13,944	490,000	115.9
4E	4.5	0.360	25, 0.014	0.005	6 Ann. 19 CW	Not swaged	40,000 90,000	8,426	13,482	462,000	109.8
5E	4.5	0.360	25, 0.014	0.005	8 Ann. 17 CW	Not swaged	40,000 90,000	8,039	12,862	450,000	111.6
6E	4.5	0.360	24, 0.014	0.005	2 Ann. 22 CW	Not swaged	40,000 90,000	7,659	12,255	470,000	117.7
1F	4.5	0.360	25, 0.014	0.005	CW	Not swaged	90,000	6,417	10,268	480,000	116.2
2F	4.5	0.360	24, 0.014	0.005	CW	Not swaged	90,000	6,911	11,057	460,000	111.8
1G	4.5	0.358	25, 0.014	0	4 Ann. 21 CW	Swaged	40,000 90,000	5,985	9,576	480,000	118.8
2G	4.5	0.358	25, 0.014	0	8 Ann. 17 CW	Swaged	40,000 90,000	5,625	9,000	480,000	120.7
3G	4.5	0.358	25, 0.014	0.002	6 Ann. 19 CW	Swaged	40,000 90,000	7,252	11,603	500,000	120.5
4G	4.5	0.358	25, 0.014	0.002	2 Ann. 23 CW	Swaged	40,000 90,000	8,084	12,934	480,000	119.8

*Exposures as of June 2, 1963.
†Annealed.
‡Cold worked.
§Unground pellets.

Table IV-11 TASK IA FAILURE DATA[45]

Task IA fuel assembly	Location of failed rod(s)	Type of rod(s) failed	Average exposure, Mwd/ton of U	Exposure in failure location, Mwd/ton of U	Heat flux in failure location, maximum, Btu/(hr)(sq ft)	Type of failure	Remarks
1D	One corner rod	CW	4,948	7,900	400,000	Longitudinal crack	RML metallurgical examination performed
2D	One corner rod	CW	4,030	6,400	399,000	Small longitudinal cracks	RML metallurgical examination performed
3D	One rod next to corner	CW	4,288	6,900	440,000		Previously reported
4D	One corner rod	CW	1,769	2,830	360,000		One corner rod has leaky weld at end plug
1E	One corner rod	CW	6,247	10,000	470,000	Longitudinal cracks	Detailed RML metallurgical examination in progress; see 1E status in text*
2E	One exterior rod O	CW	7,920	12,672	470,000	Longitudinal crack	Crack was not detected by visual observation at VBWR pool; very high sipping signal; RML examination in progress; see Fig. 1*
3E	One rod X adjacent to corner	CW	8,715	13,944	490,000	Large longitudinal crack ~4 in. long	Visual examination at VBWR pool showed crack. RML examination in progress; see Fig. 2*
4E	One exterior rod midway between corners	Ann.	8,426	13,482	462,000	Circumferential cracks	This is the first observation in the HPD program of a crack not in the longitudinal direction. Also it is the first annealed, free-standing rod to fail; see Fig. 3*
5E	?		8,039	12,862	450,000	?	Potential failure by sipping indication, visual examination in VBWR pool showed no crack; RML examining
6E	Corner rod A	CW	7,659	12,255	470,000	Longitudinal cracks	With 4E initial failure detected by in-core sampler
2F	?		6,911	11,057	460,000	?	Visual examination at VBWR pool showed no crack; high sipping signal
1G	One interior rod	CW	5,985	9,600	480,000	Longitudinal cracks	RML metallurgical examination performed; see text* for burst test results on sound rods
2G	Two interior rods	CW	5,625	9,000	480,000	Longitudinal cracks	RML metallurgical examination performed
3G	Three exterior rods on one side, including a corner rod	CW	7,252	11,600	500,000	Longitudinal cracks	RML visual examination performed
4G	One exterior rod adjacent to corner	CW	8,000	13,000	480,000	Longitudinal cracks	Visual examination in VBWR pool

*Refers to material in Ref. 45.

Table IV-12 DETAILS OF HPD PROJECT SPECIAL FUEL ASSEMBLIES[23]

Assemblies Fabricated by Swaged-over-Pellet Process

Assembly 1S	
Purpose	To irradiation-test marginal quality and good quality 12-mil-thick cladding with as-sintered pellets
Cladding	0.012-in.-thick type 304 stainless steel
Fuel	3.5% sintered UO_2* ground to an as-sintered distribution
Rods	Swaged to zero gap; 12 rods have good quality cladding and pellets with 0.010-in.-diameter range; 12 rods have marginal quality cladding and pellets with 0.006-in.-diameter range; 1 rod has a 0.015-in.-diameter hole through cladding, is three-pass swaged over powder, and has 0.015-in.-thick cladding
End plugs	Current standard machined design
Assembly 4S	
Purpose	To irradiation-test a prototype mechanical design for Consumers fuel that provides for easy removal of fuel rods
Cladding	0.014-in.-thick type 304 stainless steel
Fuel	4.5% sintered UO_2 ground to 0.003-in.-diameter tolerance
Rods	Pellet type fuel
End plugs	Current standard machined design
Assembly 6S	
Purpose	To irradiation-test 8- and 10-mil cladding rods fabricated from commercially available material and utilizing a statistical approach to the relaxation of various manufacturing and design variables
Cladding	0.010- and 0.008-in.-thick type 304 stainless steel
Fuel	3.5% sintered UO_2 ground to simulate as-sintered pellets; 40% of pellets <94% of theoretical density; balance of pellets >94% of theoretical density; pellets to have varying degrees of chips
Rods	Swaged to zero gap; 13 rods to have 10-mil cladding and 12 rods to have 8-mil gap cladding; both cladding sizes to have 9 rods, each containing up to 0.002-in. cladding defects; 4 rods in each cladding size to have X-ray rejectable weld defects
End plugs	Standard machined design
Assembly 3S	
Purpose	To irradiation-test fuel rods fabricated by the Calrod tandem rolling process
Cladding	0.015-in.-thick type 304 stainless steel
Fuel	3.5% fused UO_2 (−6 mesh)
Rods	Rolled to 88.5% ± 1% density
End plugs	Collapsible design

Assemblies Fabricated by the Swaged-over-Powder Process

Assembly 2S	
Purpose	To irradiation-test fuel rods fabricated by three-pass swaged-over-powder process
Cladding	0.015-in.- and 0.010-in.-thick type 304 stainless steel
Fuel	3.5% fused UO_2 (−6 mesh)
Rods	Swaged to 92% ± 1% density using multiple pass techniques; 13 rods to have 15-mil cladding and 12 rods to have 10-mil cladding
End plugs	Collapsible design

Assemblies Fabricated by Swaging and Vibratory-Compaction Process

Assembly 7S			
Purpose	To irradiation-test fuel rods fabricated by vibratory compaction and two-pass swaging		
Cladding	0.010-in.-thick type 304 stainless steel (vibratory compacted); 0.016-in.-thick type 304 stainless steel (two-pass swage)		
Fuel	3.5% fused UO_2 (−6 mesh, conditioned)		
Rods	Vibratory compacted to 86% of theoretical density (12); two-pass swaged to 90% of theoretical density (13)		
End plugs	Current standard machine design and drawn cup		
Assembly 5S			
Purpose	To irradiation-test two-pass swaged UO_2 rods having 90% of theoretical density and hot-swaged UO_2 rods having 95% of theoretical density		
Swage process	Three-pass cold	Hot	Two-pass vibratory compacted
No. of rods	5	10	10
Cladding thickness	0.010	0.016	0.008
UO_2 density	91%	95%	90%

*All UO_2 is 4.0% enriched and arc fused. Supplied by Spencer Chemical Co.

Table IV-13 TASK IB DESIGN AND OPERATIONAL DATA[45]

Task IB fuel assembly	Enrichment, %	Rod diameter, in.	No. of rods and cladding thickness, in.	Type of fuel	Initial tubing condition	Fabrication process	Powder density as fabricated, %	Cladding yield strength as fabricated, psi*	Average bundle exposure,† Mwd/ton of U	Peak bundle exposure, Mwd/ton of U	Peak heat flux, Btu/(hr)(sq ft)	Max. average power density to date, kw/liter
1S	3.5	0.400	25, 0.012	Unground pellets	CW‡	Swaged to 0- to 5-mil gap		105,000	1,800	2,851	380,000	86
1SM	3.5	0.400	21, 0.016	Powder	Ann.§	Tandem rolled	88 to 89	90,000	4,500	7,182	380,000	100
			4, 0.012	Powder	CW	Vibratory compacted	86 to 88	100,000		2,851	380,000	86
2S	3.5	0.400	12, 0.016	Powder	Ann.	Swaged	94	95,000	4,500	7,100	385,000	92.7
			12, 0.010	Powder	Ann.	Swaged	93					
3S	3.5	0.400	4, 0.012	Pellet	CW	Swaged to 0- to 1-mil gap		100,000	4,500	7,182	380,000	100
			21, 0.016	Powder	Ann.	Tandem rolled	88 to 89	90,000				
4S	4.5	0.36	16, 0.014	Pellet	Ann.	Not swaged		40,000	5,734	9,174	492,000	106.1
			9, 0.014	Pellet	CW	~5-mil gap		90,000				
5S	4.0	0.400	5, 0.010	Powder	Ann.	Swaged	90.5	95,000	4,000	6,339	425,000	109.2
			10, 0.008	Powder	Ann.	Swaged	87 to 90	95,000				
			10, 0.016	Powder	Ann.	Hot swaged	95					
6S	3.5	0.400	12, 0.010	Unground pellets	Ann.	Swaged to 1-mil gap		45,000	5,500	8,441	410,000	106.7
			13, 0.008	Unground pellets	Ann.			52,000				
7S	3.5	0.400	12, 0.016	Powder	Ann.	Swaged	90 to 91	95,000	3,800	6,098	460,000	95.2
			13, 0.012	Powder	CW	Vibratory compacted	86 to 88	100,000				
8S	4.0	0.400	16, 0.010	Powder	Ann.	Swaged	91 to 92	95,000	3,600	5,637	527,000	101
9S	4.0	0.400	16, 0.010	Powder	Ann.	Swaged	91 to 92	95,000	3,722	5,956	490,000	120
10S	4.0	0.430	12, 0.010	Powder	Ann.	Swaged	89 to 92	95,000	2,100	3,385	450,000	93
			4, 0.010	Pellet	Ann.	Swaged		50,000				
11S	5.0	0.430	4, 0.010	Pellet	Ann.	Swaged to 3- to 4-mil gap		40,000	0	0	0	
			12, 0.010	Powder	Ann.	Swaged	89 to 91	95,000				
12S¶												

*Yield strength at 0.2% offset; room temperature.
†Exposure as of June 2, 1963.
‡Cold worked.
§Annealed.
¶Plan to build using annealed rods from failed E assemblies.

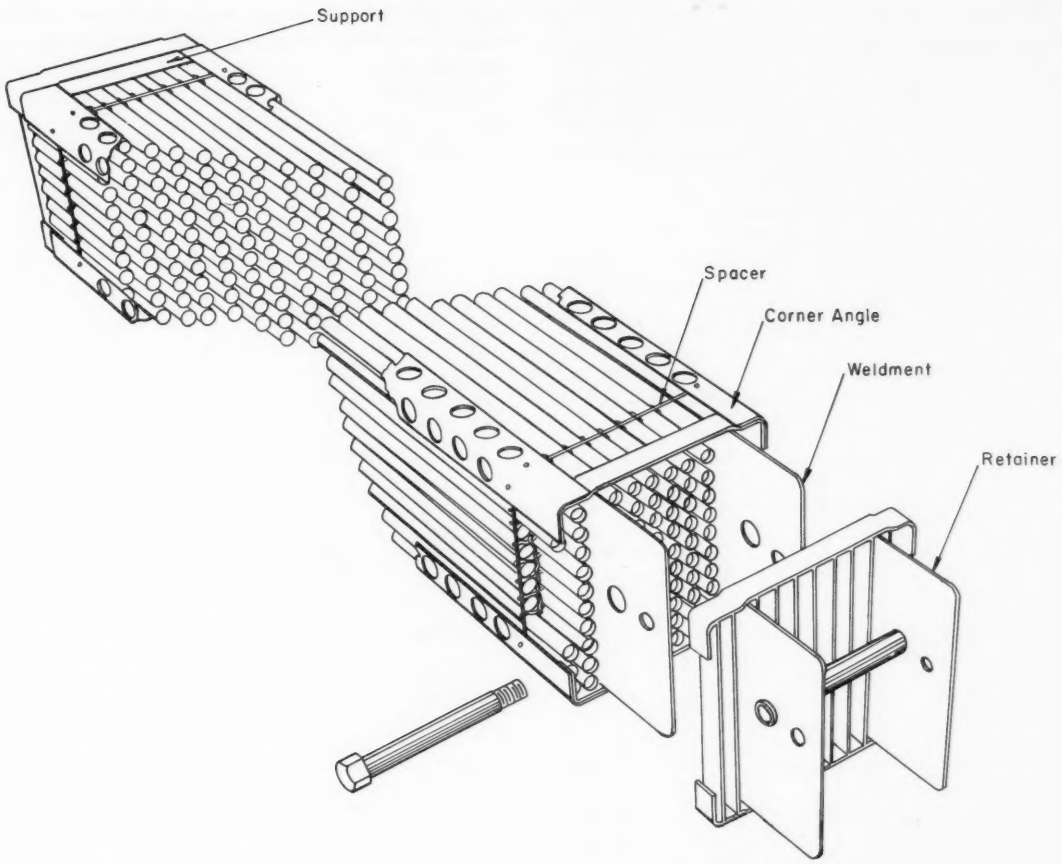

Fig. IV-5 Preliminary development of fuel bundle.[22]

Task I — Measurement of Fission Gas Pressure in Operating Fuel Elements. Objective: Direct measurement of fission gas pressure in UO_2-filled fuel rods, as functions of temperature and fuel configurations. Measurements to be made over an extended period of time during transient and steady-state reactor operation.

Task IIA — Loop Modification. Objective: Design, fabrication and installation of GETR Pressurized Water Loop modifications required by Task IIB experimental program.

Task IIB — Performance of UO_2 Fuel. Objective: Obtain a relationship between the amount of fuel rod central melting and the burn-up that can be attained before fuel-cladding interaction results in rod failure.

A number of progress reports have been issued and are cited as Refs. 35 to 41.

The results obtained under Task I of the UO_2 program are summarized in Ref. 42. The pressure transducer used in the reactor is shown schematically in Fig. IV-6; briefly, the pressure within the fuel rod was measured by increasing the pressure in the tube connected with the source of equalizing pressure until the contacts opened. The fuel elements listed in Table IV-15 were studied. The temperature profiles in the elements were calculated using the UO_2 conductivity data of Bates[43] and some unpublished UO_2 conductivity data of Lyons.[44] For comparison these data are shown in Fig. IV-7. Equivalent gap conductances of 440 and 1762 Btu/(hr)(sq ft)(°F/ft) were assumed. The results are quoted as follows:[42]

> ... These experiments have indicated that fission gas release is negligible from UO_2 operated below the recrystallization temperature. For operation at higher power levels the fractional fission gas release is directly comparable to the volume fraction of fuel operating above the recrystallization temperature.

Table IV-14 TASK IB FAILURE DATA[45]

Task IB fuel assembly	Location of failed rod(s)	Exposure in failure location, Mwd/ton of U	Heat flux in failure location (peak), Btu/(hr)(sq ft)	Remarks
1S	None			No failures; see 1SM
1SM	None			1SM has been reconstituted from fuel rods originally in 3S and 1S, the purpose being to allow irradiation to continue on the tandem-rolled rods
2S	One 0.016-in. rod, one 0.010-in. interior rod	7,100	385,000	Longitudinal crack ~8 to 9 in. long in 0.010-in. cladding; RML ultrasonic examination revealed crack in 0.016-in. cladding
3S	Four corner pellet rods	7,183	380,000	Gross longitudinal cracks varying to very small intergranular and transgranular cracks; RML metallurgical examination performed on one corner rod
3S	Two tandem-rolled rods			Two tandem-rolled rods show indications of cracks by ultrasonics
4S	None			No failures
5S	?			Ultrasonic techniques show many small indications; cracking not observed visually
6S	Two rods, B and D, adjacent to corners on one side	8,441	410,000	Large cracks visible in two rods
7S	One swaged exterior rod adjacent to corner	6,100	460,000	Longitudinal crack, ultrasonic techniques verified; RML examination planned
8S*	One corner rod	5,638	527,000	Small cracks* visible in one rod
9S				No failures
10S*	One corner pellet rod	3,387	458,000	Small longitudinal crack* in one rod
11S				Bundle has not been irradiated to date

*Some difficulty in verification exists among several observers. Ultrasonic examination will be performed.

Table IV-15 FUEL RODS IRRADIATED WITH PRESSURE TRANSDUCERS[42]

	Rod S-1	Rod S-1A	Rod S-2	Rod S-3	Rod P-1	Rod P-2
Enrichment, %	4.0	4.0	7.08	3.84	3.0	6.65
Fuel density ρ/ρ_0, %	98	98	98	93.2	89.4	90.0
Fuel type	Pellet	Pellet	Pellet	Pellet	Powder	Powder
Fuel diameter, in.	0.496	0.496	0.481	0.496	0.500	0.500
Maximum heat flux	348*	334*	532*	348*	223‡	453‡
Maximum burnup,† Mwd/ton	1549	1718	3115	1712	674	1270
Gap, in.	0.004	0.004	0.014	0.004		
Fuel weight, g	957	880.5	897	935	945	946
Fuel length, in.	28.6	26.3	28.3	28.5	28.75	27.5
Void volume, cm^3	5.5	3.5	9.6	4.4	6.3	3.9
Typical oxygen-to-uranium ratios	2.008	2.007				

*Heat flux was 1000 Btu/(hr)(sq ft) in position N-10 at 36 Mw of reactor power.
†At time of removal from reactor.
‡Heat flux was 1000 Btu/(hr)(sq ft) in position O-10 at 40 Mw of reactor power.

These conclusions are based on data taken with rod S-2, since the other rods experienced mechanical difficulties or were of insufficient enrichment to get the maximum temperature above the recrystallization temperature.

The direct measurement experiment was terminated on Sept. 12, 1962. Presumably no further irradiation of the transducer-equipped rods will be made, although the results reported to date indicate that the technique is feasible. It would be of interest to irradiate the powder-filled rods at a higher heat flux, if possible, for comparison to the pellet-filled-rod gas release.

Task IIA is concerned primarily with modification and operation of a pressurized-water loop in the General Electric Test Reactor (GETR). This loop, the PWL loop, is being used to irradiate samples under the High-Performance UO_2 Program (HPP). The loop can accommodate a rod bundle composed of four rods, each with an outside diameter of about $\frac{1}{2}$ in. and an active length of 34 in. Another facility used for the program is the so-called "Trail Cable" facility. This facility, a part of the GETR installation, can accept a single fuel rod of the same geometry as that to be employed in the PWL loop with the exception of length; the Trail Cable capsule has a length of 5 in. The Trail Cable facility was used to obtain calibration data on the UO_2 before the full-length rods were irradiated in

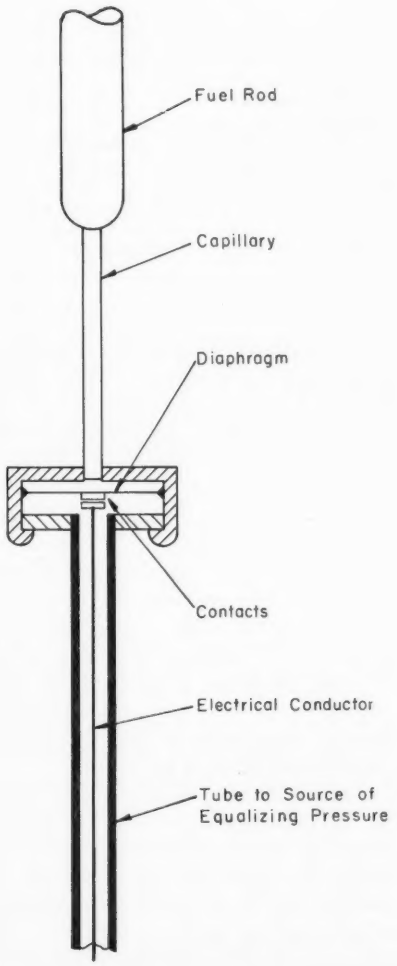

Fig. IV-6 Schematic of transducer.[42]

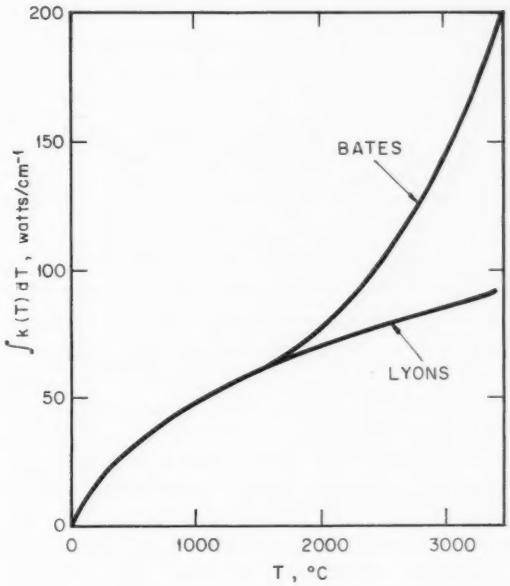

Fig. IV-7 $\int_0^T k(T)\,dT$ vs. T for UO_2 having 95% of theoretical density.[42]

Table IV-16 OPERATING DATA FOR PWL LOOP: HIGH-PERFORMANCE UO_2 PROGRAM

GETR cycle No.	PWL assembly No.	Burnup, Mwd/metric ton	Approximate peak heat flux, Btu/(hr)(sq ft)
33	EPT-6	1180	630,000
34	EPT-8	1442	790,000
35	EPT-10	1182	1,010,000
36 to 39	EPT-COM	1516	1,200,000
40	EPW-6/8	9.8	722,000
40	EPW-6/8A	11.7	800,000
41	EPT-12	2239	1,350,000

the PWL loop. The operation of the Trail Cable facility was coordinated with remote metallurgical examinations of the irradiated capsules to obtain as much information as possible concerning UO_2 temperature distribution and thermal conductivity.

The nomenclature for the assemblies irradiated in the PWL loop is given in Table IV-16, along with other pertinent data. The results of the first three experiments involving EPT-6, -8, and -10 are summarized in Ref. 40. The irradiation conditions are summarized in Table IV-17. The fuel rods contained sintered UO_2 pellets that had 95% of the theoretical density, a diameter of $\frac{1}{2}$ in. (nominal), and a total active length of 34 in. The results of the postirradiation examinations indicated increases in the fuel-rod diameter, and the increase in the fuel-rod volume corresponding to the increase in the outside diameter is shown in Fig. IV-8. Reference 40 makes the following comment on the swelling:

> Considered as an entity, all of the different bits of evidence collected in the above post-irradiation examination point to an association between the clad swelling and the UO_2 melting that occurred in the fuel rods. Recent measurements have indicated a fairly large volume increase (~7 percent) in UO_2 upon melting ... which could generate the necessary force to produce clad swelling ....

Surprisingly, similar rods that had been irradiated in the Trail Cable facility had not exhibited dimensional changes after operating at similar thermal performance. This difference has been attributed to the different lengths of the two rods. In the long PWL fuel rod, the molten oxide was contained between two relatively cold, nonplastic sets of fuel pellets, whereas the short Trail Cable rod contained a molten core over essentially its whole length, and the molten oxide expanded into a plenum. Metallographic examination of a transverse section of one of the rods in assembly EPT-10, at the point of maximum swelling, revealed cracks along the outer portion of the cladding surface. Probably some had propagated through the cladding, since puffs of fission gas had been noted during operation of EPT-10.

Since expansion of molten UO_2 was responsible for the cladding swelling, the EPT-COM assembly was designed with hollow oxide pellets to accommodate the expanded oxide. The hollow core was an 80- to 90-mil hole drilled in each of the fuel pellets at the center line. Figure IV-9 shows that extensive UO_2 melting and fuel relocation occurred during irradiation. The fuel in all four rods in assembly EPT-COM under-

Table IV-17 PARAMETERS FOR EURATOM PWL FUEL-ASSEMBLY IRRADIATION

Assembly designation	Fuel enrichment, %	Fuel-column length, in.	Fuel-rod peak surface heat flux (average), Btu/(hr)(sq ft)	Assembly thermal power, kw	Average burnup, Mwd/ton	Irradiation period
EPT-6	1.5	34 ± ¼	645,000	200	1180	4/23/62 to 5/19/62
EPT-8	2.2	34 ± ¼	895,000	260	1442	6/1/62 to 6/24/62
EPT-10	3.0	31 ± ¼	1,010,000	310	1182	7/3/62 to 7/19/62

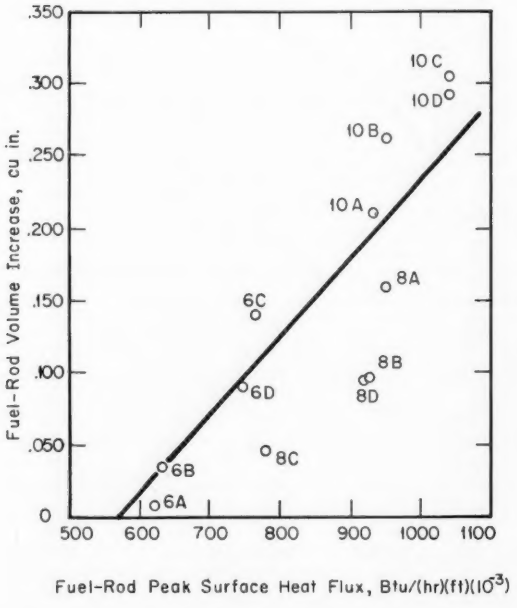

Fig. IV-8 Fuel-rod volume increase vs. peak surface heat flux at startup.[40]

Since expansion of molten UO_2 was responsible for the cladding swelling, the EPT-COM assembly was designed with hollow oxide pellets to accommodate the expanded oxide. The hollow core was an 80- to 90-mil hole drilled in each of the fuel pellets at the center line. Figure IV-9 shows that extensive UO_2 melting and fuel relocation occurred during irradiation. The fuel in all four rods in assembly EPT-COM under-

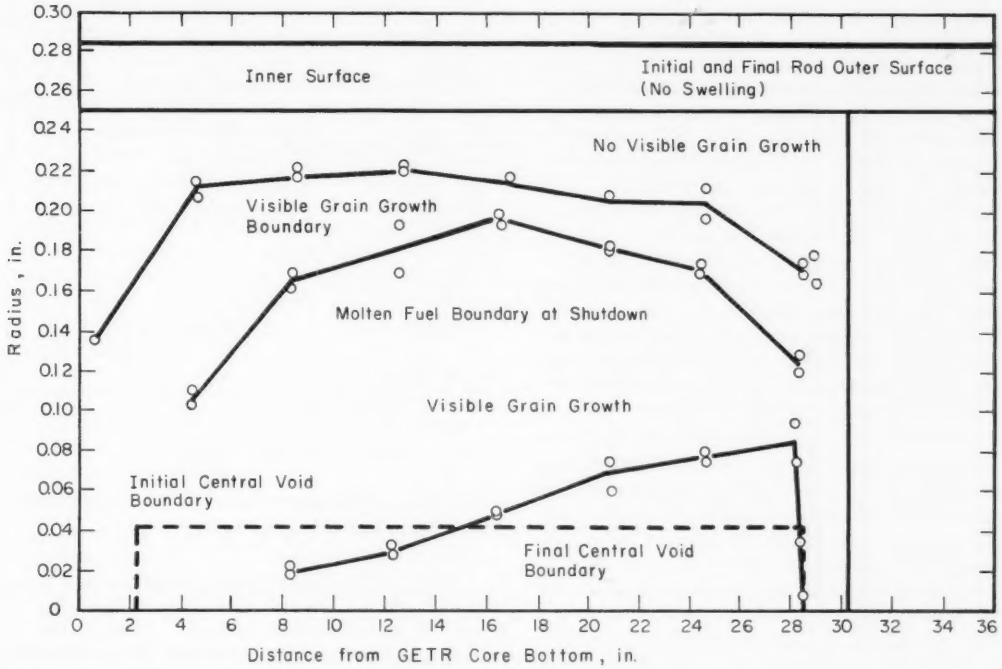

Fig. IV-9 Fuel microstructure boundaries of a rod from assembly EPT-COM.[41]

went some center melting; but of the four, only one rod, the rod in which the heat flux was highest, was swollen. This result was interpreted as an indication that the 80-mil hole was marginal for containing the UO_2 on melting, and assembly EPT-12 was designed with a 140-mil hole. Assembly EPT-12 was still in the GETR PWL loop as of the writing of Ref. 41 and apparently was performing satisfactorily.* The initial startup for the GETR, when the EPT-12 assembly was in place, was programmed to prevent sudden power changes of appreciable magnitude, since it was desired to minimize severe internal volume changes in the fuel rods of EPT-12.

Assemblies EPW-6/8 and -6/8A contained swaged-powder fuel rods. These were prepared from arc-fused powder, denitrided at 1650°C for 4 hr in H_2 before loading. The powder was vibrationally compacted into tubing that was 0.656 in. in outside diameter by 30 mils in wall thickness (Zircaloy-2) and was swaged in two passes to the final outside diameter of 0.565 in. The final oxide density was 90%. Several fuel rods were made by vibrational compaction alone — without swaging — to a final density that was 86% of theoretical. Assembly EPW-6/8, containing all swaged rods, underwent about 10 hr of irradiation in the PWL loop; at that point the reactor scrammed owing to high radiation levels in the loop. Examination of the assembly revealed a longitudinal split in the cladding of the rod in the position of highest relative power for the assembly. Two of the sound rods from the assembly and two rods fabricated by only vibrational methods were reassembled into EPW-6/8A and placed in the PWL loop for GETR cycle 40. Soon after startup, when the power was being increased from 25 to 27 Mw, one of the two swaged rods failed; the failure occurred in the swaged rod having the higher power density. The details of the irradiation and subsequent examination of these assemblies are contained in Refs. 41 and 44. The following quotation illustrates current thinking on the causes of the failures:[41]

> It should be emphasized that the RML investigations of these two failures are incomplete. No firm

*A later progress report,[46] however, notes that, during subsequent irradiation, assembly EPT-12 failed with significant release of activity.

conclusion can be made concerning the failure mechanism until the examinations are finished. However, on the basis of the evidence presently available, the failures seem to be basically the result of clad swelling similar to that previously observed in the pellet fuel rods. The magnitude of the clad swelling for a given surface heat flux in the case of the swaged fuel appears to be equal to or greater than that previously experienced with pellet fuel despite its lower fuel density .... This may be the result of lower thermal conductivity in the powder fuel with a resultant large degree of fuel melting. The clad swelling coupled with a generally less ductile cladding due to swaging resulted in actual loss of the clad integrity. (The pellet fuel rods experienced significantly larger increases in diameter than the first powder fuel rod failure and did not rupture.)

It is likely that the first powder rod failure was associated with a localized weakness in the cladding. This conclusion is based on the failure being away from the zone of maximum swelling and the circumferentially nonuniform swelling of the UO_2 cross section in the failure zone. The source of the clad weakness has not been identified.

The mechanism for the second powder rod failure appears to have been much more complex. The failure was more severe than the first in terms of the activity release to the loop.

A section of the cladding approximately $\frac{1}{4}$ inch wide by one inch long was lost from the rod and the appearance of the remaining edges of the clad indicates that the clad had melted. The general diameter increase of the rod at the axial location of failure is approximately 80 mils. Two possible mechanisms for the clad melting can be postulated. One is that a heat transfer "burnout" may have occurred at the failure zone as a result of flow starvation from the clad swelling, particularly if the swelling at the failure orientation significantly exceeded the uniform swelling measured at the cross section. A second is that the clad may have fractured, expelling the outer rim of unmelted fuel and permitting molten UO_2 to contact the cladding. The post-irradiation examination has produced some evidence favoring the latter theory. The loss of fuel and cladding makes it difficult to obtain a complete picture of what occurred.

The vibratory compacted fuel rods had approximately four percent lower density than the swaged fuel rods and do not appear to be subject to clad swelling, at least up to a heat flux of approximately 800,000 Btu/hr-ft^2. To confirm this conclusion it is planned to replace the original swaged powder assembly in the irradiation schedule for the program with fuel rods fabricated by vibratory compaction alone. This assembly [was] scheduled for irradiation in the GETR during April 1963. If this irradiation is successful, the remaining higher thermal performance powder fuel rods will also be vibratory compacted.

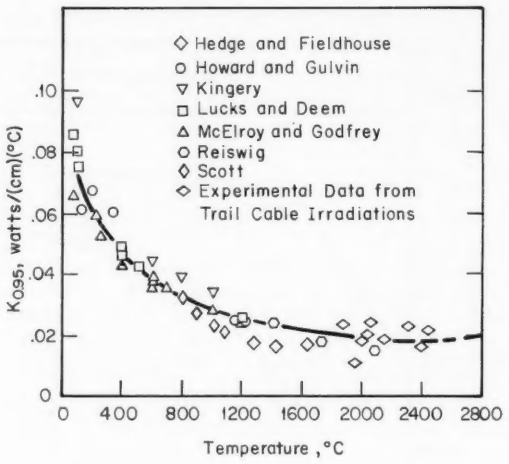

Fig. IV-10 Thermal conductivity vs. temperature for UO_2 having 95% of theoretical density.[41]

Analyses of irradiated pellet-fuel capsules in the Trail Cable facility have resulted in increased knowledge of fuel melting limits and thermal conductivity. Figure IV-10 summarizes the results from various experimenters; the integral of kdT from zero to melting temperature has been experimentally determined as 86 ± 3 watts/cm. The Trail Cable data in Fig. IV-10 do not indicate the improvement of UO_2 thermal conductivity at elevated temperatures which has been postulated elsewhere.[43]

References

1. W. H. Cook, Fuel Cycle Program. A Boiling Water Reactor Research and Development Program, First Quarterly Report, August 1960–September 1960, USAEC Report GEAP-3558, General Electric Company, Atomic Power Equipment Department, Oct. 10, 1960.
2. General Electric Company, Atomic Power Equipment Department, Fuel Cycle Program. A Boiling Water Reactor Research and Development Program, Second Quarterly Report (covering the period) October 1960–December 1960, USAEC Report GEAP-3627, July 1961.
3. J. A. Hodde (Comp.), Fuel Cycle Program. A Boiling Water Reactor Research and Development Program, Third Quarterly Report, January 1961–March 1961, USAEC Report GEAP-3709, General Electric Company, Atomic Power Equipment Department, June 1961.

4. J. A. Hodde (Comp.), Fuel Cycle Program. A Boiling Water Reactor Research and Development Program, Fourth Quarterly Report, April 1961–June 1961, USAEC Report GEAP-3781, General Electric Company, Atomic Power Equipment Department, Aug. 1, 1961.
5. J. A. Hodde (Ed.), Fuel Cycle Program. A Boiling Water Reactor Research and Development Program, Fifth Quarterly Report, July 1961–September 1961, USAEC Report GEAP-3835, General Electric Company, Atomic Power Equipment Department, Oct. 10, 1961.
6. J. A. Hodde, General Electric Company, Atomic Power Equipment Department, Jan. 31, 1962. (Unpublished)
7. J. A. Hodde (Comp.), Fuel Cycle Program. A Boiling Water Reactor Research and Development Program, Seventh Quarterly Progress Report, January 1962–March 1962, USAEC Report GEAP-3935, General Electric Company, Atomic Power Equipment Department, Apr. 30, 1962.
8. J. A. Hodde (Comp.), Fuel Cycle Program. A Boiling Water Reactor Research and Development Program, Eighth Quarterly Progress Report, April 1962–June 1962, USAEC Report GEAP-4048, General Electric Company, Atomic Power Equipment Department, July 10, 1962.
9. C. L. Howard (Comp.), Fuel Cycle Program. A Boiling Water Reactor Research and Development Program, Ninth Quarterly Progress Report, July 1962–September 1962, USAEC Report GEAP-4094, General Electric Company, Atomic Power Equipment Department, Oct. 25, 1962.
10. C. L. Howard (Comp.), Fuel Cycle Program. A Boiling Water Reactor Research and Development Program, Tenth Quarterly Progress Report, October–December 1962, USAEC Report GEAP-4159, General Electric Company, Atomic Power Equipment Department, Jan. 14, 1963.
11. C. L. Howard (Comp.), Fuel Cycle Program. A Boiling Water Reactor Research and Development Program, Eleventh Quarterly Progress Report, January–March 1963, USAEC Report GEAP-4215, General Electric Company, Atomic Power Equipment Department, Apr. 5, 1963.
12. C. J. Baroch, J. P. Hoffman, and W. C. Rous, AEC Fuel Cycle Program. Design and Fabrication of the Basic Fuel Assemblies, USAEC Report GEAP-3653, General Electric Company, Atomic Power Equipment Department, Mar. 15, 1963.
13. S. J. Paprocki (Ed.), Progress on the Use of Gas-Pressure Bonding for Fabricating Low-Cost Ceramic, Cermet, and Dispersion Fuels, USAEC Report BMI-1372, Battelle Memorial Institute, Aug. 25, 1959.
14. S. J. Paprocki (Ed.), Progress on the Use of Gas-Pressure Bonding for Fabricating Low-Cost Ceramic, Cermet, and Dispersion Fuels, Phase II Report on AEC Fuel-Cycle Program, USAEC Report BMI-1475, Battelle Memorial Institute, Nov. 7, 1960.
15. S. J. Paprocki (Ed.), Progress on the Use of Gas-Pressure Bonding for Fabricating Low-Cost Ceramic, Cermet, and Dispersion Fuels, USAEC Report BMI-1555, Battelle Memorial Institute, Nov. 24, 1961.
16. C. J. Baroch, C. B. Boyer, and S. N. Porembka, Evaluation of Failed Hot Gas Isostatic Pressed Fuel Rods, USAEC Report GEAP-4206, General Electric Company, Vallecitos Atomic Laboratory, Mar. 20, 1963.
17. C. J. Baroch, Design and Fabrication of Fuel Rods Containing Low Temperature Sintered Pellets, USAEC Report GEAP-4257, General Electric Company, Atomic Power Equipment Department, May 15, 1963.
18. C. J. Baroch, Design and Fabrication of Coextruded Stainless Steel Clad UO_2 Fuel Rods, USAEC Report GEAP-4282, General Electric Company, Atomic Power Equipment Department, June 1963.
19. J. G. Hunt, D. F. Kaufman, and P. Loewenstein, Hot Extrusion of UO_2 Fuel Elements. Fundamental and Applied Research and Development in Metallurgy, Final Report for the Period July 1, 1960 Through June 30, 1961, USAEC Report NMI-1245, Nuclear Metals, Inc., Oct. 31, 1961.
20. L. K. Holland, High Power Density Development Project, First Quarterly Progress Report (covering the period) April–June 1960, USAEC Report GEAP-3543, General Electric Company, Atomic Power Equipment Department, July 1, 1960.
21. L. K. Holland, High Power Density Development Project. Third Quarterly Progress Report, October–December 1960, USAEC Report GEAP-3632, General Electric Company, Atomic Power Equipment Department, Jan. 1, 1961.
22. L. K. Holland, General Electric Company, Atomic Power Equipment Department, July 1, 1961. (Unpublished)
23. L. K. Holland, High Power Density Development Project. Sixth Quarterly Progress Report, July–September 1961, USAEC Report GEAP-3884, General Electric Company, Atomic Power Equipment Department, October 1961.
24. R. L. Holladay, High Power Density Development Project. Seventh Quarterly Progress Report, October–December 1961, USAEC Report GEAP-4001, General Electric Company, Atomic Power Equipment Department, Jan. 1, 1962.
25. R. L. Holladay, High Power Density Development Project. Tenth Quarterly Progress Report, July–September 1962, USAEC Report GEAP-4096, General Electric Company, Atomic Power Equipment Department, Oct. 1, 1962.
26. R. L. Holladay (Comp.), High Power Density Development Project. Eleventh Quarterly Progress Report, October–December 1962, USAEC Report

GEAP-4155, General Electric Company, Atomic Power Equipment Department, Jan. 1, 1963.

27. W. D. Fowler and J. W. Lingafelter, High Power Density Development Project. Design and Fabrication of High Power Density Fuel Assemblies for VBWR Irradiation Testing, USAEC Report GEAP-3609, General Electric Company, Atomic Power Equipment Department, Nov. 1. 1960.
28. W. R. DeHollander, Vibrational Compaction of Uranium Dioxide, USAEC Report GEAP-4032, General Electric Company, Vallecitos Atomic Laboratory, Mar. 1, 1962.
29. E. A. Lees, Fabrication of Fuel Elements by Swaging, USAEC Report GEAP-3918, General Electric Company, Vallecitos Atomic Laboratory, May 21, 1962.
30. C. M. Ryer, Powder Fuel Processing by Two-Pass Swaging. The Effect of Particle Size and Distribution, USAEC Report GEAP-3891, General Electric Company, Vallecitos Atomic Laboratory, Apr. 10, 1962.
31. W. V. Cummings, D. R. Lewis, and R. E. Blood, Examination of 304 Stainless Steel Cladding from Cold-Swaged and Rolled Fuel Rods, USAEC Report GEAP-3997, General Electric Company, Atomic Power Equipment Department, July 1962.
32. W. D. Fowler, General Electric Company, Vallecitos Atomic Laboratory, April 1962. (Unpublished)
33. J W. Lingafelter, E. A. Lees, and R. J. Seely, Erosion Flow Testing of Purposely Defected Stainless Steel Clad Compacted UO_2 Powder Fuel, USAEC Report GEAP-4020, General Electric Company, Atomic Power Equipment Department, February 1962.
34. T. C. Rowland and J. S. Atkinson, Power Cycling of High Power Density Fuel Specimens Clad with 10-mil Wall Stainless Steel, USAEC Report GEAP-4069, General Electric Company, Atomic Power Equipment Department, October 1962.
35. B. Weidenbaum, High Performance UO_2 Program. Quarterly Progress Report No. 2, July–September 1961, USAEC Report GEAP-3771-2, General Electric Company, Vallecitos Atomic Laboratory, Oct. 1, 1961.
36. B. Weidenbaum, High Performance UO_2 Program. Third Quarterly Progress Report, October–December 1961, USAEC Report GEAP-3771-3, General Electric Company, Vallecitos Atomic Laboratory, Jan. 2, 1962.
37. B. Weidenbaum, High Performance UO_2 Program. Quarterly Progress Report No. 4, January–March 1962, USAEC Report GEAP-3771-4, General Electric Company, Vallecitos Atomic Laboratory, Apr. 1, 1962.
38. B. Weidenbaum, High Performance UO_2 Program. Quarterly Progress Report No. 5, April–June 1962, USAEC Report GEAP-3771-5, General Electric Company, Atomic Power Equipment Department, June 1962.
39. B. Weidenbaum, High Performance UO_2 Program. Quarterly Progress Report No. 6, July–September 1962, USAEC Report GEAP-3771-6, General Electric Company, Atomic Power Equipment Department.
40. B. Weidenbaum, High Performance UO_2 Program. Quarterly Progress Report No. 7, October–December 1962, USAEC Report GEAP-3771-7, General Electric Company, Atomic Power Equipment Department, Apr. 16, 1963.
41. B. Weidenbaum, High Performance UO_2 Program. Quarterly Progress Report No. 8, January–March 1963, USAEC Report GEAP-3771-8, General Electric Company, Atomic Power Equipment Department, Apr. 15, 1963.
42. M. B. Reynolds, The Measurement of Free Fission Gas Pressure in Operating Reactor Fuel Elements, USAEC Report GEAP-4135, General Electric Company, Vallecitos Atomic Laboratory, Jan. 23, 1963.
43. J. Lambert Bates, Thermal Conductivity of UO_2 Improves at High Temperatures, *Nucleonics*, 19(6): 83 (1961).
44. M. F. Lyons, R. C. Nelson, B. Weidenbaum, and T. J. Pashos, UO_2 Swaged Powder Fuel Rod Failures at High Thermal Performance Conditions. Preliminary Results, USAEC Report GEAP-4197, General Electric Company, Atomic Power Equipment Department, Mar. 1, 1963.
45. R. L. Holladay (Comp.), High Power Density Development Project. Thirteenth Quarterly Progress Report, April–June 1963, USAEC Report GEAP-4309, General Electric Company, Atomic Power Equipment Department, July 1, 1963.
46. B. Weidenbaum, High Performance UO_2 Program. Quarterly Progress Report No. 9, April–June 1963, USAEC Report GEAP-3771-9, General Electric Company, Atomic Power Equipment Department, July 15, 1963.

Section

V

Power Reactor Technology

Control and Dynamics

Period Meters

It is well known that the time constants of devices for measuring neutron flux levels are long at low flux levels. For pulse type detectors this is a fundamental result of considerations of signal-to-noise ratio. The instrument must examine a relatively large number of pulses to determine whether an observed change in pulse rate represents a true change in the average flux level or a statistical fluctuation. Current type detectors (ion chambers) are, of course, subject to the same fundamental limitation, but often the time constant is set at some larger value by the practical necessity of producing a voltage signal of useful size across the inherent electrical capacitance of the detector and its connecting cable.

The time constants of instruments used at low flux levels are of particular interest when the instruments provide period information, for it is evident that the instrument cannot assess the true period accurately unless its time constant is short relative to the period; and they are of particular importance because period information is often used to actuate low-level safety circuits. Two recent papers[1,2] illuminate the behavior of period circuits at low flux levels by computing the period meter output as a function of time during a reactor power transient. References 1 and 2 describe digital computer programs for the Ferranti Mercury computer which compute the outputs of period meters during startup transients resulting from specified programs of reactivity addition to the critical or subcritical reactor. The period meter considered in Ref. 1 consists of a mean-level current ionization chamber, a vacuum diode for a logarithmic device, and the usual d-c amplifier, differentiator, and meter. The circuit elements that determine the dynamic response of the meter are shown schematically in Fig. V-1. Reference 2 is similar to Ref. 1, except that it treats a period meter utilizing count rate as input. The detector is a pulse ionization chamber, and several diode pumps are used to give the logarithmic characteristic. The program allows for time delays in the diode pump circuits and in the period meter.

The calculated response of a period meter, with the circuit characteristics listed in Fig. V-1, is shown in Fig. V-2 for a power excursion caused by the addition of reactivity at the rate of 2% per minute to an initially critical reactor. The reactor assumed is graphite moderated, with an effective prompt-neutron lifetime of 1×10^{-3} sec; however, the behavior is not sensitive to neutron lifetime over the range of periods in the figure. Of more significance is the assumed relation between reactor power level and ion chamber output. This is taken as 2×10^{-3} amp per watt of reactor power and in the actual case would be strongly dependent on the ion chamber location.

In addition to the inverse periods, $\bar{\alpha}$, indicated by the period meter when the transient is initiated at various power levels, Fig. V-2 shows plots of the true inverse period, α, of the reactor and the inverse period that would be indicated by the meter if the logarithmic amplifier were perfect, i.e., if the dynamic response of the circuit element shown in part *a* of Fig. V-1 were perfect. The curves for initial powers of 100 kw and higher correspond very closely to this curve. The reference points out that the dynamic response involves both a phase lag, which in Fig. V-2 causes the low-power curves to indicate periods that are much too long for a number of seconds after the beginning of the transient, and an overshoot that at some later time causes each low-power curve to rise above the curve for the perfect logarithmic

amplifier, $\bar{\alpha}_1$. Thus, for example, if the period-meter indications were being used to actuate a scram at a period of 2 sec ($\alpha = 0.5$), the scram would occur sooner if the transient started at a power of 100 watts than if it started at one of the higher (or lower) power levels considered. Similarly, if the scram were set for a period of 1.1 sec ($\alpha = 0.9$), the initial power level of 10 watts would provide the earliest scram.

Usually a delay of several seconds in the recognition of a short period at very low power levels need not be interpreted as hazardous, inasmuch as the power must rise many decades before the level becomes dangerous (in Fig. V-2 the power rise is of the order of 10^3 before the period meter begins to show a short period on the 1-watt curve). Curves like those of Fig. V-2 do, however, emphasize the importance of locating period sensors close enough to the reactor core to avoid large attenuation of the neutron flux. They are also useful to the reactor operator for clarifying the observed performances of period meters at low power levels.

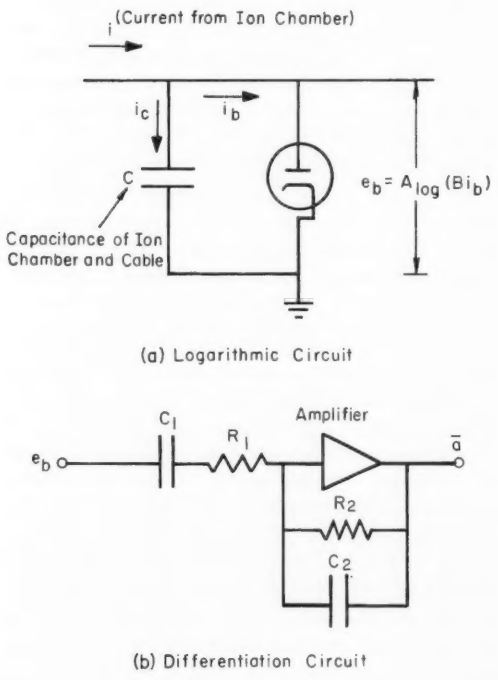

Fig. V-1 Schematic components of period-meter circuit.[1] For the curves shown in Fig. V-2, the following values were used for the circuit elements: C = 2000 picofarads; time constant of C_1, R_1 = 1.0 sec; time constant of C_2, R_2 = 1.0 sec; gain of logarithmic element = 0.1 volt/neper (1 neper = 8.686 db); gain of differentiator = 10 sec.

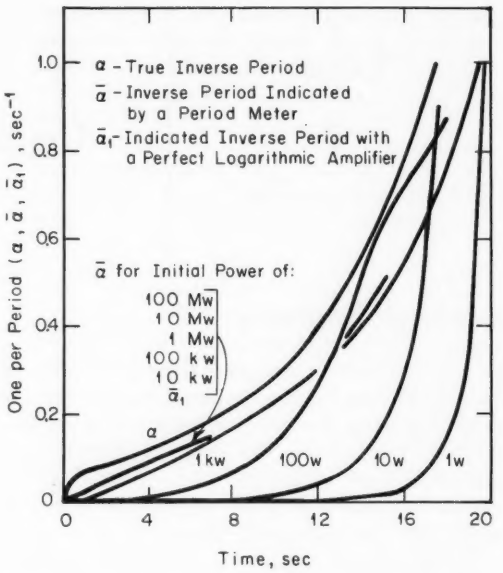

Fig. V-2 Calculated indications of period meter during ramp addition of reactivity to an initially critical reactor.[1] The reactivity addition rate is 2% per minute, and the power levels indicated specify the reactor power at the beginning of the reactivity addition. The mean prompt-neutron lifetime for the reactor is 1×10^{-3} sec, the delayed-neutron characteristics are those of U^{235}, and the ion chamber sensitivity and location are such that the current is 20 μa at the full reactor power of 100 Mw. The characteristics of the period-meter circuit are given in Fig. V-1.

Transducers

Input transducers are devices that transform a nonelectrical physical quantity into a measurable electrical quantity; transducers of various types are essential parts of nuclear reactor control systems. To incorporate these devices into a reactor system, the designer needs to know temperature and radiation-damage limitations. This important information is supplied by Ref. 3. Tables that give temperature range, measurement range, and fast-neutron and gamma-flux thresholds are presented for displacement, pressure, strain and torque, force, temperature, and radiation transducers. Often the limitations are merely best estimates, since the experimental data on actual trans-

ducers and sensing elements are limited. The threshold values quoted were established by contacting users and manufacturers, by extrapolation of irradiation-damage information on the materials of construction, and by relating actual empirical information on irradiated transducers. The limiting components of the transducers for nuclear applications are the organic insulators and dielectrics, the lubricants, and the damping oils. Of considerable interest to the nuclear industry, because of the importance of temperature transducers in reactor instrumentation, is the fact that in thermocouples radiation causes composition changes that change the calibrations. Computer programs have been used to determine the extent of the changes, and the results have been tabulated; chromel was found to undergo very slight transmutation. Temperature transducers may also be subject to other radiation effects such as effects on insulation, connectors, leads, and sealing compounds.

Servomechanism Reliability

Studies and discussions of the reliability of reactor control systems are fairly numerous. Two reviews have appeared in a recent issue of *Nuclear Safety*.[4,5] Reference 6 is a recent British study of the application of redundancy techniques to the automatic control of nuclear reactors to improve reliability. The study considers circuit redundancy, where the circuit is considered to include all components from the instrument sensors to the control-rod drives.

References

1. J. D. Cummins, Period Meter Output During Startup Transients, British Report AEEW-R-231, November 1962.
2. J. D. Cummins, Pulse Counting Period Meter Output During Startup Transients, British Report AEEW-R-245, December 1962.
3. W. E. Chapin, D. J. Hamman, and E. N. Wyler, The Effect of Nuclear Radiation on Transducers, USAEC Report REIC-25, Radiation Effects Information Center, Apr. 19, 1963.
4. E. Siddall, Reliability of Reactor Control Systems, *Nucl. Safety*, 4(4): 1 (June 1963).
5. E. P. Epler, Reliability of Reactor Systems, *Nucl. Safety*, 4(4): 72 (June 1963).
6. L. A. J. Lawrence and R. J. Scotcher, A Study of Servomechanism Reliability in Nuclear Reactor and Plant Control Systems, British Report AEEW-R-220, December 1962.

Section

VI

Power Reactor Technology

Containment, Radiation Control, and Siting

Low-Pressure Containment Building

Two recent reports[1,2] give containment information that is of use in those applications where low leakage rates are required, but where the maximum pressure and permissible leakage limits are not so stringent as to demand the use of a welded-steel containment shell. Reference 1 reports measurements of air leak rates through structural components of concrete and metal-panel buildings. The leak-rate data were used to generate empirical constants for use in analytic expressions that can be used to predict the air flow rates through the building components as a function of size, method of construction, and pressure differential. In addition to the information on walls, information is presented on doors, louvers, butterfly valves, caulking materials, and paints. Also presented are the preferred design methods for reducing leakage, descriptions of procedures for predicting and locating leak paths, and procedures for calculating the expected leakage from a real structure. It is suggested[1] that with improved construction methods the leak rate for a large metal-panel building can be reduced to 1% of the contained volume per day at a pressure of 0.5 psi. Large concrete buildings can be constructed to give a leak rate of 1% of the contained volume per day at a pressure of 5 psi.

A recent leak-rate test of two identical concrete structures shows how important design and inspection during construction will be in order to reduce the leak rate to 1% of the contained volume per day.[2] The tests were done on two reinforced-concrete structures intended to contain nuclear critical experiments at the Argonne National Laboratory. Each structure was in the form of a rectangular box with inside dimensions of 30 by 40 by 30 ft high. Three of the concrete walls and the roof were 4 ft thick, and the remaining wall was 5 ft thick. The wall thicknesses were dictated by biological shielding requirements. The structures were designed to withstand a large pressure loading from a sudden energy release and its subsequent internal pressure, but they were not designed to be leaktight. After construction had been completed, the structures were pressurized to detect areas of gross leakage, and reasonable and practical measures were taken to eliminate or minimize these leaks. For instance, at the surface joints of opening frames the concrete was routed out to form a groove that was filled with the high-temperature mastic. This was also done around all nozzles, pipes, and conduits. When leaks persisted past door frames, epoxy resin was pumped through tapped holes in the door frame to fill the void between the steel and concrete. Also, where leakage was detected through large areas of concrete, about 4 in. of concrete were chipped out back to the reinforcing bars, and expanding grout was troweled into the void created by the removed concrete. All form ties were carefully grouted. Even after all these efforts to plug known leaks and suspected areas, one cell showed a loss of approximately 23% of its contained air per day, whereas the other cell showed a loss of approximately 10% at an internal pressure of 10 psig. To further reduce the leakage, the interior surfaces of the concrete were painted with Carboline 305 that reduced the leakage rates to 8 and 6% per day. From this it can be concluded that concrete placed in the conventional manner, even in 4- and 5-ft thicknesses, is pervious to air.

Structural pressure tests were run on one of the concrete cells. The purpose of the tests was to observe and compare experimental with analytical strains and stresses in the reinforcing

steel in the concrete walls. Forty-four strain gauges were placed on the reinforcing steel on both the interior and exterior walls by removing the covering concrete. The cell was treated analytically by homogenizing the steel and concrete into a composite. The steel cross-sectional area was transformed into equivalent concrete area. The moments, shears, stresses, and strains were calculated, using the moment distribution method for longitudinal frame bent, traverse frame bent, and a rectangular box frame, which represented hypothetical 1-ft-wide sections cut vertically or horizontally through the walls and ceiling. A sample calculation is shown in the report. The analytical results and the experimental results were compared at internal pressures of 2, 4, 6, 8, and 10 psig, giving like results at all locations except at reentrant corners. The calculated results were brought into agreement at the reentrant corners by applying the proper stress-concentration factors. The stress-concentration factors produced agreement with measured results at all locations except at the corner of one of the cell entrances. The calculational procedure predicted a compressive strain when, in fact, a tensile strain was measured.

Moisture Separators and Particulate Filters

A recent review in *Power Reactor Technology*, 6(3): 20-21, described an activated-carbon filter that in combination with a particulate filter would constitute the ventilation-air exhaust filter system for the Savannah River Plant (SRP) reactor buildings.[3] These buildings are not pressure-containment buildings; therefore in the event of an accident the released fission products would be carried by the ventilating air through the exhaust filter system where the fission products would be removed. Since the reactors are cooled and moderated by water, a power-surge accident might be expected to introduce entrained water or fog into the ventilation air which could interfere with the particulate system. A report that describes a satisfactory particulate filter and moisture separator to complete the above filter system has been issued.[4]

The filtration system was designed to remove 99+% of the particles of sizes 0.3 μ and larger from the exhaust stream. The exhaust stream that would be expected after a power-surge accident would consist of wet steam for 30 sec at 7000 scfm per filter, followed by 1 lb of water per minute entrained in the exhaust air for a period of 10 days. The rated filter flow is 1000 scfm. Furthermore, the filter system has to work after accumulating dust over a three-month exposure to normal exhaust air.

Preliminary tests on commercially available particulate filters with an air-water fog indicated flooding, with some of the filters rupturing. The amount of water incident on the filters was reduced through the use of moisture separators upstream of the filters. Although the moisture separator removed sufficient water to keep the particulate filter from plugging, it still allowed enough moisture to be incident on the filter to eventually saturate the filter medium. Therefore the filter medium has to have good water-repelling characteristics, good wet strength, and permeability for air in order to continue to function over the length of the accident. The filter must also retain these characteristics when exposed to 90°C air-water fog conditions that are expected following the accident. The details of the tests and the results are presented in the report.

The moisture separator that will be used in the SRP reactor building is 2 ft by 2 ft by 2 in. thick and is rated for 1600 scfm of air at 0.95 in. of water. Each separator is made of several mats of Teflon yarn wrapped over stainless-steel reinforcing wire. The particulate filters, rated at 1000 scfm of air at 0.94 in. of water, consist of 230 sq ft of glass-asbestos fiber medium about 0.02 in. thick with aluminum corrugations separating the folds on both sides. The specifications for both units are given in the appendixes of the report.

Iodine Removal

This is the third in a series of review articles on iodine removal from the atmosphere. The series began in *Power Reactor Technology*, 5(4): 29-33, and continued in *Power Reactor Technology*, 6(3): 20-21. So far these reviews have covered several papers on the behavior of radioactive iodine released in containment buildings and methods of removing this iodine from the building atmosphere to minimize the amount escaping from the building. Several more reports from the United Kingdom Atomic Energy Au-

thority on the removal of iodine from gas streams and containment buildings have been issued.[5–8]

Reference 5 investigates the performance of the scrubber that was originally installed in the cooling system of the British Experimental Pile O to remove iodine from the shutdown flow of air in the event of an accidental release of fission products. Although the caustic soda scrubbers have since been replaced by the more efficient activated-charcoal beds, the test results may be of interest. The scrubbers consisted of four columns with a total cross-sectional area of 26 sq ft, with each column containing a 6.25-ft height of 1-in. mild-steel Raschig rings. The recommended air flow was 3000 cfm with a liquid throughput of 325 gal/min. The scrubber liquor was a 5% caustic soda solution containing some carbonate. The four columns are mounted on a 700-gal horizontal sump tank from which the scrubber liquor is circulated around the scrubber system by a pump that delivers the liquor from the base of the sump tank to each column via a header and feed lines. The air passes countercurrent to the scrubber liquor, entering the bottom of the column and leaving from the top.

Six tests were run to measure the iodine decontamination factor (DF) of the scrubber system. The iodine used in the tests contained a trace amount of radioactive I^{131} that was counted to determine the DF. The first, third, and fifth tests consisted of introducing iodine vapor, by heating sodium iodide, into the air stream just before its entrance into the scrubber. In the second test the iodine vapor was passed over a hot (900 to 1000°C) tungsten wire and then into a glass aspirator where the submicron particles of tungsten and iodine would mix, thus encouraging the iodine to adsorb on the particles. In this way the efficiency of the scrubber for the removal of particulates could be measured. Test 6 was similar except that lead fumes were used to form the submicron nuclei. In test 4 nothing was introduced into the air stream. The measured results in test 4 came from the iodine deposited on the surfaces from previous experiments and absorbed back into the air stream. In test 5 the liquor was changed from caustic soda to sodium carbonate. The test results are shown in Table VI-1.

If test 1 is disregarded, the scrubber appears to give a DF of about 30 for iodine vapor and does not appear to be sensitive to the change in liquor; but tests 2 and 6 show that the DF is reduced by the introduction of particulate nuclei on which the iodine can be adsorbed and pass through the scrubber. In the case of a fuel-element meltdown, presumably many particulate nuclei would be released along with the iodine, thus reducing the effectiveness of the scrubber.

Table VI-1 IODINE DECONTAMINATION FACTOR FOR LIQUID SCRUBBER[5]

Test No.	1	2	3	4	5	6
DF	250	10.5	32	33	29	1.4

Reference 6 discusses the removal of iodine from the atmosphere by sprays; it is primarily a theoretical treatment of the effect of sprays in removing molecular iodine and iodine-containing particles. The molecular iodine is removed from the atmosphere by a water spray primarily by absorption in the water, and the iodine adsorbed on condensation nuclei is removed primarily by the spray by impaction. The two modes of removal require different analytical treatments.

The molecular iodine is assumed to be absorbed by water drops by a diffusion process. It is assumed further that the equilibrium concentration or partition of iodine between air and water follows Henry's law. So that the most efficient use of a water spray can be obtained, each drop should contain an equilibrium concentration of iodine when it reaches the building floor. The analysis shows that equilibrium concentration in the water drop is a function of the water-drop size and the height through which the drop falls. This relation for the attainment of 99% saturation with iodine, for 20 and 100°C water temperatures, is shown in Fig. VI-1. For example, in a containment building that is 10 m in height, the water drops would have to be $<1000\ \mu$ in diameter. The percentage of iodine removed by the water as a function of temperature for several different air-to-water volume ratios is shown in Table VI-2.

It can be seen that for reasonable quantities of water in the spray, very little iodine is actually removed by the spray because of the equilibrium vapor pressure between air and water. The ways suggested for increasing the amount of iodine removed by the spray are (1) continuous removal of the water from the floor of the containment building and (2) combining the iodine chemically in the water.

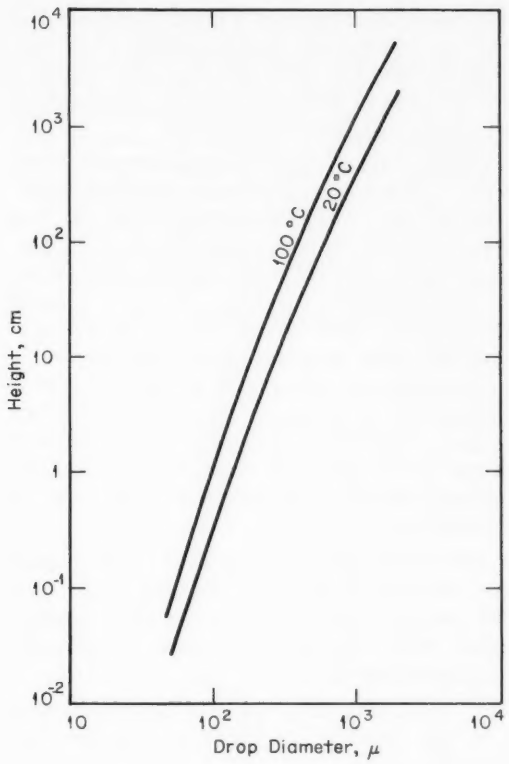

Fig. VI-1 Height in which a falling water drop reaches 99% saturation with iodine.[6]

The iodine and other fission products that are adsorbed on particulate matter in the atmosphere or are released from the fuel in particulate form are removed from the atmosphere mainly by three processes, all of which depend on the size and density of the particles. These processes are (1) diffusion to solid and liquid surfaces, (2) fallout under gravity, and (3) impaction on solid or liquid surfaces. Diffusion is a slow process, and fallout is rapid only for large particles, >10 μ. Sprays can be used to increase the impaction surfaces. Analysis shows that particles of sufficient size and density (>1 μ in diameter and 10 g/cm^3) can be efficiently removed from the atmosphere with drops traversing the atmosphere and impacting with the particles. The calculated removal rates, λ, for 1-, 2-, and 5-μ particles for a water flow rate of 10 g/sec per square meter of floor area for water drops of 100, 200, 500, and 1000 μ, are shown in Table VI-3. The optimum diameter of the water drops in the spray is about 500 μ. If the flow rate is increased to 100 g/(sec)(m^2) the removal rates in Table VI-3 increase by a factor of 10. A flow rate of about 100 g/(sec)(m^2) for 15 min will reduce the air concentration of >1-μ particles to 0.1% of the original concentration.

Table VI-2 IODINE REMOVAL BY WATER AT VARIOUS AIR-TO-WATER VOLUME RATIOS[6]

Air-to-water volume ratio	Iodine removal, %, at the indicated temperature	
	20°C	100°C
1	99	91
10	92	52.5
100	54	9.9
1000	10.5	1.1

Table VI-3 REMOVAL RATES OF PARTICLES BY WATER DROPS[6]

[Water Flow Rate Is 10 g/(sec)(m^2)]

Water-drop diameter, μ	Removal rates (λ), sec^{-1}, at the indicated particle size		
	1 μ	2 μ	5 μ
100	4.5×10^{-5}	1.35×10^{-3}	3×10^{-3}
200	5.2×10^{-4}	4.5×10^{-3}	9×10^{-3}
500	9×10^{-4}	7.2×10^{-3}	1.4×10^{-2}
1000	6×10^{-4}	5.5×10^{-3}	1.0×10^{-2}

Sprays seem to be reasonably efficient in removing molecular iodine and particles of diameter greater than 1 μ but are extremely inefficient in removing the biologically important particles of submicron size. The type of reactor and the method of release seem to have a great deal to do with the chemical nature and the size of particulate iodine released.[9,10] More research on particulate size released from the various types of reactors is required before the effectiveness of sprays can be determined.

A recent British report on the behavior of iodine in low concentrations has been issued.[7] These iodine-release experiments were done in a laboratory with a volume of 1500 m^3. The tests included a measurement of the iodine lost to the laboratory surfaces as a function of time after release, as well as several tests in which absorbers and filters were used to remove iodine from the air.

The iodine loss from the air was assumed to be principally by deposition on the laboratory surfaces and not from leakage or removal by the absorbers and filters that were in operation during the deposition measurements. This assumption is reasonable, since the laboratory was fairly leaktight and of such a size that at least 1000 min would be required to pump all the air in the room through the systems under test. The principal surfaces present in the laboratory are shown in Table VI-4. The reproducibility of

Table VI-4 PRINCIPAL SURFACE MATERIALS AND AREAS IN THE LABORATORY[7]

Type of surface	Area, sq ft
Linoleum (floor)	2,500
Glass	2,500
Asbestos board (walls)	3,500
Painted	13,000
Total	21,500

the concentration of iodine in the air as a function of time was poor. Several runs with an initial iodine concentration of 5 $\mu g/m^3$ gave air concentrations that differed by a factor of 30 early in the run with the difference decreasing to a factor of 10 at 200 min after the iodine release. An explanation for the discrepancy early in the run was that the rate of mixing in the air was quite slow, giving large variations at the sampling position. No explanation was given for the variation at later times. So that the effect of changing the initial iodine concentration could be explored, tests were run in which the initial concentration was varied from 0.5 to 500 $\mu g/m^3$. The resulting ratios of air concentration to initial concentration as functions of time all fell within the spread of the 5 $\mu g/m^3$ results, thus showing no measurable effect of initial concentration. Condensation nuclei from dusty air, as well as nuclei produced by Bunsen burner flames and by burning magnesium, were used to investigate the effects on deposition rate, but again no significant changes were detected. In all tests the prominent feature was the rapid disappearance of the iodine from the air in the room. At the end of the first hour about 98% of the released iodine was no longer airborne, and at the end of 3 hr about 99.7% was no longer airborne. The exact deposition mechanism is not completely understood, but an additional experiment was done to determine if gravitational settling did occur; although the results were not conclusive, they did show that no more than 10% of the total deposition could be accounted for by this mechanism.

Several iodine absorber and filter systems were tested to determine their efficiency in removing low-concentration iodine from air. The types of systems tested were activated carbon, gas coke, magnesite, copper mesh, silver mesh, scrubbers, absolute filters, and combinations of absorbers and filters. The activated-carbon system was most effective. In combination with a good particulate filter, a 2-in.-deep activated-carbon bed was better than any other single system. The filter removes the particulates carrying iodine that pass through the carbon bed, whereas the elemental iodine is removed by the carbon bed.

Reference 8 is a review of the work done on the behavior of iodine by the aerosol group of the Atomic Energy Research Establishment since 1959. The following tests are reviewed and summarized:

1. The behavior of iodine in large containers
2. The behavior of iodine at very low concentrations in air and CO_2
3. Adsorption of iodine on surfaces
4. Adsorption of iodine on particulate matter
5. Adsorption of iodine on charcoal
6. Chemistry of iodine at low concentrations

Also included in the report is a review of the work being done presently and a discussion of work that needs to be done before a complete solution of the problem can be expected.

References

1. R. L. Koontz, C. T. Nelson, L. Baurmash, S. E. Becker, and C. V. Di Pol, Low-Pressure Containment Buildings. Component Tests and Design Data, USAEC Report NAA-SR-7234, Atomics International, Mar. 15, 1963.
2. S. H. Fistedis, A. H. Heineman, and M. J. Janicke, Testing of Containment Capabilities of Reinforced Concrete-Shielded Enclosures, USAEC Report ANL-6664, Argonne National Laboratory, March 1963.
3. G. H. Prigge, Application of Activated Carbon in Reactor Containment, USAEC Report DP-778, Savannah River Laboratory, September 1962.
4. A. H. Peters, Application of Moisture Separators and Particulate Filters in Reactor Containment,

USAEC Report DP-812, Savannah River Laboratory, December 1962.

5. F. G. May and J. B. Morris, Performance of the BEPO Scrubber for Iodine Removal, British Report AERE-M-1163, February 1963.
6. V. Griffiths, The Removal of Iodine from the Atmosphere by Sprays, British Report AHSB(S)R-45, Dec. 3, 1962.
7. J. B. Morris and C. H. Rumary, Tests on Absorbers for Iodine at Low Concentrations, British Report AERE-R-4219, February 1963.
8. A. C. Chamberlain, A. E. J. Eggleton, W. J. Megaw, and J. B. Morris, Physical Chemistry of Iodine and Removal of Iodine from Gas Streams, to be published in *J. Nucl. Energy*.
9. G. W. Parker, G. E. Creek, and W. J. Martin, Fuel Element Decomposition Products, paper presented at Seventh AEC Air Cleaning Conference, October 10–12, 1961, Held at Brookhaven National Laboratory, Upton, N. Y., USAEC Report TID-7627, pp. 263-283.
10. W. J. Megaw, R. C. Chadwick, A. C. Wells, and J. E. Bridges, The Oxidation and Release of Iodine-131 from Uranium Slugs Oxidizing in Air and Carbon Dioxide, *J. Nucl. Energy: Pts. A and B*, 15(4): 176-184 (December 1961).

Section

VII

Power Reactor Technology

Components

Sodium-Heated Steam Generators

A summary report[1] has been compiled on the current state of the art of sodium-heated steam generators. The report contains information on six plant-size units and several model-size units. A general design description, operating experience, and bibliography are given for each unit. A summary of the performance of the plant-size units is given in Table VII-1.

The steam generator for the Experimental Breeder Reactor I (EBR-I) consists of 31 single-tube heat exchangers, each about 10 ft long. Nine exchangers serve as economizers, 18 as evaporators, and four as superheaters. A typical cross section is shown in Fig. VII-1, illustrated as an evaporator. The economizers and evaporators are mounted vertically, and the superheaters are horizontal. The inner tube is of triple-wall construction that consists of two layers of nickel with a copper core. The three individual tubes were assembled, drawn together, and bonded by thermal diffusion to obtain good heat transfer. The water (or steam)

Table VII-1 PERFORMANCE SUMMARY OF PLANT-SIZE STEAM-GENERATOR UNITS[1]

	EBR-I	SRE natural circulation	SRE once through	EFAPP	EBR-II	HNPF
Full-load heat transferred per unit, Mw(t)	3.92	20	20	143	62.5	85 (reentrant)
Type of unit	Falling film	Recirculating pancake tube	Once-through double-wall tube	Once-through single-wall tube	Recirculating duplex tube	Recirculating double-wall tube
Number of units per plant	1	1	1	3	1	3
Steam temperature, °F	529	654	825	780	840	833
Steam pressure, psig	393	600	605	900	1250	825
Feedwater temparature, °F	214	425	311	380	550	304
Feedwater flow per unit, lb/hr	3630	51,500	88,800	476,000	268,000*	251,000
Liquid-metal temperature						
In, °F	583	850	900	820	866	875
Out, °F	419	580	440	520	588	559
Liquid-metal flow, lb/hr	124,700	546,000	718,000	5,300,000	2,500,000	2,820,000
Manufacturer	Argonne National Laboratory	Combustion Engineering, Inc.	Babcock & Wilcox Co.	Griscom-Russell Co.	Argonne National Laboratory	Griscom-Russell Co.

*Blowdown of 20,000 lb/hr.

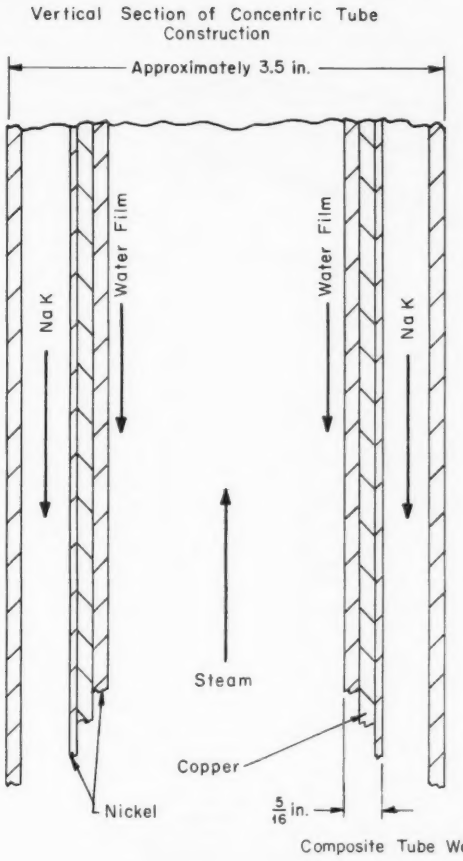

Fig. VII-1 Detail of single-tube evaporator for the Experimental Breeder Reactor I.

flows through the tube, and the NaK flows (countercurrently) through the annulus. Leak detection to the copper core zone is provided at each end of the tubes.

The natural-circulation unit (steam generator) for the Sodium Reactor Experiment (SRE) is made up of two evaporators, one steam drum, and one superheater. The evaporators and superheater are vertical shells filled with many pancake coils stacked on top of each other. A horizontal section of an evaporator, showing a single coil, is illustrated in Fig. VII-2. The evaporator shells are about 5 ft in diameter and about 8 ft high, each containing 48 coils. The coils are of double-wall construction with mercury in the annulus. In the evaporator the inner tube is type 347 stainless steel, and the outer tube is carbon steel. The sodium flows inside the coils, and the steam is generated on the shell side. Water enters at the bottom of the shell, and saturated steam passes out the top to the steam drum and then flows to the superheater. The superheater construction is similar, except that the steam flows inside the tubes and the sodium is on the shell side. Both inner and outer tubes of the coil are type 347 stainless steel. This steam-generation system has been operated up to approximately two-thirds power without significant difficulties.

In the once-through unit (steam generator) for the SRE, the water enters subcooled at one end and emerges as superheated steam at the other end. The unit is a U-shaped shell-and-tube heat exchanger. Sodium flows inside the shell from one end to the other, and the water or steam flows inside the tubes in counterflow. Figure VII-3 shows the general arrangement of the shell and the nozzles and also shows a section view of the tube-sheet design. Double-wall tubes are used with mercury in the annulus. The outside diameter of the outer tube is $^{11}/_{16}$ in. The shell has a diameter of 19 in. and a developed length of 80 ft. Both inner and outer tubes are type 304

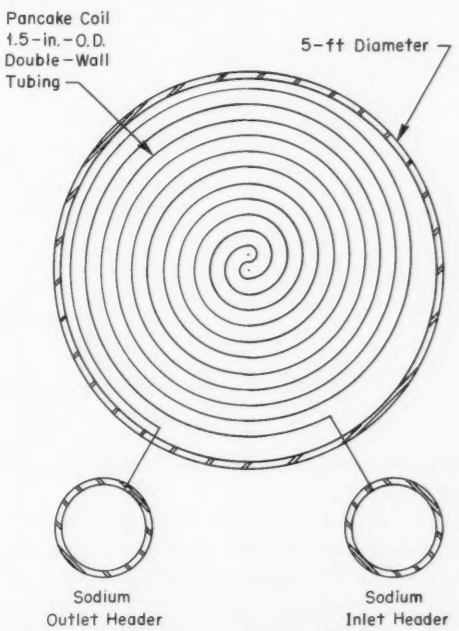

Fig. VII-2 Natural-circulation evaporator for the Sodium Reactor Experiment.

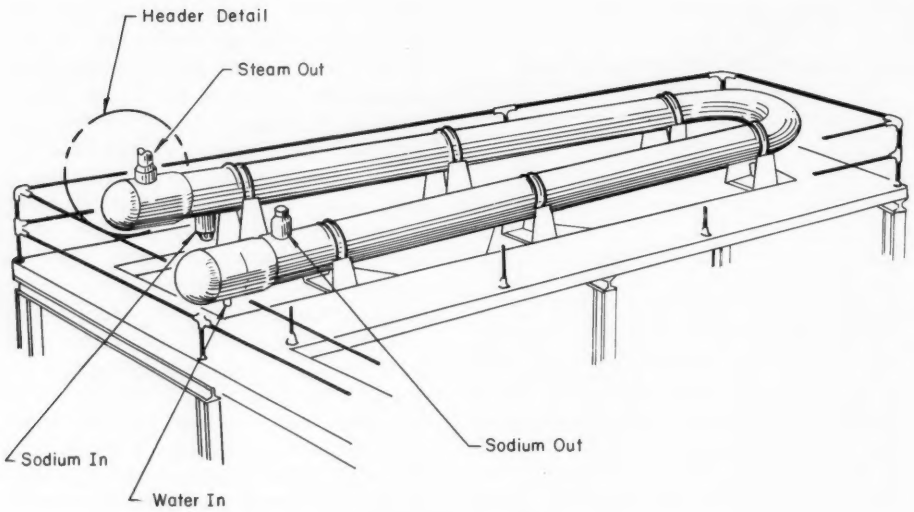

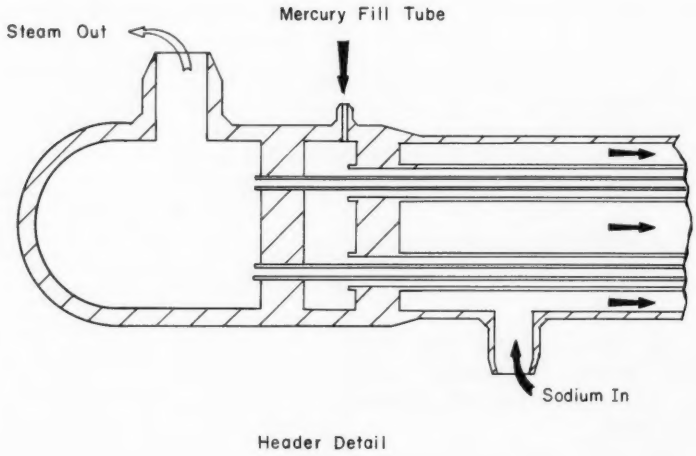

Fig. VII-3 U-tube once-through steam generator for the Sodium Reactor Experiment.[1]

stainless steel, and the shell is the same material.

The unit has operated about 16,000 hr, and for about half of this time the power levels approached 20 Mw(t). During a recent shutdown an inspection was made of the steam-side internals, which disclosed no observable deposits or corrosion. One significant operating phenomenon is the stratification of sodium on the shell side. There are no shell-side baffles (other than eggcrate tube supports), and the denser sodium sinks to the bottom. This adversely affects the uniformity of the outlet steam temperature. The difficulty might be avoided by mounting the U shell vertically.

The Enrico Fermi Atomic Power Plant (EFAPP) has three identical steam generators, one in each coolant loop. The steam generator, schematically shown in Fig. VII-4, is a once-through type unit, with the fluids in counter-

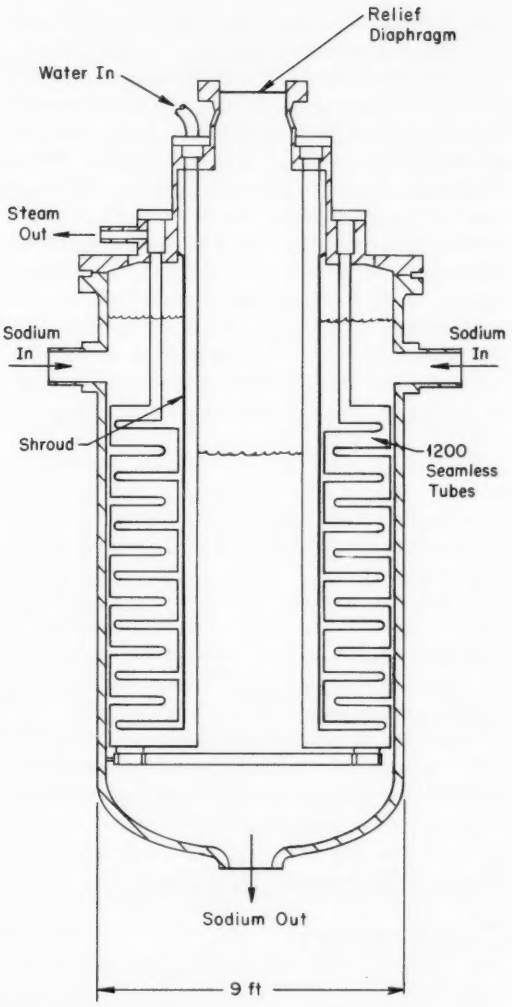

Fig. VII-4 Steam generator for Enrico Fermi Atomic Power Plant.[1]

flow. The sodium enters the shell near the top, flows downward over the tubes, and leaves the shell at the bottom. Each unit has 1200 seamless single-wall tubes that are $\frac{5}{8}$ in. in diameter and 0.042 in. thick; the tube material is 2.25% chromium–1.0% molybdenum alloy steel. The tubes are installed in the form of serpentine involutes, trombone nested in banks of eight. The feedwater enters the tubes at the top center and flows down the straight tubing in the central region of the unit. The water then enters the involutes at the bottom, flows upward, and leaves as superheated steam. Before operation it was discovered that some of the tubes were cracked as a result of stress corrosion. The defective tubes were replaced and stress relieved. The plant has only recently started operation, and no operating experience has been reported.

Banks of shell-and-tube heat exchangers comprise the steam generator for the EBR-II (Fig. VII-5). Eight identical units arranged in parallel form the natural-circulation evaporating section. The saturated steam collects in a steam drum and then flows through two superheater units. The original design specified four superheater units, which were never completed be-

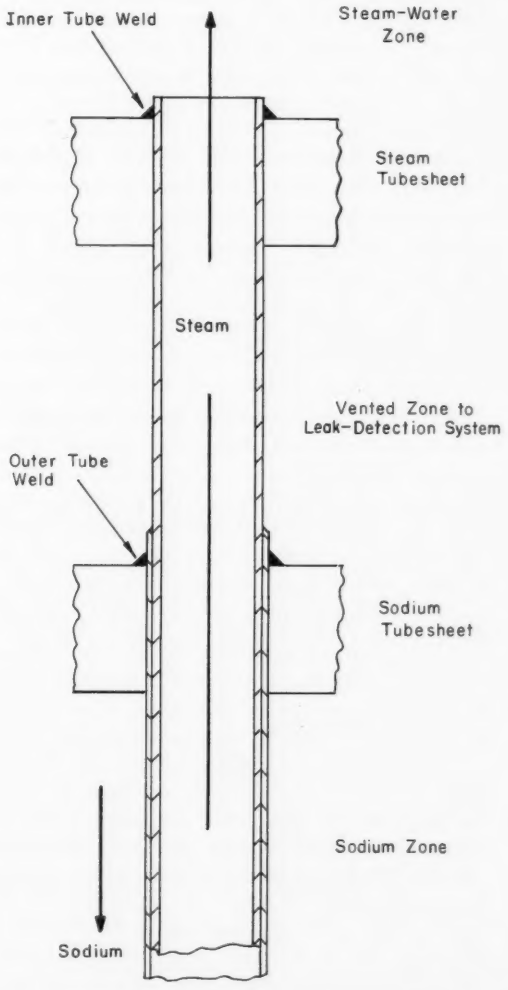

Fig. VII-5 Header detail at top of evaporator for the Experimental Breeder Reactor II.

cause of a tube-sheet welding problem. As a substitute measure two evaporative type units, slightly modified, were fabricated for superheater service. The shells are 20 in. in diameter, 30 ft long, and stand vertically. Sodium, on the shell side, enters at the top and leaves at the bottom. Water flows in at the bottom, and saturated steam flows out at the top. There are 73 double-wall tubes (1.438 in. in diameter) per shell made from 2.25% chromium and 1.0% molybdenum steel. The shell is made of the same material.

Some of the duplex tubes were metallurgically bonded, and some were bonded only mechanically. Figure VII-5 shows the details of assembly of the duplex tubes into the tube sheets. The design specification required that the weld of the outer tube to the sodium tube sheet have a penetration less than the thickness of the outer tube; i.e., there was to be no weld between the outer tube and inner tube in making this joint. This outer-tube weld was successful in the evaporator units with tubes having a wall thickness of approximately 0.10 in. and an outside diameter of 1.438 in. However, a successful weld was never achieved in the superheater units with smaller, thinner tubes (0.052 in. in wall thickness and 0.596 in. in outside diameter).

The design of the evaporators and superheaters incorporated fixed tube sheets. Cold springing of the tubes to satisfy the differential expansion was accomplished by elongating the shell (probably by thermal expansion) about $\frac{1}{8}$ in. during the process of welding the tubes to the tube sheets. Upon completion of that process, the shell returned to its original length, compressing (or springing) the tubes. No operating experience has yet been accumulated with the EBR-II steam generators.

The Hallam Nuclear Power Facility (HNPF) has three steam generators, one in each coolant loop. They feature bayonet type tubes, as shown schematically in Fig. VII-6. The outside diameter of the bayonet is 1.33 in. Tubes of this type are mounted horizontally in two different shells to form the separate evaporator and superheater units of a complete steam generator. A review of these steam generators was presented in *Power Reactor Technology*, 5(3): 46-47. The double-wall-tube material is 2.25% chromium – 1.0% molybdenum alloy steel in the evaporators and 5.0% chromium – 0.5% molybdenum alloy steel in the superheaters. There is no operating experience reported at this time. It is reported[1] that the double-wall construction and leak-monitoring system approximately triple the cost of the HNPF steam generators.

Of the six plant-size steam generators discussed in the report,[1] only one features a single-wall separation between the water and the liquid metal. The other five generators use double-wall construction. Two of these use mercury to create a good thermal bond, and three depend on mechanical and metallurgical bonding to achieve good thermal continuity.

Gas-Heated Steam Generators

In a gas-cooled nuclear power plant, the steam generator is one of the most expensive components, and its design has a strong influ-

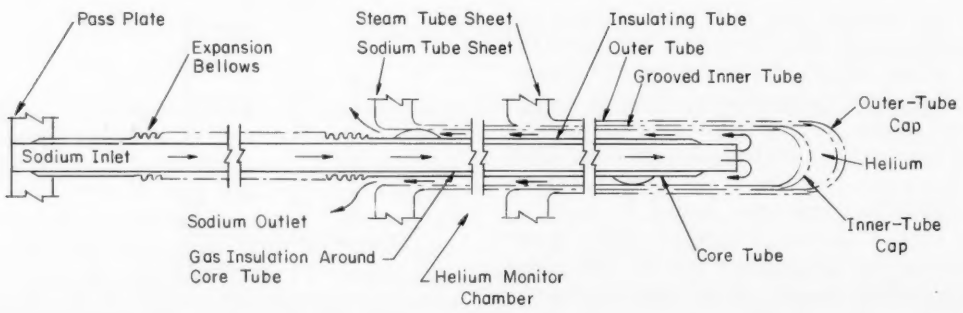

Fig. VII-6 Bayonet tube of the Hallam Nuclear Power Facility steam generator.[8]

ence on the overall plant layout. A parameter study on steam generators for high-temperature gas-cooled reactors has been carried out at Oak Ridge National Laboratory and is reported in Ref. 2. The objective of the study was to provide a sound basis for the optimization of steam-generator design and for the evaluation of the relative merits of major design features. The quantitative study was limited to once-through designs, inasmuch as it was decided that previous design studies had clearly shown the advantages of the once-through type for high-temperature gas-cooled reactor applications. The major parameters of the study were:

1. Axial-flow and cross-flow arrangements
2. Coolant gas (helium, carbon dioxide, nitrogen)
3. Coolant-gas pressure
4. Coolant-gas temperature
5. Steam pressure
6. Steam temperature
7. Tube diameter

The report[2] presents charts to facilitate the design of both axial-flow and cross-flow generators. In addition, it lists 10 important design implications revealed by the study, which may be summarized as follows:

1. When the gas pressure and the mean temperature difference are sufficiently high to give an average heat flux above 30,000 Btu/(hr)(sq ft), the smallest and least expensive steam-generator design employs axial gas flow over bare tubes.

2. Conversely, when the gas pressure and mean-temperature difference give an average heat flux of less than 30,000 Btu/(hr)(sq ft), the smallest and least expensive design employs cross flow of the gas over finned tubes.

3. In axial-flow units the best inside tube diameter is 0.4 to 0.6 in. In cross-flow units there is a tube support problem for tubes smaller than 1.0 in.

4. Croloy tubes should be usable, in suitable designs, for gas temperatures up to 1150 to 1250°F. There is little economic incentive to go to higher gas temperatures that would require refractory alloys, since the higher material cost would offset the thermal advantage.

5. For plants designed to produce steam at pressures of the order of 2500 psi, the reactor inlet gas temperature should be at least 650°F.

6. Important reductions in size and cost in axial-flow units are obtained by increases in gas pressure up to about 500 psi. Above this pressure the benefits of further pressure increases are small.

7. For axial-flow steam generators, the pumping-power-to-heat-removal ratio in the generator should be about 0.5% for minimum cost.

8. The extra cost and complication of a reheater is more than justified by the reductions in fuel-cycle costs and reactor-system capital costs resulting from higher efficiency.

9. A configuration that offers many practical advantages is one using U tubes so arranged that the legs straddle an annular baffle. The hot gas rises up the center and returns downward through the outer annulus, in counterflow to the steam-water.

10. Control considerations indicate that the hot gas temperature entering the steam generator should not be more than 100 to 150°F above the superheated-steam outlet temperature.

In summary:[2] "The results indicate that the least expensive and most promising unit for high-temperature high-pressure gas-cooled reactor plants employs axial-gas flow over 0.5-in.-diameter bare U-tubes arranged with their axes parallel to that of the shell. The proposed design is readily adaptable to the installation of a reheater and is suited to conventional fabrication techniques."

Liquid-Metal Pumps

An electromagnetic pump of unique design has been fabricated and tested at Atomics International.[3] The pump features a rotating magnetic field produced by a mechanically rotating armature, whereas a conventional electromagnetic pump has no moving parts. A schematic cross section of the pump is shown in Fig. VII-7. The liquid flows in an annulus that surrounds the armature, or rotor, and is separated from the rotor and the surrounding magnetic circuit by stainless-steel walls; the rotor thus operates in a normal air environment. The rotor is made of laminated steel plates and is wound helically with field coils, having an appearance similar to the rotor of a d-c motor. The rotor windings are energized by d-c current, and the rotating field induces eddy currents into the liquid metal in the annulus (part *a* of Fig. VII-8). The path of the flux

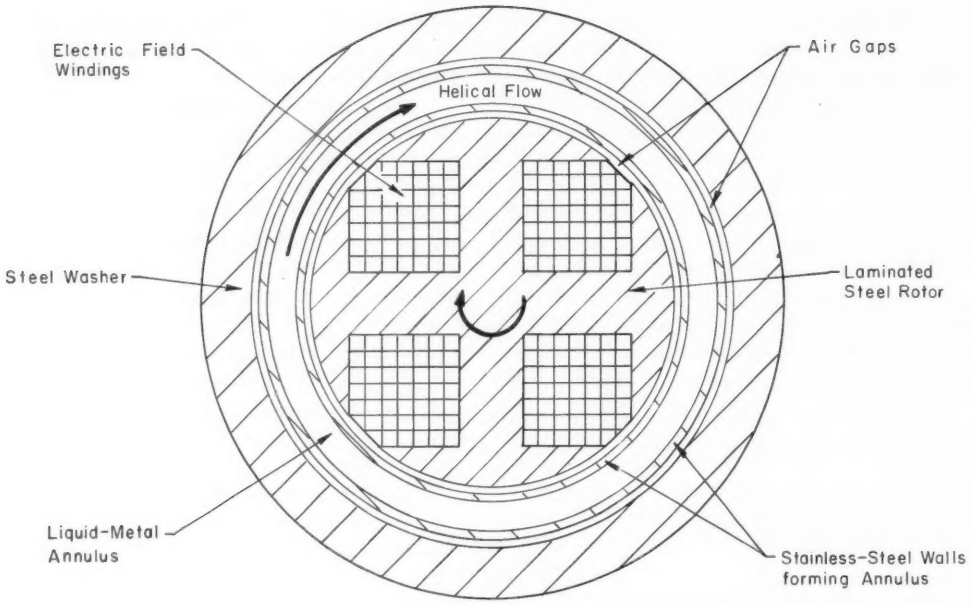

Fig. VII-7 Schematic cross section of helical-rotor electromagnetic pump.

extends radially from the poles through the liquid-metal annulus and connects circumferentially in the outer ring of steel washers (part *b* of Fig. VII-8). The reaction between the moving flux field and the induced current in the liquid metal produces a force on the liquid metal (part *c* of Fig. VII-8), moving it in a helical path, from intake to discharge. With the rotor having a helical configuration, the report[3] indicates that guide vanes are not essential to direct the flow. The helical-rotor electromagnetic pump avoids the necessity for a high-current low-voltage power supply that is characteristic of d-c electromagnetic pumps of conventional types. In addition, it is said to be more efficient than conventional electromagnetic pumps, because the direction of liquid-metal flow is at every point parallel to the driving force. Figure VII-9 shows an exploded view of a typical pump of the helical-rotor type.

A full-size prototype pump has been designed, fabricated, and evaluated in a test loop. The pump delivers 2200 gal of sodium per minute (at 600°F), with a pressure rise of 34 psi and with an efficiency of 26%. The pump completed 1000 hr of testing without loss of performance. The drive motor is rated at 200 hp at 1740 rpm, and the shaft speed is geared down to 374 rpm for the magnetic rotor, which draws 25 amp of direct current at 175 volts.

The report[3] states that the helical-rotor pump can be designed for many applications, ranging from low flows to over 50,000 gal/min, with liquid-metal temperatures up to 2200°F or higher.

Another interesting liquid-metal pump, under development for mobile nuclear plants, is reported in Ref. 4. The application requires high pumping efficiency, small size, low weight, and high reliability. The pump package consists of a shaft-sealed centrifugal pump directly driven by an air turbine. The shaft is vertical, with a single-stage axial-flow air turbine on top and a single-stage unshrouded impeller on the bottom. The shaft is supported with ball and roller bearings that are lubricated and cooled with oil under forced feed. An important feature of the pump is the dynamic shaft seal, in which a liquid-metal-to-inert-gas interface is achieved in a high centrifugal force field.

All the major components have been individually evaluated, and a 3000 gal/min pump has been fabricated and tested using NaK at temperatures up to 1300°F. The report[4] states that the testing has verified the soundness of the

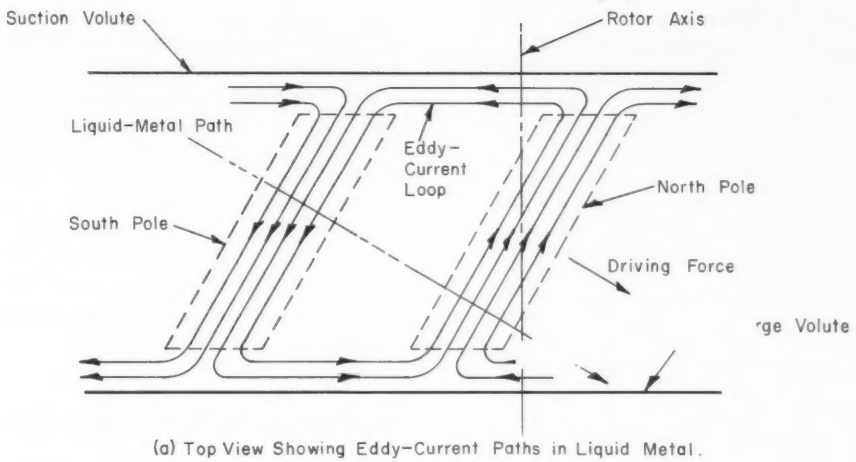

(a) Top View Showing Eddy-Current Paths in Liquid Metal.

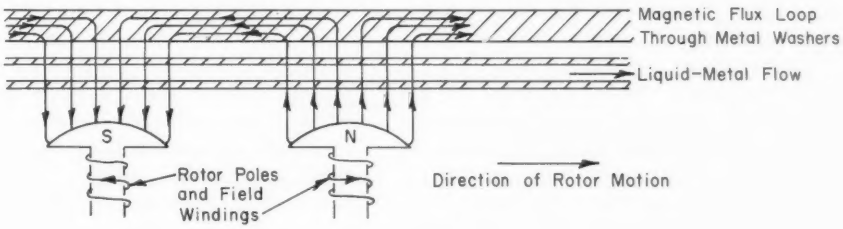

(b) End View Showing Magnetic Flux Paths.

(c) Vector Description of Driving Force on Liquid Metal.

Fig. VII-8 Schematic design of pumping principle.

design philosophy. The air turbine and pump impeller are basically somewhat mismatched (i.e., the turbine should operate at a higher speed and the impeller at a lower speed); however, the simplicity, compactness, and mechanical reliability attained with a single shaft are considered more important than the slight reduction in maximum efficiency due to the mismatch. The dynamic shaft seal proved to operate satisfactorily.

Canned Pump for Organic Service

The development of a canned pump for high-temperature organic service (up to 850°F in Santowax) was completed in the Experimental Organic-Cooled Reactor program (EOCR) before the program was terminated. A description of the pump and its testing program is

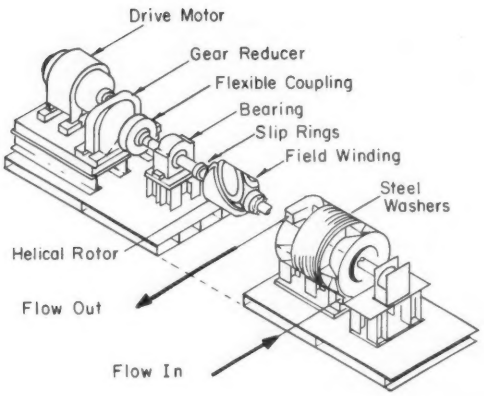

Fig. VII-9 Exploded view of helical-rotor electromagnetic pump.[9]

reported in Ref. 5. Actually two pumps were developed, one having a single pumping stage and the other having two stages; otherwise the pumps were similar. The design flows were 5 and 15 gal/min, respectively. The pump has one moving part, a rotor-impeller assembly completely immersed in Santowax. The pump casing is designed to minimize the intermixing of the fluid between the pump chamber and the rotor cavity; the rotor-cavity fluid is independently circulated through a heat exchanger to remove the bearing and rotor heat. Although the poor lubricating properties of Santowax posed a design problem, the fluid bearings operated satisfactorily during the testing period. The tests have indicated a tendency for gases to build up in the rotor cavity and for overheating to result. This problem has been solved by the installation of a self-venting system. Life tests of the pumps had been planned, but they were not completed because of the termination of the EOCR program.

Butterfly-Valve Cavitation Test

An experimental test program on cavitation in a butterfly valve is reported in Ref. 6. Although critical values for cavitation can be theoretically computed, disagreements were found in the existing calculational and experimental information, and tests were performed to ensure that the throttling valves (butterfly type) in the Pathfinder atomic power plant will always operate in the cavitation-free range. The Pathfinder is a boiling-water reactor with integral superheating. The cooling-moderating water for the core is recirculated through three loops, each having a constant-speed pump, and the amount of recirculation flow is controlled with a 20.5-in.-diameter butterfly valve in each pump discharge line. A similar, but smaller (8-in.-diameter), butterfly valve was tested. The experimentally determined values of the cavitation number were then used to determine the cavitation-free control range of the reactor system valves.

Fuel-Handling Equipment

New equipment for fuel handling has been designed, fabricated, and put into service in the SRE.[7] Although the original fuel-handling machine was well proved with more than 1000 fuel-transfer manipulations, the experience indicated certain areas of weakness in the design which were not only troublesome but which could lead to future difficulties. The new fuel-handling machine will have the following improvements in characteristics and capabilities:

1. Ability to handle deformed or damaged elements
2. Improved cask maintenance and decontamination
3. Decreased cask leakage
4. Improved ability to recover from equipment failure at critical times
5. Ability to inspect cask contents
6. Ability to determine the cask grapple load weight

References

1. Atomic Power Development Associates, Inc., Sodium Heated Steam Generator Summary, USAEC Report TID-18072, Sept. 19, 1962.
2. A. P. Fraas and M. N. Ozisik, Steam Generators for High-Temperature Gas-Cooled Reactors, USAEC Report ORNL-3208, Oak Ridge National Laboratory, Apr. 23, 1963.
3. R. S. Baker, Theory, Design, and Performance of Helical-Rotor, Electromagnetic Pump, USAEC Report NAA-SR-7455, Atomics International, May 31, 1963.
4. R. W. Kelly, G. M. Wood, and H. V. Marman, Development of a High Temperature Liquid Metal Turbopump, *J. Eng. Power*, 85A(2): 99 (April 1963).
5. R. G. Young, Chempump Performance for High

Temperature Organic service, USAEC Report IDO-16844, Phillips Petroleum Company, Mar. 15, 1963.
6. N. P. Grimm, Pathfinder Atomic Power Plant. Butterfly Valve Cavitation Test, USAEC Report ACNP-62004, Allis-Chalmers Mfg. Co., Mar. 20, 1963.
7. E. O. Dryer, E. L. Brown, and W. J. Freede, SRE Reactor Fuel Handling Equipment, USAEC Report NAA-SR-5599, Atomics International, Feb. 1, 1963.
8. Atomics International, Final Summary Safeguards Report for the Hallam Nuclear Power Facility, USAEC Report NAA-SR-5700, Apr. 15, 1961.
9. Electromagnetic Pump, *Mech. Eng.*, 85(5): 70 (May 1963).

Section

VIII

Power Reactor Technology

Design and Construction Practice

Humboldt Bay and Big Rock Point

By Walter Mitchell III

In September 1962 the Big Rock Point Nuclear Power Plant, owned by Consumers Power Company, reached criticality. Five months later unit No. 3 (the nuclear unit) of the Humboldt Bay Power Plant, owned by the Pacific Gas & Electric Company, went into operation. The plants, which were designed and built by the same contractors during roughly the same period, provide an unusual opportunity for comparison, since they have equal ratings and employ variations of the basic boiling-water reactor type. Both plants were built by the Bechtel Corporation as prime contractor to the owners, and the General Electric Company furnished the reactors, turbine-generators, and other electrical apparatus. Each installation consists of a direct-cycle boiling-water reactor, a power-extraction system, and associated service facilities. The reactors are thermal, heterogeneous light-water-cooled and -moderated units that are fueled by slightly enriched UO_2 clad in stainless steel. In both cases bottom-entering control rods are used. The most obvious differences in the plants lie in or result from the methods of coolant recirculation and steam separation: the Big Rock Point reactor[1] is a forced-circulation external-steam-drum unit that is housed in a conventional, spherical steel containment vessel; the Humboldt Bay reactor is a natural-circulation design with internal separation that utilizes the pressure-suppression containment concept. Both plants are designed for an ultimate generating capacity that is about half again as great as the initial capacity of 50 Mw(e), but the values given in the following tables, figures, and discussions pertain to the 50-Mw plants.

	Big Rock Point	Humboldt Bay
Location	Charlevoix, Mich.	Eureka, Calif.
Start of construction	June 1960	November 1960
Date critical	September 1962	February 1963
Thermal power, Mw	157	165
Gross electrical output, Mw	>50	>50
Gross thermal efficiency, %	>31.8	>30.3
Net electrical output, Mw	>47.9	>48.5
Net efficiency, %	>30.5	>29.4
Reactor pressure, psia	1050	1035
Coolant saturation temperature at operating pressure, °F	550.6	549
Turbine pressure, psia	1015	1015

General Mechanical and Hydraulic Characteristics

A comparison of the sizes and arrangements of the reactors and recirculation systems of the two plants is given in Fig. VIII-1, which shows schematic elevations of the nuclear steam-supply systems. The major components are drawn to the same scale to give a size comparison between the nuclear steam-supply system of the external separation forced-circulation reactor and the internal natural-circulation reactor.

The general coolant-flow paths in the two reactors and the numbers of major components in the coolant systems are indicated in Fig. VIII-1. In the Big Rock system, an open bypass connection between the suctions of the two recirculating pumps permits some circulation of water through the two downcomers connected to a pump that is shut down, thus preventing insertion of cold water into the reactor when the pump that has been shut down is started. If both pumps are inoperative but free to rotate, the elevation of the steam drum provides sufficient natural-circulation driving head to per-

mit operation of the Big Rock Point reactor at about 50% load.

The cores of both reactors consist of vertical fuel bundles that are laterally spaced to provide vertical slots for the passage of cruciform control rods. In the Big Rock Point plant, the fuel bundles are unshrouded and fit within flow channels that are semipermanent components of the core structure. The Humboldt Bay bundles have integral shrouds and are held at the top and at the bottom by the permanent core support structure. Thus in principle the Big Rock Point bundles are placed within already formed flow channels, whereas the Humboldt Bay bundles form their own channels. Figure VIII-2 gives horizontal cross sections of the reactor pressure vessels and illustrates the arrangement of the major components of the cores.

Each core flow channel in the Big Rock Point reactor is attached to the top of a support tube. The channel-and-support-tube assemblies, which by virtue of their lateral

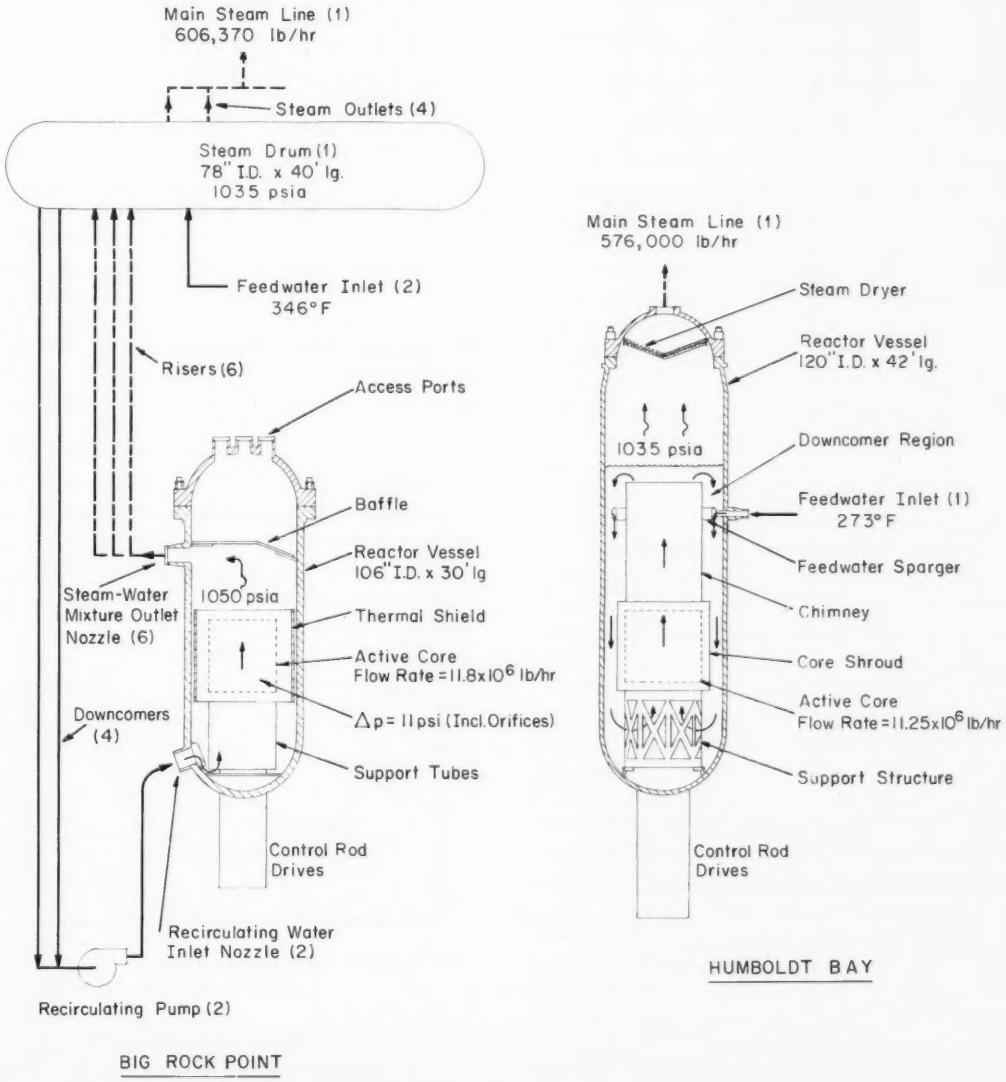

Fig. VIII-1 Schematic elevations of nuclear steam supply systems.

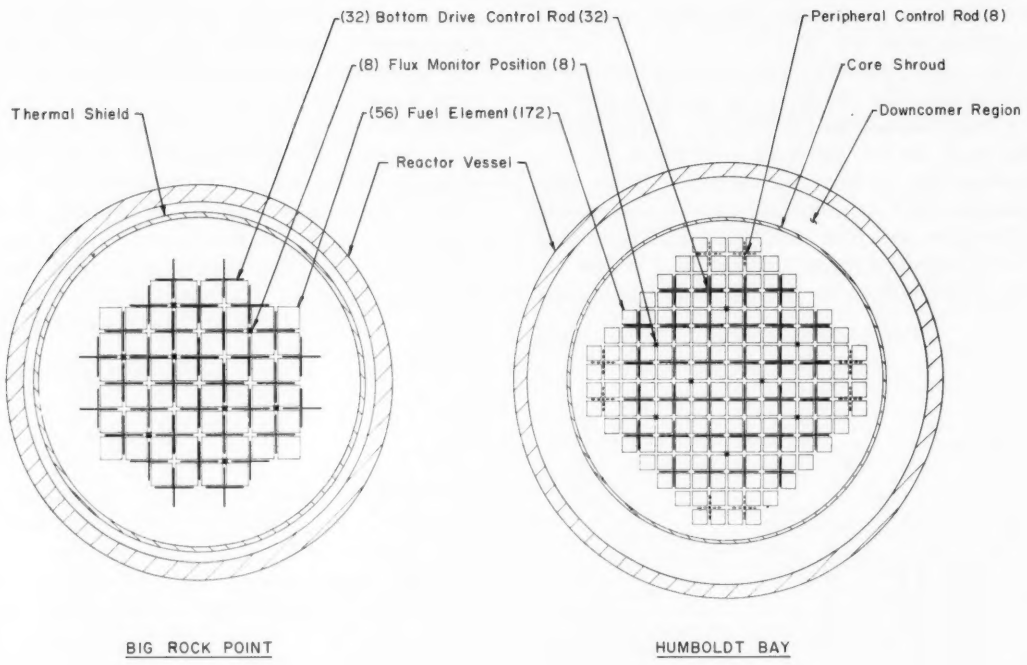

Fig. VIII-2 Horizontal cross sections through reactor vessels.

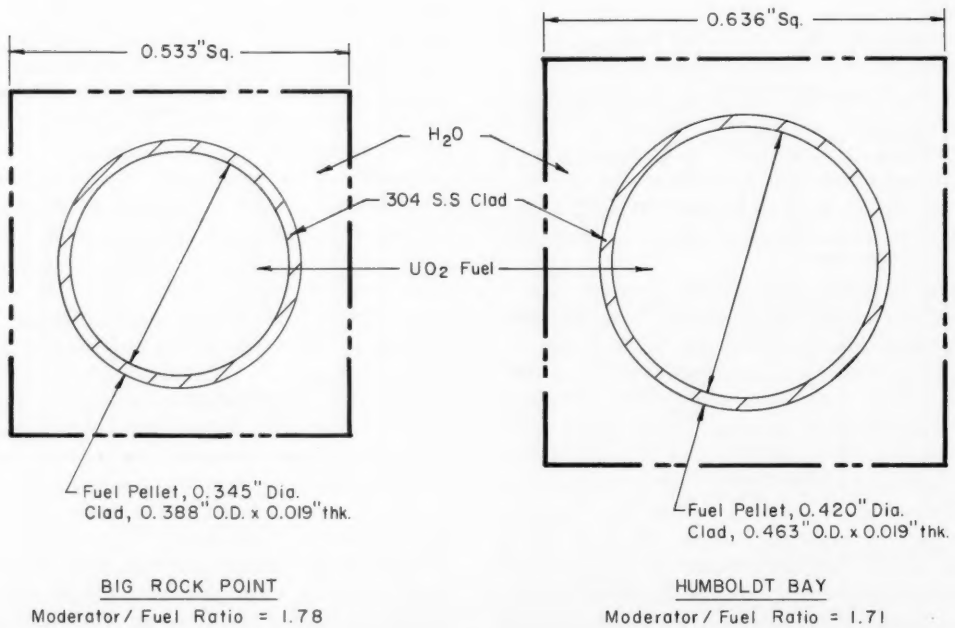

Fig. VIII-3 Cross sections through fuel-rod cells.

spacing provide guidance for the control rods, are positioned by a core support at the bottom and by a guide assembly at the top. The core support is a circular plate that rests on brackets in the reactor vessel near its bottom. The brackets position the core support plate relative to the control-rod-drive penetrations in the vessel bottom head. Support-tube adapters, which align the bases of the channel-and-support-tube assemblies with the control-rod penetrations, are bolted to the support plate. Coolant for each fuel channel enters the bottom of the support tube, which is held clear of the support plate by the adapter. The upper ends of the channel-and-support-tube assemblies are radially supported and are aligned by a top guide assembly that is attached to a thermal shield. The top guide assembly consists of a grid of movable beams that serve as hold-downs for the channel-and-support-tube assemblies but which permit removal of the assemblies through the top of the vessel. The annular steel thermal shield supports the guide assembly and is itself supported by brackets attached to the reactor vessel wall. The baffle plate above the outlet nozzles of the reactor vessel is segmented. The segments can be unlocked and swung upward to allow access to the core from the vessel head nozzles.

At their bottoms the fuel bundles of the Humboldt Bay reactor plug into a core plate that is held by the core shroud. The shroud itself is atop a support structure that is attached to the reactor vessel bottom head. The support structure is perforated and permits recirculation flow from the downcomer region to enter the central part of the vessel, where flow is reversed and the coolant enters the bottom of the active core region. Cruciform guide tubes for the control rods extend from the nozzles in the vessel bottom head to the core plate and furnish additional support. At its top the core shroud supports and positions the chimney structure, which provides radial positioning for the top ends of the fuel bundles. The ring type feedwater sparger located near the top of the chimney structure is supported by brackets attached to the vessel wall.

	Big Rock Point	Humboldt Bay
Reactor vessel		
Height, ft	30	42
Inside diameter, in.	106	120
Wall thickness, excluding cladding, in.	$5\frac{1}{4}$	$4\frac{5}{16}$
Material	Carbon steel	Carbon steel
Cladding thickness, minimum, in.	$\frac{5}{32}$	$\frac{1}{4}$
Cladding material	S.S.	S.S.
Design pressure, psia	1715	1265
Design temperature, °F	650	650
Approximate initial nil ductility transition temperature, °F	10	10
Safety valves, number and location	6, on steam drum	4, on vessel head
Steam drum		
Length, ft	40	
Inside diameter, in.	78	
Wall thickness, excluding cladding, in.	$4\frac{3}{8}$	
Material	Carbon steel	
Cladding thickness, minimum, in.	$\frac{5}{32}$	
Cladding material	S.S.	

Core Details

The basic fuel units in both reactors are rod type elements, made up of stainless-steel tubes containing stacks of cylindrical UO_2 pellets. Figure VIII-3 shows a cross section of a typical rod-moderator cell for each reactor and gives dimensions and moderator-to-fuel ratios of the cells. Most of the fuel rods in both reactors are of full core length. Pellets of UO_2 are placed in the jacket tube in an uninterrupted stack, and a plenum is provided at the top of the stack to accommodate expansion and released fission gases. A coil spring and wafer in each plenum keep the stack of UO_2 pellets in the proper position, and welded plugs are used to seal the fuel rods at each end.

The fuel rods are arranged in a square array to form the fuel bundles shown in Fig. VIII-4. The rods are positioned at the top and at the bottom by fittings that form the handles and bases of the bundles, and wire spacers provide radial spacing at three axial locations in each bundle. The spacers, each of which consists of a double layer of crimped wire grids and a surrounding band, are positioned axially by special, segmented fuel rods that fit through sleeves in the spacers. The Big Rock Point bundle has four of these segmented rods, one at each corner, whereas the Humboldt Bay bundle uses a single segmented rod at its center. Construction of the segmented rods is similar to that of the full-length rods but with correspondingly shorter fuel and plenum lengths. The Big Rock Point bundle is held together axially by 32 fuel rods with special, threaded end plugs which screw into the base of the bundle and which are attached to the bundle handle with safety-wired nuts. In the Humboldt Bay bundle, eight rods are used in a similar manner, and the integral flow shroud adds stiffness to the assembly. In

both bundles the rods not used for axial restraint have unthreaded end plugs that slide into holes in the top and bottom fittings. Springs are installed between all rods and the top fitting to accommodate thermal expansion. The Big Rock Point bundle, which has no integral flow liner but fits into a fixed flow channel in the reactor core, is equipped with pad type external spacers on each of the three axial spacer assemblies. Each Big Rock Point bundle has 12 special fuel rods, three in each corner of the bundle, which are smaller in diameter and have thicker jackets

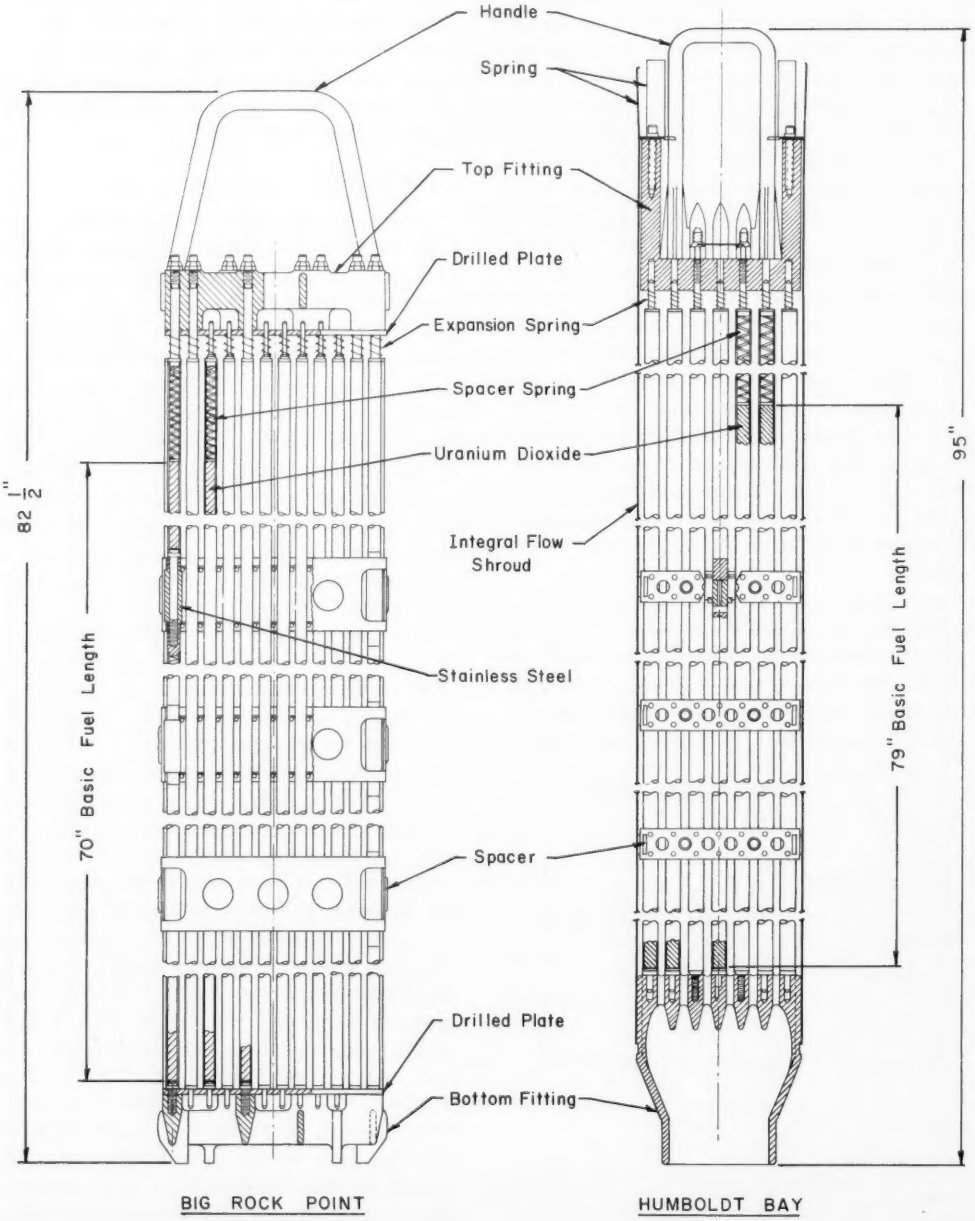

Fig. VIII-4 Fuel bundles.

than the standard rods, to reduce the power peaking caused by the water in the control-rod channel (see Fig. VIII-5). These 12 special rods include the four segmented rods used to support the wire-spacer assemblies. Their dimensions are shown in Fig. VIII-5, which is a horizontal section through a typical portion of the core.

The control rods for both reactors are made up of poison tubes containing boron carbide which are assembled into a cruciform structure by a surrounding steel sheath, as indicated in Fig. VIII-5. These control elements are similar to those in the Dresden reactor which were described in *Power Reactor Technology*, 5(3): 34. The control rods are guided on the four core

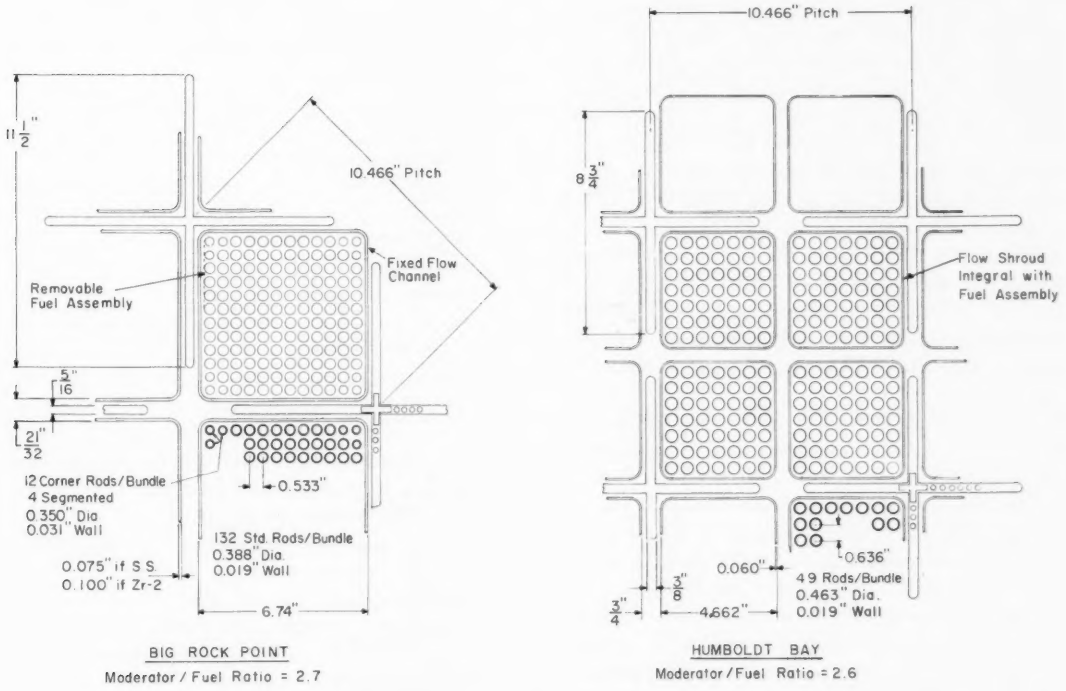

Fig. VIII-5 Horizontal cross sections through typical core regions.

The geometrical relations between the major components of the cores of the two reactors are illustrated by Fig. VIII-5. The components include the groups of fuel rods, as provided by the fuel bundles; the flow channels, which are defined by the integral fuel-bundle shrouds in the Humboldt Bay core and by the preinstalled flow channels in Big Rock Point; the control-rod passages, formed by the radial spacing of the fuel-element or flow-channel assemblies; and the control rods themselves. In the Big Rock Point core, the flow channels may be either stainless steel or Zircaloy, depending on the core loading and the shutdown control requirements. The thicknesses of the channels of both materials are shown in Fig. VIII-5.

channels that they contact by stellite rollers at the top and bottom of each blade. Heat generated in the poison rods is removed by coolant that flows through holes in the sheaths and by contact heat transfer from the rods to the sheaths.

In addition to the regular, bottom-driven control rods shown in Fig. VIII-5, the Humboldt Bay reactor can be equipped with a system of peripheral control rods. These cruciform rods enter the core from the top and are provided to assure that an adequate cold shutdown margin is available even if any one of the central, bottom-driven control rods sticks in the withdrawn position. It was found that the peripheral control rods were not needed with the first core of the Humboldt Bay reactor. Consequently rods

and drives were removed from the vessel prior to power operation.

Both reactors are provided with liquid-poison injection systems that provide a backup means of shutting the reactor down and holding it subcritical in the event that the control rods are not able to do so. Both systems, which are pressurized by bottled nitrogen gas, utilize sodium pentaborate solutions.

As mentioned above, either stainless-steel or Zircaloy flow channels can be used in the core structure of the Big Rock Point reactor. It is intended that the stainless-steel channels be used during initial operation of the reactor to reduce the excess reactivity that will exist prior to the establishment of an equilibrium program of partial-core refueling. The initial core of the Humboldt Bay reactor will contain up to 96 poison curtains which are made of borated stainless steel and which are hung from the top grid in such a way that they surround groups of four fuel assemblies. The curtains will be removed during the life of the first core to maintain reactivity.

	Big Rock Point	Humboldt Bay
Fuel and core		
Fuel material	UO_2	UO_2
Initial enrichment, % U^{235}	3.2	2.6
Weight of UO_2 in core, lb	19,300	34,600
Average fuel exposure, first core load, Mwd/ton of U	10,000	10,000
Equivalent core diameter, in.	62.5	77.5
Active core height, in.	70	79
Fuel-rod array in bundle	12 by 12 square	7 by 7 square
Number of bundles in core	56	172
Reactivity requirements		
Temperature, Δk_{eff}	0.025	0.015
Voids, Δk_{eff}	0.019	0.021
Xenon and samarium, Δk_{eff}	0.031	0.031
Fuel depletion and maneuvering, Δk_{eff}	0.127	0.133
Initial reactivity requirement, Δk_{eff}	1.202	1.200
Control elements		
Number of central control rods	32	32
Number of peripheral control rods		8
Shape of peripheral control rods		Cruciform
Control-rod poison material	B_4C	B_4C
Number of poison curtains (maximum)		96
Shape of poison curtains		Plate
Poison-curtain material		Borated S.S.
Single control rod, maximum worth, $\Delta k/k$	0.042	0.038
Liquid poison		
Material	Sodium pentaborate solution	
Volume, gal	850	365
Worth, $\Delta k/k$	0.25	0.20

Heat Removal

In view of the differences in the basic modes of operation of the reactor plants, their heat-removal and steam-generation characteristics are of particular interest. A comparison of the principal thermal characteristics of the two systems is given in the following table.

	Big Rock Point	Humboldt Bay
Average power density, kw/liter	45	27
Peaking factors		
Gross	1.94	2.62
Local	1.65	1.38
Overpower	1.27	1.25
Maximum at overpower	4.07	4.53
Linear power density, kw/ft of fuel rod		
Average	3.34	2.97
Maximum	10.5	10.8
Maximum at overpower	13.3	13.5
Fuel-jacket heat flux, Btu/(hr)(sq ft)		
Average	110,000	80,600
Maximum	352,000	292,100
Maximum at overpower	447,000	365,100
Burnout ratio, minimum at overpower	1.5	2.0
Coolant flow rate through core, 10^6 lb/hr	11.8	11.25
Core inlet subcooling, Btu/lb	14.0	12.1
Core inlet velocity, ft/sec		
Maximum	6.3	4.56
Minimum	5.1	4.37
Steam volume fraction		
Average core exit	0.41	0.48
Maximum channel exit	0.57	0.64
Average over core length	0.21	0.20
Average steam quality, core exit, %	4.9	6.3
Steam quality entering drum, %	5.2	
Average steam surface separation velocity, ft/sec		0.90
Average downcomer velocity, ft/sec		1.73

Effects of Circulation Mode on Reactor Design

The difference in performances that are achievable with natural and forced circulation is most clearly apparent in the comparison of core power densities in the preceding tabulation, where the power density in the Big Rock core is shown to be 1.67 times that in the Humboldt Bay core. Since the inlet subcooling is nearly the same in both cases and since the steam-void fractions do not differ greatly, the improvement in power density in the Big Rock reactor can be regarded rather directly as the benefit received from forced circulation — at least to a first approximation. That is to say,

both reactors use about the same total coolant flow rate (see table), but to achieve this total, the natural-circulation core must provide a larger cross-sectional area for coolant flow. The actual situation is not quite as simple as that, since the Humboldt Bay core is some 13% longer than that at Big Rock Point, and the design relations that involve core length as a variable are not simple ones.

The fuel arrangement and design must, of course, be compatible with the heat-transport capabilities of the coolant system. Apparently the fuel centerline temperature is the limiting consideration in heat removal from the fuel elements in both cores. For ceramic fuel elements of a given basic design this consideration sets, to a good first approximation, the maximum power that can be extracted from a unit length of fuel element. The preceding table shows that the maximum power generation per foot of fuel element is very nearly the same for the two cores. If one considers, for simplicity, that the designer has fixed the coolant-flow area in a way that is characteristic for the type of recirculation (natural or forced) to be used, then he has left the interdependent design variables of fuel-rod diameter and moderator-to-fuel ratio to vary in order to match the required total length of fuel rod with the required coolant-flow area. Either one of these may be chosen freely but not both. In the cases considered here, the designers have chosen very nearly the same moderator-to-fuel ratio for the two cores (see Fig. VIII-5). This choice strongly involves the interrelated reactor physics characteristics of steam-void coefficient of reactivity, temperature defect, and fuel enrichment. Once a moderator-to-fuel ratio has been chosen, there is no longer any room for variation of fuel-rod diameter. In the cases considered here, where the moderator-to-fuel ratios are nearly equal, it is clear that the fuel-rod diameter must be smaller in the Big Rock core if advantage is to be taken of the higher coolant-flow velocity provided by the forced-circulation system.

In the forced-circulation case the coolant-flow velocity is a design parameter that the designer may vary at will for design optimization. Presumably the power density in a core like that of Big Rock Point could be increased still further by increasing the coolant-flow velocity along with other design modifications. If the linear power-generation limit for the fuel elements is considered fixed, one might increase the power density by moving the fuel rods closer together and increasing the coolant-flow velocity. This would decrease the moderator-to-fuel ratio and increase the steam-void coefficient of reactivity, the temperature defect, and the fuel-enrichment requirement. Or one might hold the moderator-to-fuel ratio constant, decrease the fuel-rod diameter, and increase the coolant flow. The major considerations in such a design variation would be the increase in fuel-fabrication cost (per kilowatt-hour), the increased neutron absorption in the fuel jackets (unless they were made proportionately thinner), and possibly the fuel-rod support problems.

Naturally the attractive way of increasing the power density in the forced-circulation case is to employ increased coolant flow (if necessary) in conjunction with fuel elements of the same size but higher power rating. Work toward the development of fuel elements of higher capability for the Big Rock Point reactor is reviewed in Sec. III of this issue of *Power Reactor Technology*.

Although high power density in the core has some advantages per se, the more important consideration is perhaps the size of the reactor vessel required for a given power generation. Here the external steam separation employed in the Big Rock Point plant would be expected to show an additional difference because considerations of recirculation flow do not determine the amount of space that must be left between the reactor core and the pressure-vessel wall. The consideration of fast-neutron shielding for the vessel wall does, of course, remain and is quite significant in determining the pressure-vessel diameter.

The comparison of reactor cross sections in Fig. VIII-5 does not show any important difference in the thickness of annulus between core and vessel. The reason for this is not apparent, but, in this case of relatively new, relatively small reactors, a number of possibilities could be visualized having little fundamental significance. It is in reactors of dimensions that begin to push the limits of pressure-vessel size that large incentives for high effective power density may develop. Now it is perhaps more to the point to examine the details of the recirculation phenomena in the natural-circulation circuit of the Humboldt Bay reactor.

The average velocity in the downcomer of the Humboldt Bay reactor is given[2] as 1.73 ft/sec.

One would judge, from quoted dimensions and flow rates, that this downcomer velocity occurs in the annular area around the chimney, and that the term "average" indicates an average over the flow area at that level. In the regions below the feedwater inlet sparger and opposite the active core region, where the core shroud forms the inner boundary of the downcomer, the flow area is decreased, and the average velocity must be considerably higher. The velocity near the top of the chimney has, of course, the greatest interest because it is in that region that the effects of velocity on gravitational separation determine the amount of carry-under in the recirculation flow. Apparently the degree of carry-under experienced is much less than that found in the small-scale steam separation tests at Argonne National Laboratory, which have been reported in Ref. 3 [reviewed in *Power Reactor Technology*, 6(2): 69-74]. In those tests the ratio of steam quality in the downcomer to that in the riser was found to be about 0.7 at 1000 psi for a downcomer velocity of 1.73 ft/sec. The successful operation of the Humboldt Bay plant can be taken as evidence that the actual ratio is not nearly that high. Estimates based on the data given in Ref. 2 indicate that the design expectation for the downcomer-to-riser quality ratio was no higher than 0.28.

The different coolant-recirculation approaches at Big Rock Point and Humboldt Bay give rise to certain incidental features of reactor design which are worth notice in passing.

Since the forced-circulation scheme of the Big Rock Point reactor permits the core to have a relatively high pressure drop, each flow channel in the core is provided with an orifice at its bottom. Although the orifices could be used to match the flow distribution to the radial power distribution, they are installed primarily to increase the single-phase pressure drop of the core. The effect of the increased single-phase pressure drop is to make individual channel flow less dependent on power, thus improving the burnout ratio and parallel channel stability. The pressure drop across the orifice is equal to slightly more than one-third of the pressure drop across the remainder of the core channel.

The lifting forces imparted to the fuel bundles by the upward-flowing coolant are small enough in both reactors that no positive fuel hold-down mechanism is required. In the Big Rock Point reactor, whose fuel bundles fit in semipermanent

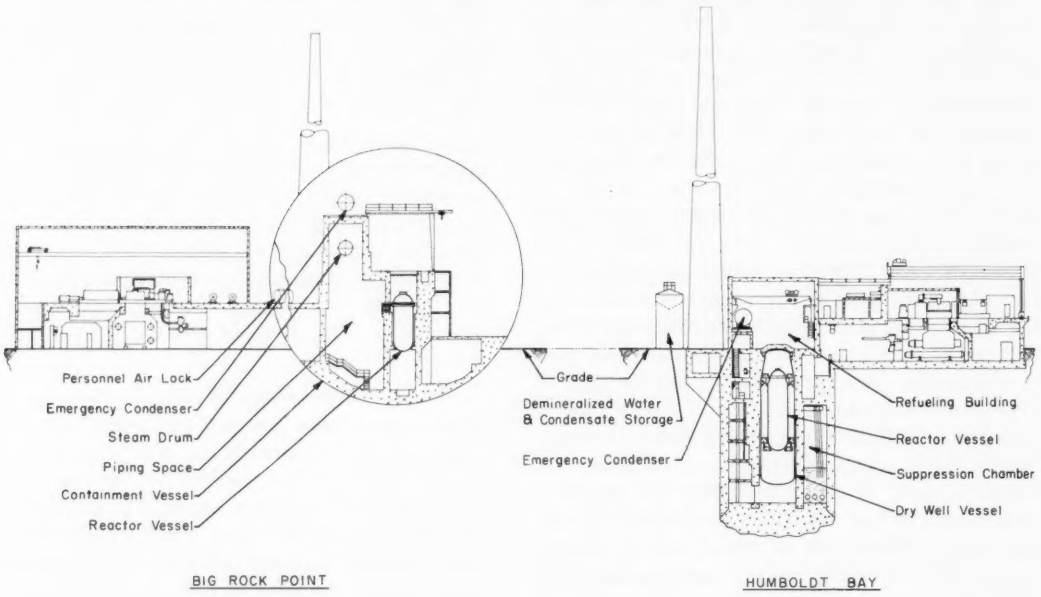

Fig. VIII-6 Plant cross sections.

flow channels of the reactor core structure, no bundle hold-down is used. In the Humboldt Bay core, where the control-rod channels are formed by the integral shrouds of surrounding fuel bundles, hold-down latches are provided for those fuel bundles which adjoin bottom-driven control rods. Consequently, if a control rod jams against a fuel bundle, the bundle cannot be lifted from the core as insertion of the rod is attempted.

One of the differences in the plants is the accessibility of the core for shutdown operations such as refueling. In Big Rock Point, ports in the vessel top head provide access to the core, although the normal refueling procedures include removal of the head. The steam dryer in the Humboldt Bay reactor has a removable center section, which permits access to the vessel internals without the necessity of removing the head.

Plant Arrangement and Containment

The basic differences in coolant schemes in the two reactors lead to striking differences in plant arrangement and containment design, for the external steam drum approach used at Big Rock Point would not fit gracefully into the pressure-suppression concept employed at Humboldt Bay. The differences are illustrated in Fig. VIII-6, which gives simplified vertical cross sections of the two plants to the same scale. In addition to showing the inherent differences in appearance of the forced-circulation plant and the internal natural-circulation plant, the drawing illustrates the conventional containment scheme employed in the Big Rock Point plant and the pressure-suppression containment utilized for Humboldt Bay.

The Big Rock Point containment vessel was designed and constructed in accordance with the *ASME Boiler and Pressure Vessel Code*, Secs. II, VIII, and IX, as modified by applicable nuclear code cases. The vessel is typical of the conventional type, except that its exposed exterior surface is insulated with a cork mastic coating protected by acrylic resin. The insulation prevents excessive temperatures inside the vessel that are caused by solar radiation, reduces heat loss in winter, provides atmospheric corrosion protection, and reduces inside surface condensation. The application of the pressure-suppression concept to the Humboldt Bay reactor was described in *Power Reactor Technology*, 6(3): 27, and will not be discussed further.

Big Rock Point	
Diameter of containment sphere, ft	130
Height above grade, ft	103
Approximate free volume, cu ft	940,000
Design pressure, psia	41.7
Design maximum temperature, °F	235
Maximum leakage rate at design pressure, %/day	0.5
Number of access air locks	3
Total number of penetrations	100
Diameter of nozzle penetrations, in.	
Maximum	24
Minimum	0.75
Humboldt Bay	
Dry well	
Vessel inside diameter, ft	17.5
Vessel overall height, ft	68
Design pressure, psia	86.7
Maximum leakage rate at design pressure, %/day	0.1
Suppression chamber and pool	
Chamber total volume, cu ft	54,300
Air space volume, cu ft	33,400
Water volume, cu ft	20,900
Vent pipe submergence, ft of water	6
Water temperature, °F	80
Air space internal pressure rating, psia	24.7
Internal pressure capability of concrete structure, psia	39.5
Maximum leakage rate at 24.7 psia, % of free-air volume per day	1.0
Refueling building	
Volume, cu ft	192,000
Minimum exterior wall thickness, in.	12
Maximum inleakage rate at a negative pressure of $\frac{1}{4}$ in. water, cfm	134

Turbine-Generator, Condensate, and Feedwater Systems

The power system for each plant includes those components which convert steam into electric power and which provide feedwater for the reactor. The major components of the systems are shown on Fig. VIII-7, which presents simplified flow diagrams for each plant. Each system utilizes a tandem-compound double-flow

	Big Rock Point	Humboldt Bay
Turbines		
Speed, rpm	3600	3600
Rating, kw	54,500	50,000
Inlet pressure, psia	1015	1015
Exhaust pressure, in. Hg abs.	3.5	3.5
Generators		
Rating, kva	70,588	70,588
Voltage	13,800	13,800
Power factor	0.85	0.85
Short-circuit ratio	0.80	0.70
Hydrogen pressure, psia	45	45
Main condensers		
Condensing surface area, sq ft	27,500	30,700
Condensing capacity during load rejection, lb/hr	948,000	810,000
Hot well capacity, gal	6000	6500
Condensate demineralizers		
Number	3	3
Size, each	Half capacity	Half capacity
Maximum flow rate, gal/(min) (sq ft)	50	50

saturated-steam turbine, which is connected directly to a hydrogen-cooled generator. Each turbine is equipped with external moisture separators in the crossover between the high-pressure and low-pressure sections, and three extraction points are provided. At its initial power rating, the Humboldt Bay system uses only two extractions: the third point can be used with a high-pressure feedwater heater to increase efficiency. The main condenser in each

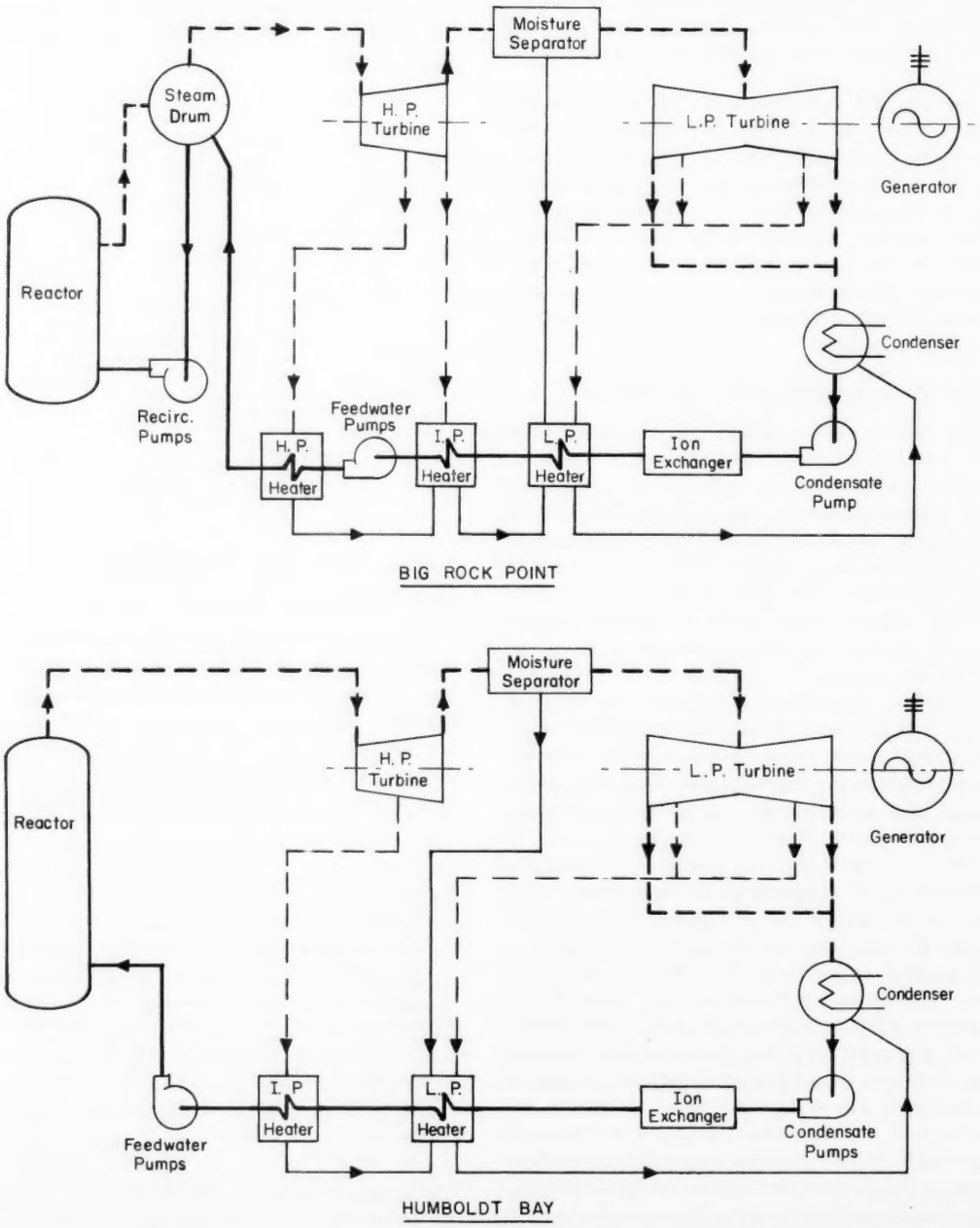

Fig. VIII-7 Simplified flow diagrams.

system is a horizontal, single-pass divided-water-box deaerating type unit of conventional construction. The condensers can accept bypass steam at reduced pressure, and they have oversize, baffled, storage type hot wells that provide a holdup time for the decay of short-lived radioactivity in the condensate. The air- and gas-removal equipment of the condensers discharges to the main exhaust stacks through oversize pipes that provide en route holdup time for further decay of radioactivity. Full-flow ion exchangers are located in the condensate system of each plant.

Control and Instrumentation

The mode of control for the plants is one in which the turbine follows the reactor output rather than system load changes. The basic control device for the turbine is an initial pressure regulator, and during normal operation the turbine admission valves are controlled by this regulator. The steam bypass valve is normally closed, and so all reactor steam flow is passed through the turbine. The occurrence of abnormal conditions, such as turbine trip, results in the opening of the bypass valve and the dumping of steam directly to the condenser. If a sudden loss of electrical load results in turbine overspeed, a speed-governor signal overrides the initial pressure-regulator signal. The governor signal initiates sufficient closure of the turbine admission valves to obtain acceptable turbine speed, but this admission-valve closure causes the reactor pressure and reactivity to rise. The increase in reactor pressure generates another signal, which opens the turbine bypass valve and dumps steam to the condenser, thereby lowering reactor pressure.

The reactor operator adjusts reactor power level by manual operation of the bottom-driven control rods. Each rod is provided with its own hydraulically operated drive mechanism that is mounted vertically in a thimble welded to one of the reactor bottom head nozzles. The basic concept of the drive mechanism is one in which a double-acting piston and a drive shaft are attached to each cruciform control element. Differential pressures across the piston are used to drive the rod into or out of the core, and a ratchet type locking device is used to hold the drive (and rod) at set positions when driving pressures have been removed. The ratchet does not interfere with insertion of the control rod into the core but must be unlatched in order to withdraw the rod. Maximum withdrawal rate of a rod is 3 in./sec, and speed of movement is controlled by a flow-metering device in the hydraulic circuit. Signals indicating control-rod positions are initiated by indicator mechanisms housed within the drive sections of the rods. A mechanism consists of a series of fixed, magnetically operated switches, each of which indicates a discrete rod position, and a permanent magnet which is carried on the rod-drive piston and which actuates the switches.

A vertical cross section of a control-rod-drive mechanism of the Big Rock Point reactor is given in Fig. VIII-8. The mechanism is representative of the assembly used in Humboldt Bay as well as Big Rock Point, and both drives are modified versions of a design originally developed for the Dresden reactor. High-pressure water, which is the actuating fluid for the hydraulic drive unit, is introduced at one of two inlet ports of the mechanism, depending on the desired direction of movement of the control rod. Internal passages in the unit direct the actuating fluid to either the top or the bottom of the piston, resulting in an unbalanced force that causes the piston to move.

The components of the ratchet type locking device are shown near the top of the mechanism in Fig. VIII-8. A collet assembly, which consists of a piston and locking fingers, is spring and gravity loaded to remain in the down position as shown on the drawing. In this position, the collet fingers engage ratchet notches in the drive piston and lock the control rod in place, thereby permitting the hydraulic driving pressures to be removed from the drive mechanism. If scram or normal insertion of the rod is desired, admission of hydraulic fluid to the up inlet will accomplish the desired movement without interference from the collet assembly. However, inadvertent opening of the valve in the down hydraulic line cannot cause rod movement out of the core. To withdraw the rod from the core, a momentary up pressure must be applied to the mechanism; this up pressure causes the collet fingers to move outward and to unlatch as the rod begins to move upward. The admission of down fluid to the unit then places a downward-acting force on the drive piston and an upward-acting force on the collet assembly. Consequently the collet assembly moves up, causing the collet fingers to be held clear of the ratchet notches of the piston rod, thereby

permitting the drive piston to move down. When the control rod has moved down to the desired position, the control valve of the down hydraulic fluid line is closed, and the drive mechanism is isolated from the control pressure. With the pressure removed the collet assembly returns to its normal position, and the collet fingers reenter the locking notches on the piston rod. Pressure within the control-rod drives is such that approximately 30 psi differential above reactor pressure is applied to the bottom of the pistons. This is not enough pressure to force the control rods into the core, but it does provide leakage past the drive seals for cooling.

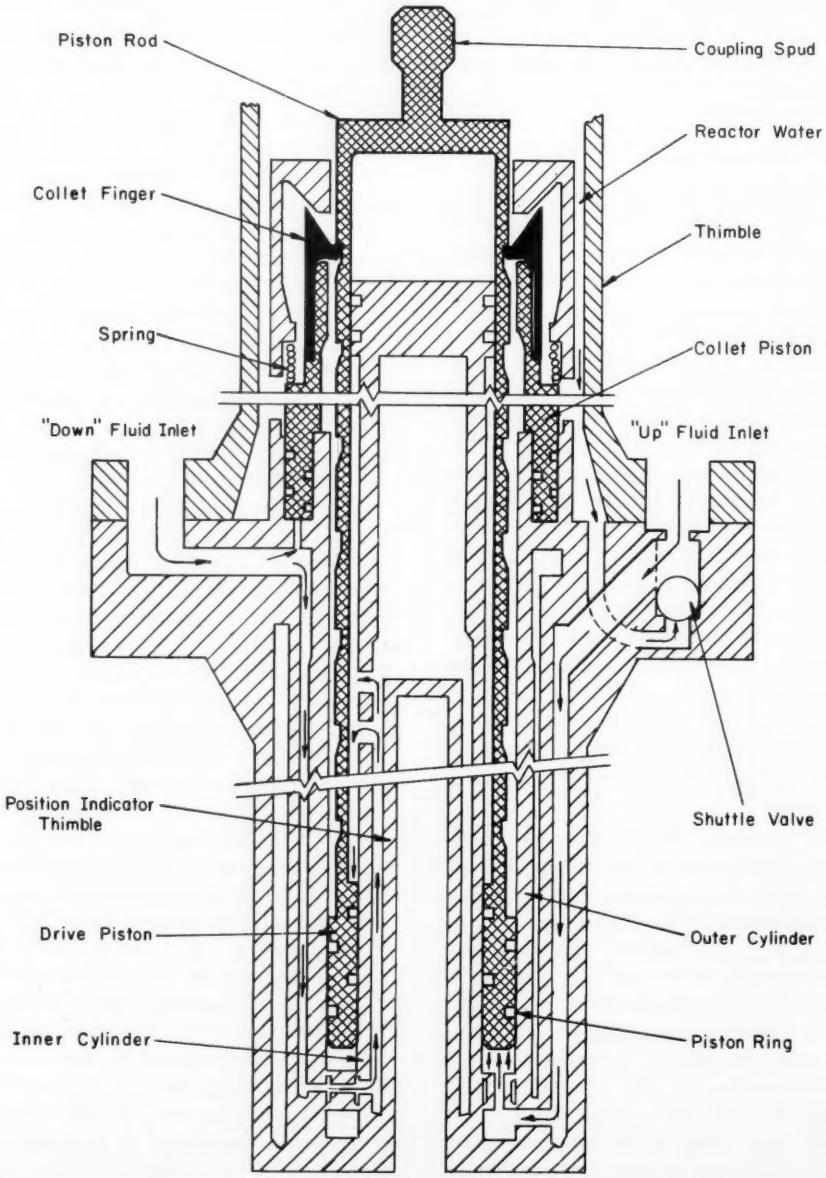

Fig. VIII-8 Control-rod-drive mechanism, Big Rock Point reactor.

In each plant the reactor neutron-monitor system consists of two separate sets of detectors: the out-of-core monitors, which provide the operators with immediate indications of neutron level within the reactor from startup to full power and which are connected to the reactor safety system, and the in-core monitors, which are used to determine the neutron-flux distribution in the core and periodically to provide data for verification of analytical predictions and major rod programming. The out-of-core monitors cover a range of nine decades by use of three subsystems that cover the start-up range, the period or intermediate range, and the power range. A block diagram of the out-of-core nuclear instrumentation of the Big Rock Point reactor, shown in Fig. VIII-9, illustrates the major features of the system provided for each plant. Although the Humboldt Bay system differs slightly from that of Big Rock Point, the principal components and interrelations between the channels are the same. Both systems incorporate revisions to earlier system drawings that were shown in *Power Reactor Technology*, 5(2): 66-67.

The in-core flux-monitor system uses miniature fission chambers as detectors and determines neutron flux in eight radial positions of the core. Detectors are located at three elevations in each radial position, so that a total of 24 in-core measurements can be taken. The three detectors for each radial core position are fabricated into a single assembly that is inserted into the core from the top. Calibration wires are inserted through nozzles located in the bottom head of the reactor pressure vessel.

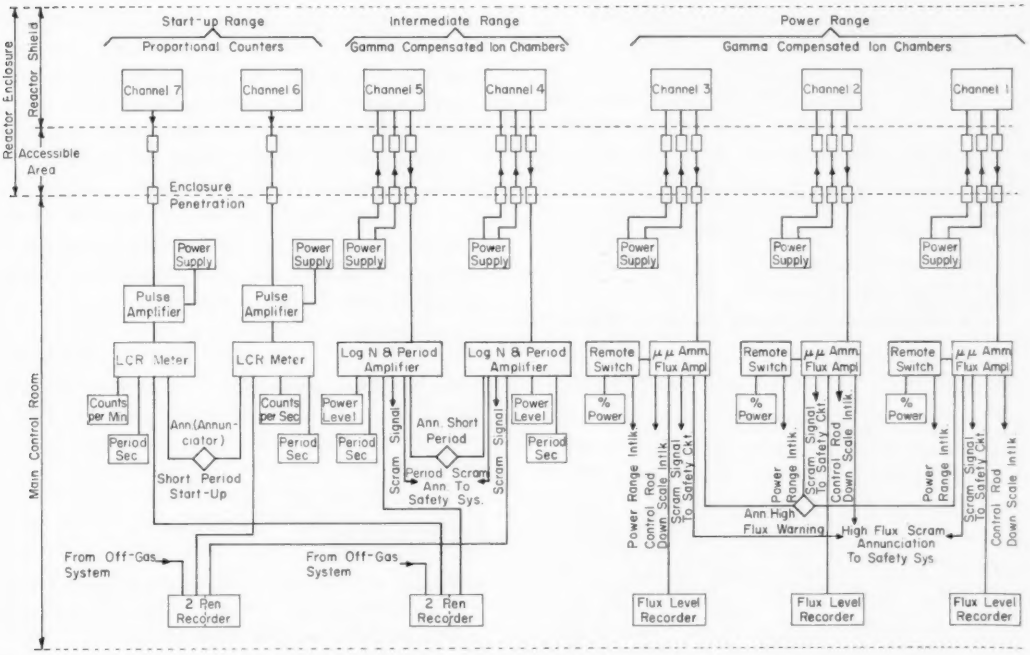

Fig. VIII-9 Out-of-core nuclear instrumentation diagram, Big Rock Point reactor.

Radioactive Waste Disposal

The principal sources of gaseous radioactivity are the off-gases from the main condenser air ejectors, the gland seal condenser, and the mechanical vacuum pumps. The air-ejector gases, which are carried to the plant stack through a holdup line to provide decay time, are passed through a high-efficiency filter

prior to entering the stack. Gases from the gland seal condenser and the mechanical vacuum pumps flow through a separate holdup pipe, which provides a shorter holdup period, and are discharged to the stack. Before release from the stack, the process gases are mixed with ventilating air, giving a significant dilution of the airborne radioactivity.

The limits on the annual average rates of release of fission and activation gases from the stacks of Big Rock Point and Humboldt Bay, as given in the Technical Specifications,[4,5] are tabulated below:

	Big Rock Point	Humboldt Bay
Holdup time for air-ejector gases, min	30	18
Holdup time for gland-seal condenser and vacuum-pump gases, sec	90	50
Minimum air flow in stack, cfm	30,000	12,000
Stack height, ft	240	250
Maximum permissible stack release rate		
Annual average, curies/sec	1.0	0.05
Instantaneous, curies/sec	10	0.5
Maximum permissible annual average stack release rate, expressed in units of μc/sec, does not exceed the permissible air concentrations for unrestricted areas, as given in 10CFR20, multiplied by	1.2×10^{10} cm^3/sec	6×10^8 cm^3/sec

Relatively low values of stack release rate for fission and activation gases are specified for Humboldt Bay because of uncertainties in the meteorology of the local coast area. The rates will be increased by a factor of 5 if meteorological tests confirm that the increase is reasonable.

The general procedures followed in liquid waste disposal are collection, dilution, and discharge, or storage following concentration by evaporation. Effluent from the liquid radioactive waste system is released under batch control, and storage tanks are provided for retreatment of effluent if required prior to discharge. The effluent is pumped to the circulating-water discharge duct, so that a large volume of nonradioactive water is available for use as a diluent.

	Big Rock Point	Humboldt Bay
Minimum waste treatment	Filtration	Filtration
Waste-filter capacity, maximum, gal/min	50	50
Nonradioactive water available for diluting waste effluent, full power, gal/min	50,000	104,000
Maximum waste inventory in system, curies	5000	10,000

Solid wastes include spent demineralizer resins, contaminated tools, equipment, and clothes, used filters, and used process equipment such as control rods or core components. Demineralizer resins are normally sluiced to a storage tank that is sufficiently large to receive wastes for approximately five years. Other solid wastes are stored in an underground concrete burial vault. Room is available for additional storage tanks or burial vaults, and, when the current facilities are full, additional storage space will be constructed or a licensed contractor will be called in to remove the accumulated solid waste material.

	Big Rock Point	Humboldt Bay
Resin storage-tank capacity, gal	10,000	10,000
Maximum waste inventory, curies	40,000	50,000

References

1. Docket No. 50-155, Final Hazards Summary Report for Big Rock Point Plant, Vols. 1 and 2, Nov. 14, 1961, and Amendments.
2. Docket No. 50-133, Final Hazards Summary Report, Humboldt Bay Power Plant Unit No. 3, Sept. 1, 1961, and Amendments.
3. M. Petrick, A Study of Vapor Carryunder and Associated Problems, USAEC Report ANL-6581, Argonne National Laboratory, July 1962.
4. Appendix A (Technical Specifications) to Provisional Operating License No. DPR-6, granted to Consumers Power Company by the United States Atomic Energy Commission.
5. Appendix A (Technical Specifications) to Provisional Operating License No. DPR-7, granted to Pacific Gas & Electric Company by the United States Atomic Energy Commission.

Section

IX

Power Reactor Technology

Specific Reactor Types

Heavy-Water Reactors

By J. R. Dietrich

The last comprehensive review of heavy-water reactors in *Power Reactor Technology* was in 4(2): 62-77. Among the points discussed in that review were the following:

1. To the extent that there is a concern about the possible depletion of nuclear fuel resources, this concern constitutes an incentive for the development of heavy-water-moderated reactors of high neutron economy.

2. The power cost estimates arrived at in studies of heavy-water-moderated reactors have tended to be higher than those estimated for the light-water reactors. The higher estimates result from the costs directly attributable to heavy water—heavy-water inventory charges and losses—and often from higher capital cost estimates. The estimated fuel costs are, in general, considerably below those for the H_2O reactors and are less dependent on uranium costs, plutonium buy-back prices, and fuel-processing costs.

3. It is generally recognized that the difference in economic environment for nuclear power generation which exists between the United States and Canada is responsible to a large degree for the differences in preference for light-water and heavy-water reactors in the two countries. It is also true, but not so generally recognized, that this difference in economic environment may also strongly affect the direction of preferred development of the D_2O reactor in the two countries.

Since the issuance of the preceding review, there have been some critical reexaminations of the heavy-water reactor type, as well as some significant technical developments, which have sharpened and illuminated these points. The reexaminations have strengthened the position of the liquid-D_2O-cooled reactor for the near term, and have, mostly by omission, deemphasized the direct-cycle boiling-D_2O pressure-tube system. Many other coolant possibilities have been examined, and several seem promising, but the organic-cooled system appears to emerge as the one most likely to give an early economic improvement over the pressurized D_2O system. In the following brief review of recent developments, these points will be discussed in more detail.

Heavy-Water Reactors and Fuel Supplies

It has long been recognized in a general way that the capability of the D_2O-moderated reactor to achieve high neutron economy and substantial reactivity lifetime with fuel of natural or near-natural enrichment is a real advantage; but the implications of that advantage in the United States, where large enrichment facilities are available, have been slow in being noticed. The AEC Report to the President[1] states that the U. S. resources of fissile isotope appear to be small in relation to the hoped-for development of nuclear power generation, and the recognition of this fact in that report has helped to give the proper emphasis to the wise use of nuclear fuel. Ironically, the relation of low-enrichment operation to fuel resource utilization had not been clearly defined prior to the Report to the President, and the report, although establishing the basis of importance for heavy-water reactors, placed no emphasis on the need for that reactor type. Since the publication of the report, heavy-water systems have been examined more carefully in relation to efficient fuel utilization, and a more precise appreciation of their conservation advantages has developed. These advantages, which were brought out in a general way in the discussion

of nuclear fuel utilization in the previous issue of *Power Reactor Technology* [6(4): 1-38], may be summarized as follows:

1. Because the heavy-water-moderated reactor can achieve high neutron economy with fuel of low enrichment, it possesses the unique ability to utilize fissile isotope effectively (i.e., to extract a large amount of energy per net gram of fissile isotope destroyed) and at the same time to minimize the amount of fissile isotope required in inventory. In a rapidly expanding nuclear power-generation system, the tie-up of fissile isotope in reactor inventory represents as effective a drain on the resource as does the actual destruction of the isotope.

2. Because of its ability to achieve long exposures with fuel of low enrichment, the D_2O-moderated reactor can minimize the effective loss of fissile isotope that results from the degradation of enrichment in the tailings from isotope separation plants and spent reactor fuel elements.

3. Because the epithermal component of the neutron energy spectrum can be low in a reactor of low enrichment, and because a low effective neutron temperature can be achieved by the use of cool moderator, D_2O reactors of the pressure-tube type can minimize the effects of the high capture-to-fission ratio (α) which afflicts plutonium in the epithermal-neutron energy regions and hence can utilize plutonium more effectively than other thermal reactors.

4. The natural-uranium D_2O-moderated reactor is probably more efficient than a diffusion plant in converting raw natural uranium to fissile isotope for the fueling of fast breeders. That is to say, if a given quantity of natural uranium is used in a natural-uranium D_2O-moderated reactor, the plutonium produced will probably provide inventory for a larger power capacity of fast breeder than would the U^{235} that could be extracted from the same quantity of natural uranium by a diffusion plant operating with a practical value of tails enrichment.

5. If it should prove desirable to operate on a thorium fuel cycle, the D_2O-moderated reactor would still retain the relative advantage of achieving high conversion ratio with low inventory requirement. Furthermore, it apparently has the capability of utilizing plutonium efficiently as a means of starting the U^{233}-thorium cycle, and its chances of breeding on that cycle are as good as or better than those of other solid-fuel reactors operating in the thermal or near-thermal energy range.

Power Cost Estimates

In the more recent studies of nuclear power plants employing heavy-water reactors, the estimated power costs have improved relative to estimates for light-water plants of comparable output, and the prospects appear good for competitiveness in plants of large size. Designers who have some experience with the uncertainties in power cost estimates are likely to discount the significance of such estimates if they are based on anything short of detailed construction drawings. However, if the current, rather favorable estimates are discounted because of uncertainties, at least the earlier, less favorable estimates should be viewed with equal, or greater, reservation.

Actually there are good reasons for improvements in the estimated economic performance. Not the least of these is the advancement of the technology, most clearly demonstrated by the operation of the NPD plant[2–5] and the advanced stage of construction of the Douglas Point Station[6,7] (scheduled[6] for full-scale commercial operation in 1965) in Canada and by the startup of the Carolinas-Virginia Tube Reactor (CVTR) in the U. S. [see *Power Reactor Technology*, 6(4): 63-81, for a review of the CVTR design]. Another important factor is the development of more favorable design concepts and the optimization of design of the particular concepts. As pointed out in the previous review, optimization and attention to design detail are of the highest importance in those reactors (for example, the heavy-water reactors) whose attractive features depend on good neutron performance. Finally, most of the more recent power cost studies have been made at higher power levels [500 Mw(e)] than the earlier studies. The economic performance of the heavy-water reactors improves relative to that of the light-water reactors as plant size increases and presumably would experience a step increase if plant size were increased further to the point that a single light-water reactor could not supply the required thermal power.

The recent power cost estimates for reactors cooled and moderated by D_2O have been made by the Du Pont Company at the Savannah River Laboratory,[8] by a joint team from the American Electric Power Service Corporation (AEPSC)

and the General Nuclear Engineering Corporation (GNEC)[9] and by the AECL Chalk River Laboratory.[10] Although each of these groups has considered several D_2O-moderated reactor types, the results for the liquid-D_2O-cooled type will suffice to show the trend of the estimates. Table IX-1 summarizes the characteristics of the reactors which were described by the three groups at a joint USAEC-AECL review[11] in May 1963. Table IX-2 summarizes the capital and fuel cost estimates for the three plants. These are somewhat more susceptible to comparison than are the estimates of power-generation cost, inasmuch as they are less affected by ground rules. However, it is clear that different groups use different criteria for the breakdown between direct and indirect costs. The inclusion of D_2O inventory at $20 per pound is for the sake of comparison only. The power cost estimates of the various groups covered D_2O prices from $17 per pound to $28 per pound, with and without depreciation, and, of course, included allowances for D_2O losses. The references should be consulted for the understanding of the ground rules necessary for the interpretation of power cost estimates. However, for purposes of orientation, it may be mentioned that the Du Pont and AEPSC-GNEC estimates were, respectively, 5.8 and 6.9 mills/kw-hr for the case of private utility financing with nondepreciating D_2O.

Other economic studies of very large heavy-water reactors have considered the production of process heat for water desalinization—in most cases with concurrent electric generation by backpressure turbines. Reference 12 (see also Ref. 13), reporting work at the Oak Ridge National Laboratory (ORNL), considers a plant of 25,000 Mw(t), employing three heavy-water-moderated reactors, each of 8333 Mw(t) capacity, cooled by boiling light water.* With municipal financing and a plutonium credit of $6.7 per gram (as nitrate), the plant is estimated to produce electric power at 1.55 mills/kw-hr and fresh water at 11.0 cents per 1000 gal, when water and electricity are sold in the ratio of 9 gal per kilowatt-hour.

Reference 12 does not make comparisons with other reactor types for the desalinization application, but a recently issued report[14] gives the results of a study of sea-water distillation by nuclear heat (with electric power production by backpressure turbines), carried out by the Bechtel Corporation for AEC. In the study[14] light-water reactors and water-cooled graphite-moderated reactors were considered in addition to organic-cooled D_2O-moderated reactors. The study utilized reactor and fuel cost information supplied by ORNL and by various contractors through the AEC Division of Reactor Development and the Savannah River and Hanford Operations Offices. The D_2O-moderated reactor was found to give the lowest cost heat, primarily because of its low estimated fuel cost.

Canadian and U. S. Approaches

The differences between the economic environments of nuclear plants in the U. S. and Canada are well known, and it has become a cliché to point out that the low capital charge rate applicable to the Canadian reactor (about 6.5% per annum) causes the balance between capital costs and fuel costs, which usually must be struck in economic optimizations, to be tipped in favor of low fuel costs. It has been recognized that this circumstance plays a large part in the Canadian choice of the heavy-water reactor and that, in combination with some other nontechnical considerations, it plays a large part in the favorable performance shown by the natural-uranium designs in the Canadian environment. What is not so generally recognized is the extent to which these effects permeate the entire Canadian design approach, making it uniquely fitted for the Canadian power economy and for the use of natural uranium. This effect may be seen by examining the characteristics of the Canadian and U. S. designs listed in Table IX-1, and it will become even more obvious if the designs are examined in detail. The most straightforward comparisons can be made between the Canadian design and the AEPSC-GNEC design, since both have rod type fuel

*This reactor is of particular interest technically, for it appears to achieve a negative coolant-void coefficient of reactivity. This has not been previously reported for D_2O-moderated reactors cooled by H_2O and, in general, has been considered very difficult, if not impossible, with natural-uranium fuel. The design described in the reference is unusual in that it uses quite massive fuel elements and a high fuel-to-moderator ratio. This entails the penalties of low specific power and reduced reactivity lifetime, but these penalties appear to be tolerable in the economics of the very large reactor system.

Table IX-1 COMPARISON OF DESIGNS FOR 500-Mw(e) LIQUID-D_2O-COOLED REACTORS*[11]

	Canadian (AECL-1730)[10]	Du Pont (DP-830)[8]	AEPSC-GNEC (NP-12344)[9]
General			
Gross thermal output, Mw(t)	1570	1838	1850
Net electrical output, Mw(e)	491	491	489
Net thermal efficiency, %	31.3	26.7	26.4
Total D_2O inventory, metric tons	350	325	390
Refueling method	On-line	Shutdown	On-line
Primary coolant system			
Design pressure, psia	1830	1730	1760
Coolant inlet temperature, °C	266	260	257
Coolant outlet temperature, °C	310	310	302
Coolant flow rate, gal/min	122,000	138,000	128,000
Maximum coolant velocity, ft/sec	30	30	40
Fuel			
Fuel material	UO_2	UO_2	UO_2
Fuel cladding	Zircaloy	Zircaloy	Zircaloy–2.5% Nb
Fuel configuration	Solid rods	Coaxial tubes	Hollow rods
Fuel bundle length, ft	1.7	15	4.5
Concentration of U^{235}, %	0.71	1.19	1.41†
Average fuel burnup, Mwd/metric ton of U	8680	14,000	19,700
Number of fuel positions	387	226	560
Core fuel inventory, metric tons of U	95.7	27.1	51.4
Reactor core			
Pressure-tube concept	Hot	Cold	Cold
Core length (including reflector), ft	21.4	19	20
Reactor diameter (including reflector), ft	~23.9	18	22
Control method	Rods	Rods	Ball columns
Number of control positions	16	23	187
Pressure-tube inside diameter, in.	4.0	4.4	3.5
Maximum heat flux, Btu/(hr)(sq ft)	330,000	850,000	620,000
Average specific power, Mw/metric ton of U	16	68	36
Mw/metric ton of total D_2O	4.5	5.2	4.8
D_2O moderator inventory, metric tons	265	163	242
Turbine plant			
Throttle steam pressure, psia	762	522	540
Throttle steam temperature, °C	265	245	246
Type of steam cycle	Reheat	Nonreheat	Nonreheat
Feedwater return temperature, °C	182	200	188
Condenser pressure, in. Hg	1.0(?)	1.5	1.5
Gross cycle efficiency, %	34.6	30.0	28.4

*Basic numbers are from Refs. 8 to 10. However, the AECL numbers, where appropriate, have been adjusted upward from the 457-Mw(e) output of Ref. 10 to the 491-Mw(e) value appropriate for this comparison.

†Optional operation to 5000 Mwd/metric ton of U possible with natural uranium.

elements in 19-rod bundles. Some of the significant items are the following:

1. Although the important coolant temperatures are not greatly different in the Canadian and U. S. designs, the thermal efficiency of the Canadian plant is substantially higher, with the result that the U. S. designs generate some 18% more thermal power for a given electrical output. The higher thermal efficiency appears to result from a slightly lower condenser pressure, the use of a reheat steam cycle, and the use of U-tube U-shell steam generators that do not restrict the temperature of the generated steam to a value less than the coolant inlet temperature to the reactor. The latter point is illustrated in Fig. IX-1. The U-tube U-shell generators are avoided in the U. S. design studies because of their estimated high capital cost.

2. The Canadian designs use a larger quantity of heavy water in the reactor tank—part of it to afford a generous 2-ft reflector—but they use a much smaller quantity of heavy water in the external coolant system to reach a total that is intermediate between that for the Du Pont and the AEPSC-GNEC designs (Table IX-1). The low external inventory results from the use of the counterflow coolant arrangement in adjacent pressure tubes, illustrated in Fig. IX-2,

which eliminates the need for return lines from one end of the reactor to the other, and apparently also from a design approach that weights very heavily the considerations of minimizing the external D_2O inventory. This approach is illustrated in Fig. IX-3, showing a bank of pumps and steam generators for the 200-Mw(e) CANDU reactor (the reactor for the Douglas Point Station). The unit shown in the figure, comprised of five pumps and four steam generators, each of the latter utilizing 10 vertical U-tube heat exchangers, serves one end of the reactor and is duplicated at the other end. The holdup of D_2O in headers and other parasitic volumes is comparatively small. Again, U. S. practice would indicate a smaller number of larger units on capital cost considerations.

3. The Canadian design produces more power per unit length of fuel element than does the U. S. design (AEPSC-GNEC) that utilizes fuel assemblies of the same (rod bundle) type. Primarily this is the result of a flatter power distribution in the Canadian reactor (apparently a maximum-to-average ratio of 1.5 vs. 2.6 in the U. S. design). The immediate reasons for the excellent power flattening achieved in the Canadian design are primarily the thick reflector and the bidirectional push-through scheme of fuel reloading. The latter is illustrated in Fig. IX-4. There is, however, a more fundamental reason why better power flattening can be achieved in a reactor designed for relatively low fuel burnup than in one designed for high fuel burnup.

Table IX-2 CAPITAL AND FUEL COST ESTIMATES FOR 500-Mw(e) LIQUID-D_2O-COOLED REACTORS[11]

	Canadian (AECL-1730)[10]	Du Pont (DP-830)[8]	AEPSC-GNEC (NP-12344)[9]
Capital costs [all costs are in millions of U. S. dollars and apply to single units of 500 Mw(e) capacity]			
Land and land rights		0.4	0.4
Structure and improvements		6.0	12.1
Reactor plant equipment		21.7	37.2
Turbine-generator equipment		27.8	25.2
Total direct cost	55.0	55.9	74.9
Indirect costs (including contingency)	36.7	29.9	27.0
Total construction cost	91.7*	85.8	101.9
Total construction cost, $/kw(e)	202	175	208
D_2O inventory at $20/lb	14.3	15.4	17.2
Total plant cost	106.0	101.2	119.1
Total plant cost, $/kw(e)	232	206	244
Fuel characteristics			
Fuel material	UO_2	UO_2	UO_2
Fuel shape	Rod	Tube	Hollow rod
Cladding	Zircaloy	Zircaloy	Zircaloy–2.5% niobium
Fabrication method	Pelletizing	Mechanical compaction	Pelletizing
Concentration of U^{235}, %	0.715	1.19	1.41
Average exposure, Mwd/metric ton of U	8680	14,000	19,700
Fuel-cycle costs, $/kg of U†			
Conversion and fabrication		21.60	71.44
Shipping (fresh and spent fuel)		2.50	19.01
Depletion of U^{235}		66.10	88.12
Reprocessing		26.08	28.88
Use of U^{235}		3.21	7.23
Net plutonium credit		(36.43)	(46.35)
Other		1.19	
Total, $/kg of U	52‡	84	168
Total, mills/kw-hr	0.80	0.94	1.35

*For a 454-Mw(e) plant.

†Costs tabulated under "Du Pont" and "AEPSC-GNEC" are for U. S. Government ownership of fuel; the AEPSC-GNEC estimate of total fuel cost under private ownership is 1.29 mills/kw-hr.

‡Throwaway fuel cycle.

In uranium-cycle reactors with reasonably high conversion ratios, the initial effect of fuel exposure is to increase the macroscopic fission cross section, because the macroscopic fission cross section of Pu^{239} is considerably higher than that of U^{235}. This usually occurs even though the reactivity may be decreasing because of the lower η of Pu^{239} and the buildup of fission products. In such reactors the macroscopic fission cross section of the fuel will go through a maximum as exposure continues and as the Pu^{239} content approaches an equilibrium value, and it will eventually decrease to a value far below its initial value. Until the fission cross section decreases below its initial value, power flattening by appropriate fuel shuffling or incremental reloading procedures may be very effective. However, when a reactor contains old fuel with substantially decreased fission cross section, the best the fuel-shuffling program can do is to flatten the neutron-flux distribution; it cannot make the old fuel bundles produce as much power, on the average, as the new ones.

At a given conversion ratio, this effect is more pronounced in low-enrichment reactors (e.g., the heavy-water reactors) than in the reactors that inherently use higher enrichment (e.g., the light-water reactors), simply because the fractional burnup of fissile isotope, for a given exposure in megawatt-days per ton, is larger in the low-enrichment reactor. The effect is felt rather strongly in the AEPSC-GNEC design.

The other effect of high-burnup fuel on power distribution occurs in the initial period of operation: not only is the initial fuel composition far different from that which characterizes the final equilibrium reloading cycle, but the nonequilibrium period lasts so long that compromises in either fuel or reactor performance during that period are quite expensive. The designer must then solve the double problem of finding a favorable equilibrium power dis-

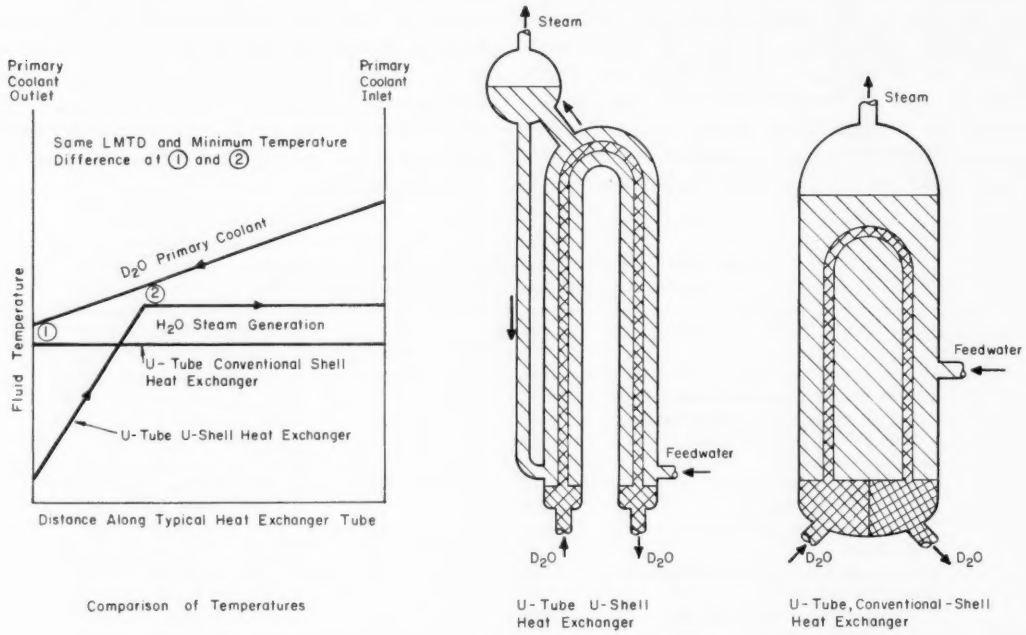

Fig. IX-1 Comparison of U-tube U-shell and U-tube conventional-shell heat exchanger. The U-shell design produces hotter steam principally because of the countercurrent flow in the feedwater—D_2O-outlet leg of the U: this countercurrent flow, in conjunction with a low feedwater inlet temperature, is used to cause the point of minimum temperature difference to occur where the D_2O temperature is relatively high.

tribution and of establishing that distribution without creating a less favorable distribution during the nonequilibrium period.

The Canadian design (relative to the AEPSC-GNEC design) utilizes much more massive fuel elements, with a consequent reduction in fabrication cost per pound of uranium. Partly this results from several of the points discussed above. The high value of average power per unit length of fuel element, along with the low cost of the natural-uranium fuel, allows the use of massive elements without an important penalty in fuel inventory charges. At the same time, the economical use of D_2O in the external circuit gives a reasonably high value of specific power relative to total D_2O, despite the fact that a low specific power relative to fuel implies also a low specific power relative to that D_2O which is in the reactor tank.

The use of the large fuel rods results also from Canadian developments directed specifically toward the problems of fuel bundles for heavy-water reactors. The fundamental difference between fuel designed for this application and fuel designed for the typical U. S. light-water reactors is that space for fission-gas accumulation cannot be provided in the heavy-water case without incurring an undesirable power peaking due to the end-peaking or Wilkins effect. Much of the Canadian fuel research has been directed toward the understanding of the behavior of fission gases in oxide fuel elements, and presumably these developments, along with the relatively low burnup of the fuel, are factored into the Canadian design. The elements specified in Ref. 10 (diameter, 0.74 in.), are considerably larger than the 0.60-in. elements specified for the CANDU reactor. In contrast to this rather massive design, the U. S. design utilizes a smaller element, with a central hole that serves the dual purpose of reducing the maximum oxide temperature and providing a space for the fission gases that may be released (Fig. IX-5).

The other U. S. design, produced by the Du Pont group, utilizes the Savannah River fuel-element approach that has been under development for some time. The massive full-length fuel elements consist of coaxial Zircaloy-clad tubes of uranium oxide (Fig. IX-6). They are fabricated by pouring fused uranium oxide powder into prefabricated Zircaloy sheaths, consolidating the powder by vibratory compaction, and swaging the composite tube over a mandrel to increase the oxide density above 90% of theoretical. At the present time the di-

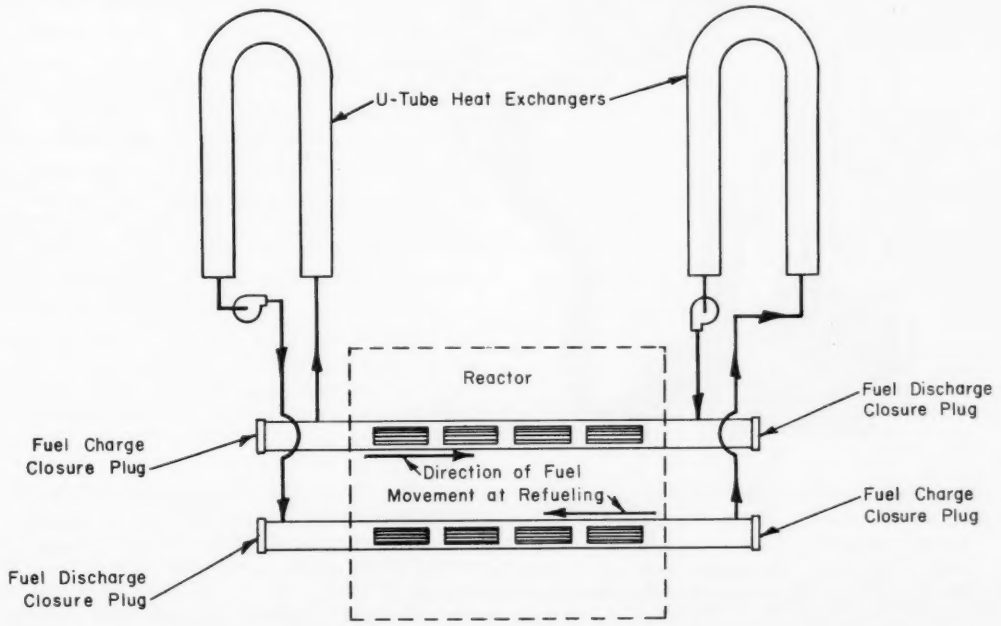

Fig. IX-2 Coolant-flow paths and fuel movement directions, CANDU reactor.

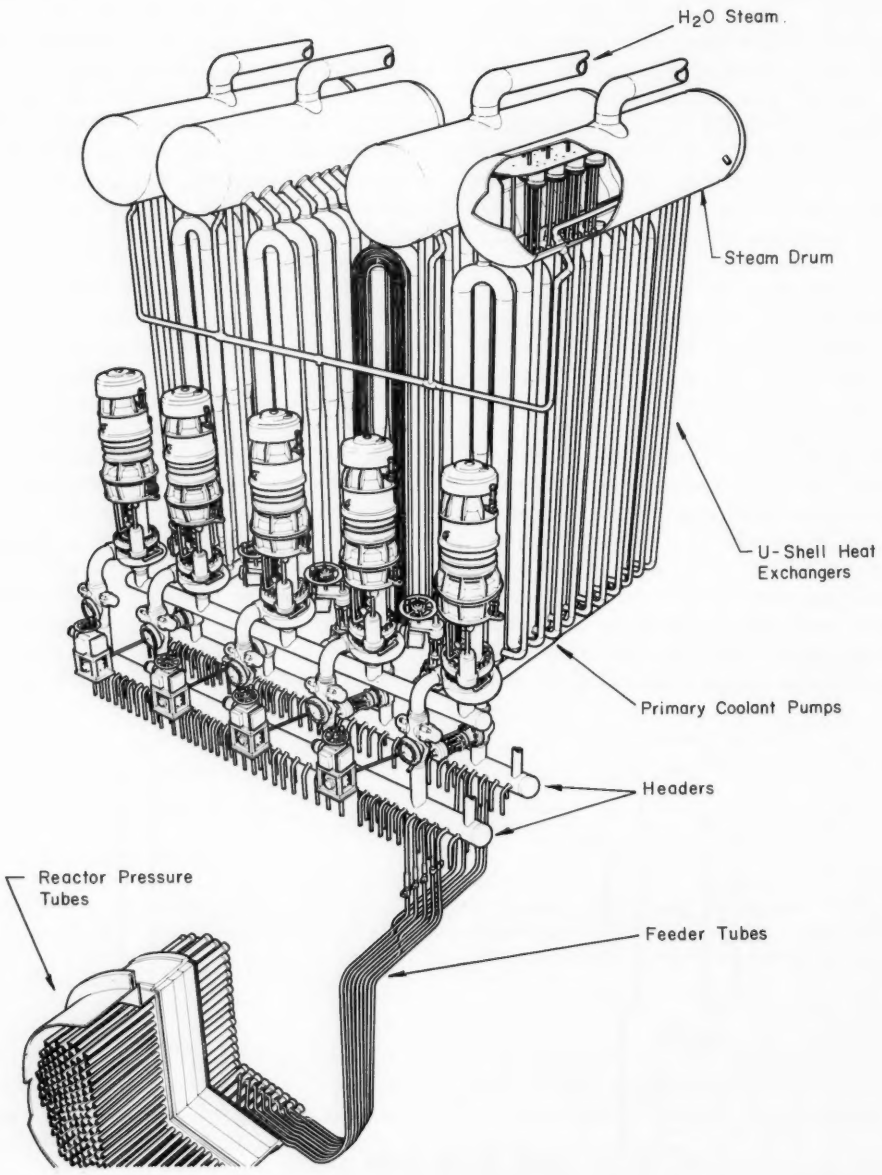

Fig. IX-3 CANDU boiler and circulating pump arrangement.[7] This bank of equipment serves one end of the reactor, and an identical bank serves the other end. The D_2O primary coolant passes through the tubes of the heat exchangers. The headers are 16 in. in outside diameter by 32 ft long, with 1.5-in. walls. The feeder tubes are of four sizes, $1\frac{1}{4}$, $1\frac{1}{2}$, 2, and $2\frac{1}{2}$ in. (normal), according to the coolant-flow requirements of the pressure tubes served.

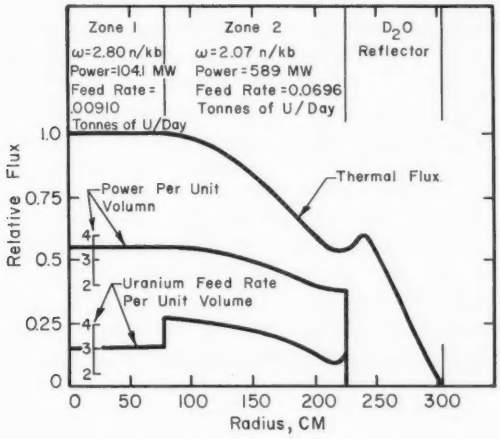

Fig. IX-4 Radial flux, power, and fuel feed distributions in CANDU.[7] Here ω is the discharge fuel exposure in neutrons per kilobarn; nvt = (neutrons/kilobarn)(10^{21}).

rect development effort on heavy-water power reactors in the U. S. consists largely of the development and testing of the tubular fuel elements, in both metal and oxide versions, at Savannah River. Some irradiation tests have been made in the Vallecitos Boiling-Water Reactor, but currently all testing is being done in the Heavy-Water Components Test Reactor (HWCTR),[15] which was constructed primarily for the development of fuel elements for heavy-water reactors. The status of elements currently under test is summarized in Table IX-3. The experience to date has been encouraging for the tubular elements containing oxide of relatively high density, but failures have been experienced in elements containing oxide in the 83% of theoretical density range. The following quotation is from Ref. 16:

> By the end of June, the maximum exposure attained by any of the fuel elements in the HWCTR was 7400 MWD/ton U in oxide tubes that were operating at a maximum $\int k\,dt$ of 22 watts/cm. However, fuel testing in HWCTR during the May-June period was interrupted three times by failures of oxide fuel assemblies. The cause of these failures has not yet been determined. Information available while this report was in preparation indicates that the failures were due to the collapse (under the hydraulic pressure of the coolant—1200 psi max.) of the outer sheathing of Zircaloy. The failures occurred only in fuel tubes that were filled with UO_2 having a density of about 83% of theoretical; oxide of 88% density gave sufficient support to the cladding that failure has not occurred. The first failure, which occurred during a power ascension on May 31, was in an assembly of eight short oxide tubes, the hottest of which had operated at a maximum $\int k\,dt$ of 50 watts/cm to a maximum exposure of about 3000 MWD/ton U. Another failure of this type of UO_2 element had occurred on April 3 shortly after a reactor shutdown. The other full-length oxide tubes failed during subsequent reactor operation: one during a startup, the other during normal operation. These latter tubes had operated at a maximum $\int k\,dt$ of 28 watts/cm and had attained maximum exposures of 4800 and 5600 MWD/ton U.

Reference 16 also describes a new vibrator that has been installed at the Savannah River Laboratory. It is expected to facilitate the attainment of high oxide density, as well as to make possible the fabrication of larger elements.

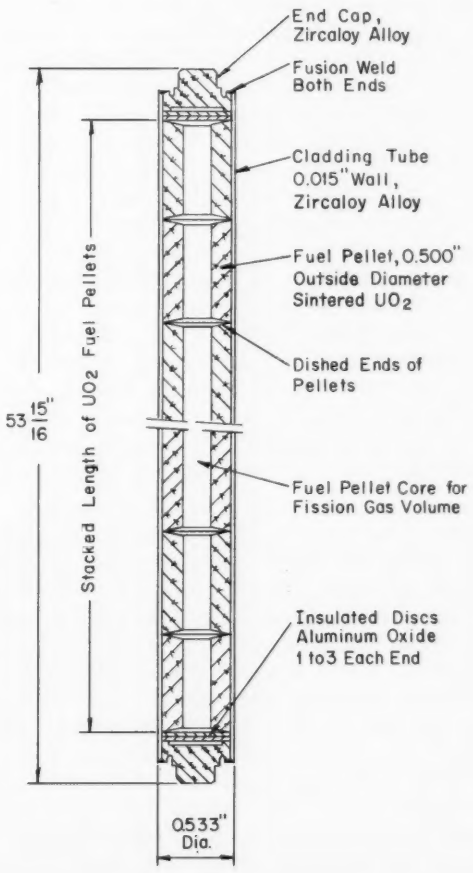

Fig. IX-5 Details of the fuel rod in the AEPSC-GNEC design.[9]

Table IX-3 FUEL IRRADIATION TESTS IN THE HWCTR,[16] JUNE 1963*

Reactor power	36 Mw
Coolant pressure	1200 psig
Coolant inlet temperature	238°C
Moderator outlet temperature	249.5°C

Position	Element number	Fuel type	Fuel assembly description	Starting date	Maximum nominal conditions								Maximum exposure,‡ Mwd/ton of U	
					Assembly power,† Mw	Specific power,‡ Mw/ton of U	Heat flux, pcu/(hr)(sq ft)	Outlet temp., °C	Surface temp., °C	Core-cladding temp., °C	Core temp., °C	$\int k\,dt$, watts/cm	Attained	Planned
37	CANDU	Oxide rod	Five 19-rod bundles of natural UO_2 pellets	10-5-62	0.83	21	117,000	262	270	289	1,250	25	2,908	9,000
38§	OT-3-2	Oxide tube	Single tube of vibratory-compacted natural UO_2	5-19-63	0.41	40	178,000	256	286	340	800	15	543	§
39	2ETWO-2	Metal tube	Unalloyed, 2.1% enriched, 2-in. OD, single tube	5-19-63	1.01	80	459,000	252	306¶	424	491		1,170	8,000
40	SOT-1-2	Oxide tube	Eight 14-in.-long tubes of 1.5% enriched UO_2	10-5-62	0.49	57	274,000	246	292	371	1,100	22	7,418	23,000
42	2ETWO-3	Metal tube	Same as position 39	6-11-63	0.96	76	436,000	251	306	418	482		533	10,000
55	SOT-5-2	Oxide tube	Eight 14-in. tubes of natural UO_2; 4 swaged, 4 vibratory compacted	5-19-63	0.48	31	292,000	249	300	393	2,030	46	457	6,000
56	SOT-1-3	Oxide tube	Same as position 40	1-6-63	0.47	53	253,000	246	288	361	1,060	21	5,665	10,000
57	SMT-1-2	Metal tube	Ten $11\frac{1}{4}$-in. alloyed (Fe,Al) natural-U tubes	5-19-63	0.47	29	249,000	250	301	357	408		436	7,500
58	OT-1-5	Oxide tube	Single tube of vibratory-compacted 1.5% enriched UO_2	1-6-63	0.60	57	262,000	248	291	367	1,120	22	5,656	23,000
59	OT-1-3	Oxide tube	Single tube of vibratory- and swage-compacted 1.5% enriched UO_2	**	0.64	55	275,000	249	294	376	1,120	22	4,832	5,000
60	OT-1-2	Oxide tube	Same as position 59	10-5-62††	0.59	51	254,000	248	287	363	1,060	21	7,041	11,000

*Data taken on June 18, 1963; exposures as of June 31, 1963.
†Based on ΔT and flow calculations; does not include gamma heating of moderator.
‡Based on an assembly power that includes gamma heating of moderator (1.09 times the power based on ΔT and flow calculations).
§Liquid loop position. The OT-3-2 fuel element is being used to commission the loop; this is not an irradiation test of fuel.
¶Temperature limited by surface boiling.
**Starting date 1-6-63; discharged 4-3-63; recharged 6-6-63; failed 6-20-63.
††Irradiated from 10-5-62 to 6-7-63 in position 42; moved to position 60 on 6-11-63.

The typical reactor design prepared by the Du Pont group[8] differs quite markedly from the typical Canadian designs (Table IX-1). The use of tubular elements rather than rod bundles and the use of slightly enriched rather than natural uranium lead to quite high specific power relative to the fuel and relative to the D_2O in the reactor because of the favorable geometry of the fuel for heat removal and the relatively thin oxide sections that were used. In the Du Pont design, on-power refueling is not used. Partial core reloading is contemplated, and radial power flattening is achieved by using higher average fuel exposures (or lower enrichments) near the center rather than near the edge of the reactor.

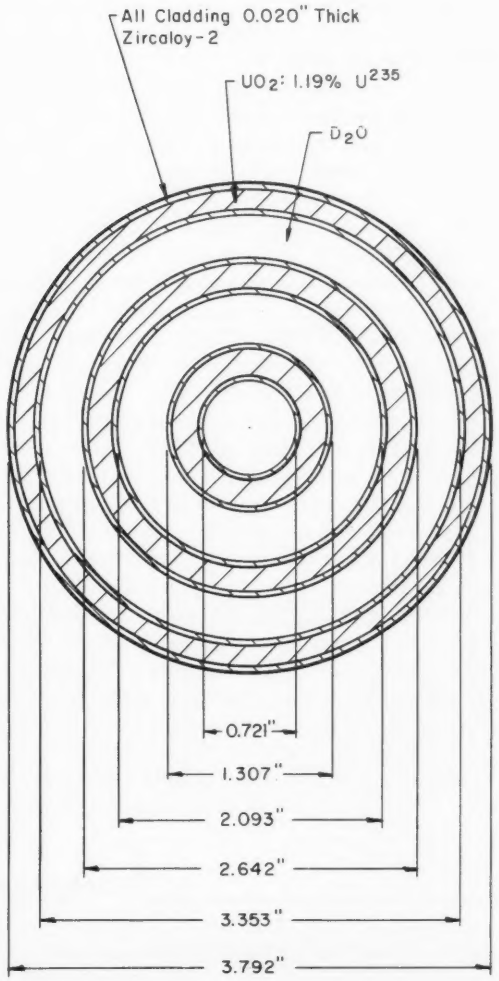

Fig. IX-6 Du Pont fuel element.

Organic-Cooled Heavy-Water Reactors

It must, of course, be recognized that the organic-cooled system has not reached nearly the same stage of development as the liquid-D_2O-cooled system. The problem of organic fouling of fuel elements is well known. Recent results indicate that the problem may be controlled by careful attention to the initial cleanup of the system, control of the halogen (chlorine) content of the coolant,[11] and suitable filtration. Fuel elements suitable for the desired operating temperatures have not been demonstrated, although the possibilities of utilizing carbide fuels, or even metallic uranium, offer some promises of nuclear and thermal performance which are absent in the aqueous-coolant cases; however, the area of uncertainty in the development of a usable fuel element lies not in the fuel material but in the cladding material. Also, a pressure-tube design has not been proved. In both of these problems a key question is whether zirconium will operate satisfactorily in contact with hot organic in the reactor environment. Canadian investigations of this question have been encouraging but are not yet conclusive. If zirconium or a low-cross-section zirconium alloy cannot be used in these applications, the sintered aluminum product (SAP) of aluminum and aluminum oxide, which has been under development for organic reactors for a number of years, provides another possibility; however, it presents problems of fabrication, particularly welding problems, and is a rather brittle material, with less high-

Although it is difficult to compare the results of economic analyses made by different groups, the comparative results of a particular group for reactors of different types should have a more straightforward interpretation. It is, therefore, the more striking that the groups which have recently looked at various advanced heavy-water reactor types have all estimated the lowest power-generation costs for the organic-cooled type. These results are listed in Table IX-4. This list includes the results of studies[17] on the organic-cooled type by Combustion Engineering, Inc., under ground rules identical to those used earlier by the AEPSC-GNEC group for studies of the D_2O-cooled and gas-cooled types.

Table IX-4 ESTIMATED FUEL CYCLE AND POWER COSTS FOR SINGLE-REACTOR PLANTS IN THE 450- to 500-Mw(e) RANGE, UTILIZING D_2O-MODERATED REACTORS WITH VARIOUS COOLANTS

Reactor coolant	Estimating group	Type of financing	Fuel	Fuel-cycle cost, mills/kw-hr	Total energy cost, mills/kw-hr
Liquid D_2O	Du Pont[8]	Private plant, AEC fuel ownership	Enriched uranium	0.94	5.79
Boiling D_2O				0.68	5.94
H_2O fog				0.68	5.65
Organic				0.69	5.02
Liquid D_2O	AEPSC-GNEC*[9]	Private plant, private fuel ownership	Enriched uranium	1.29	6.94
Boiling D_2O				1.09	6.84
CO_2 gas				1.66	9.08
Organic	Combustion Engineering*[17]	Private plant, private fuel ownership	Enriched uranium	0.72	5.50
Liquid D_2O	AECL[10]	Canadian utility	Natural uranium	0.80	3.86
H_2O fog				0.86	3.89
Boiling H_2O				0.69	3.77
Organic				0.42	3.45

*These two studies used identical ground rules.

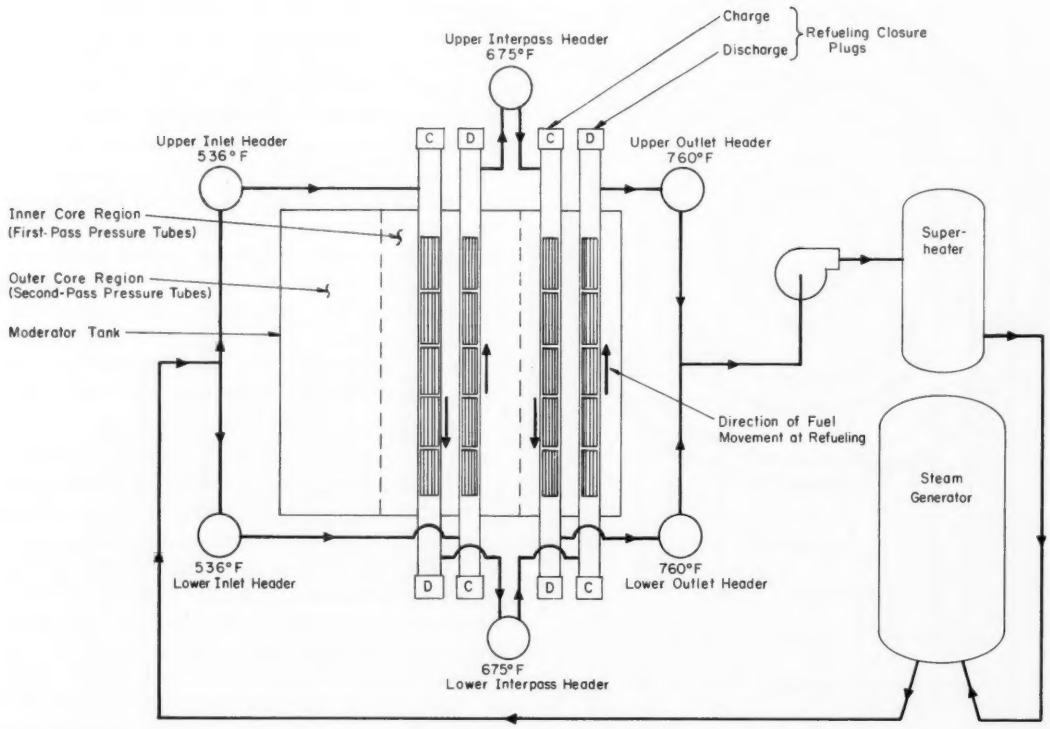

Fig. IX-7 Coolant-flow paths and fuel movement directions, Combustion Engineering organic-cooled reactor.

temperature strength than would be desirable. The organic-cooled design studies that have served as the basis for the economic evaluations discussed here have all utilized SAP-clad fuel elements. All of them have had also, either as the reference design or as a backup design, composite pressure tubes that, in one way or another, place SAP in contact with the organic but utilize Zircaloy for its strength properties and low neutron absorption.

It is hardly surprising that the organic coolant appears attractive in this application, for the low-vapor-pressure characteristic of the organic is particularly attractive in the pressure-tube concept. The use of a separate nonorganic moderator reduces the rate of organic decomposition to a fraction of that experienced in a reactor that is both moderated and cooled by an organic liquid. Further, as discussed above in connection with the D_2O-cooled reactors, the traditional approach of attempting to improve economic performance through working the fuel harder and increasing the specific power may well yield limited returns when applied to low-enrichment D_2O-moderated reactors. If this is the case, the well-known deficiencies of the organics as heat-transfer fluids may prove to be relatively unimportant in this application, particularly since their use eliminates most of the ex-reactor D_2O inventory that is associated with the D_2O-cooled types and thus reduces the importance of a high specific power relative to the in-reactor D_2O. It is possible also that specific design approaches can be utilized to minimize the poor heat-transfer properties while exploiting the relatively high-temperature capabilities of the coolant. An approach of this type, which was utilized in the Combustion Engineering design study, is illustrated in Fig. IX-7. Serious work toward the development of organic-cooled heavy-water reactors is under way in Canada with the WR-1 Test Reactor[18] at the Whiteshell Nuclear Research Establishment in Manitoba, and in Europe under the ORGEL (Organique-Eau Lourde) program,[19–21] sponsored by Euratom.

References

1. U. S. Atomic Energy Commission, Civilian Nuclear Power, a Report to the President—1962, Nov. 20, 1962.
2. Nuclear Canada Issue of *Nucleonics*, 18(10): (October 1960).
3. Nucleonics Reactor File...No. 13, NPD on the Line, *Nucleonics*, 20(11): 47 (November 1962).
4. I. N. MacKay, General Description of Nuclear Power Demonstration Plant, paper presented at the Winter Meeting of the American Nuclear Society, Washington, D. C., November 1962 (and other papers on NPD details presented at the same session).
5. L. G. McConnell, Commissioning and Initial Operation of NPD, The Eighth AECL Symposium on Atomic Power, Held at Chalk River, Ontario, Sept. 24, 1962, Canadian Report AECL-1599, pp. 40-42, September 1962, (This report also contains papers on NPD development and construction.)
6. D. L. S. Bate, Status Report on the Douglas Point Project, The Eighth AECL Symposium on Atomic Power, Held at Chalk River, Ontario, Sept. 24, 1962, Canadian Report AECL-1599, pp. 54-68, September 1962.
7. Atomic Energy of Canada Ltd., Douglas Point Nuclear Generating Station, Canadian Report AECL-1596.
8. D. F. Babcock, R. R. Hood, L. Isakoff, J. C. Jensen, D. S. St. John, and J. W. Wade, An Evaluation of Heavy-Water-Moderated Power Reactors, Status Report as of March 1963, USAEC Report DP-830, Savannah River Laboratory, June 1963.
9. American Electric Power Service Corp. and General Nuclear Engineering Corp., East Central Nuclear Group Inc. Heavy Water Moderated Reactors Evaluation Study, Report NP-12344, Oct. 15, 1962, in three volumes: I, Summary and Conclusions; II, Design Bases and Plant Comparisons; III, Plant Designs.
10. Atomic Energy of Canada Ltd., Power Reactor Development Evaluation, A Summary Report by a Committee of AECL Staff, Canadian Report AECL-1730, May 1, 1963.
11. D. G. Boyer and D. P. Dunlop, USAEC/AECL Review of Heavy Water Reactor Evaluation Studies, Minutes of Meeting Held at Toronto, Ontario, May 23–24, 1963.
12. Irving Spiewak, A Large Desalinization Reactor Based on Current Technology, *Nucleonics*, 21(7): 64 (July 1963).
13. Sargent & Lundy, Saline Water Conversion Power Reactor Plants, USAEC Report SL-1998, Jan. 11, 1963.
14. Bechtel Corp., Large Reactor Study for Sea Water Distillation. Final Report, USAEC Report TID-19267, July 1963.
15. L. M. Arnett, D. Randall, C. P. Ross, B. C. Rusche, and C. D. Taylor, Final Hazards Evaluation of the Heavy Water Components Test Reactor (HWCTR), USAEC Report DP-600, Savannah River Laboratory, December 1962.
16. R. R. Hood and L. Isakoff (Comps.), Heavy Water Moderated Power Reactors Progress Report,

May-June 1963, USAEC Report DP-855, Savannah River Laboratory, August 1963.

17. Combustion Engineering, Inc., March 1963. (Unpublished)
18. F. W. Gilbert, WR-1 Fits Organic Coolant to Canadian Program, *Can. Nucl. Tech.*, 2(2): 37 (Spring 1963).
19. J. C. Leny, ORGEL—A European Concept, *Nucl. Eng.*, 6(67): 508 (December 1961).
20. J. C. Leny, ORGEL: A European Power Reactor Design, *Trans. Am. Nucl. Soc.*, 5(1): 103 (June 1962).
21. J. C. Leny, ESSOR: Specific Test Reactor for the ORGEL Program, *Trans. Am. Nucl. Soc.*, 5(1): 104 (June 1962).

Section

X

Power Reactor Technology

Unconventional Approaches

Design Study of Thermionic Nuclear Plant

A recent report[1] describes a feasibility study of a water-cooled thermionic nuclear power plant of the portable medium-power (PM) class, which was carried out for the Atomic Energy Commission by the Martin Co.

The major design criteria established before the beginning-of-life study were:[1]

(1) The plant is to have a net power output of 1000 kwe, 60-cycle 3-phase ac at 480 volts. The plant is to be of the preassembled type, meeting the air-transportability requirements of the C-130A aircraft (i.e., maximum size—$8\frac{1}{2}$ ft × $8\frac{1}{2}$ × 30 ft; maximum weight—30,000 lb). In addition, the plant and modules are to be designed for minimum on-site erection and operating requirements.

(2) The reactor is to be cooled with either a natural or forced circulation water system.

(3) Thermionic converters are to be incorporated within the fuel elements. They are to be of the low temperature cesium plasma type, utilizing a refractory metal cathode that also serves as cladding for the fuel in each device.

(4) The reactor core is to be designed for a minimum of 10,000 fueled power hours.

(5) An air-cooled heat rejection system for minimum size and weight (air at 80°F maximum, −60°F minimum) is to be incorporated in the design.

(6) A theoretical analysis is to be conducted to determine plant nuclear, thermal, and electrical responses during startup, gradual load changes, and step transients.

The study included a cost analysis; however, this review will confine its attention to the reactor design features. Previous reviews in *Power Reactor Technology*, which covered only the principles of thermionic electric generation, may be found in 3(1): 6-14 and 3(3): 48-50. Reference 2 is a good discussion of general principles and is of more recent date.

A thermionic converter transforms nuclear heat directly into electricity without the intermediate step of conversion to mechanical energy. It accepts heat at a high temperature T (in a nuclear thermionic reactor, this heat is sup-

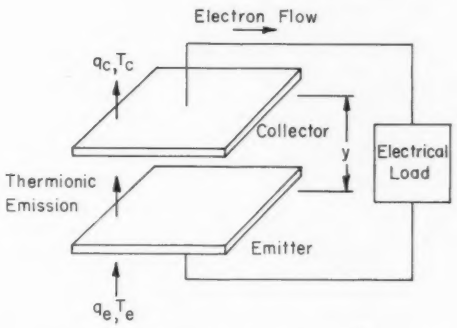

(a) Schematic of Thermionic Converter Diode.

q_e – Heat Rate from Nuclear Fuel Emitter.

T_e – Temperature of Emitter.

q_c – Heat Rate Rejected from Collector.

T_c – Temperature of Collector.

y – Interelectrode Spacing.

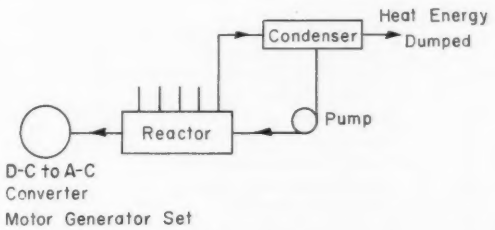

(b) BWR, Direct Cycle, Forced Circulation.

Fig. X-1 Schematic of nuclear thermionic converter.

plied by the fissioning fuel), rejects heat at a lower temperature T_c, and generates electric energy. It also performs according to the thermodynamic principles applicable to all heat cycles. The converter consists of two electrodes (part *a* of Fig. X-1), the emitter or cathode and the collector or anode. The emitter receives heat, q_e, and delivers electrons with positive kinetic energy. The emitted electrons cross the interelectrode spacing, y, to the collector, doing work against the electrical load and dissipating additional energy, which must be rejected as heat, in the collector. The characteristic space-charge barrier formed in the interelectrode spacing, which can place a severe limit on the current density, can be alleviated by reducing the spacing to a few microns and/or by the introduction of positive ions. The latter remedy is usually applied by filling the gap with an easily ionized gas (e.g., cesium) that becomes partially ionized by electron collisions.

The main characteristics of the reactor described in Ref. 1 are listed in Table X-1. All the electrical generation is by thermionic means. The heat rejection is by means of a forced-circulation boiling-water system in a direct

Table X-1 NUCLEAR THERMIONIC POWER PLANT: SUMMARY OF CONCEPTUAL DESIGN CHARACTERISTICS[1]

Overall performance data	
Thermal power, Mw(t)	16
Electric power, Mw(e), net	1
Core life, full-power hours	10,000
Design pressure, psia	150
Average core coolant temperature, °F	358
Core design characteristics	
Geometry	Right-circular cylinder (approximately)
Diameter, average, in.	40.2
Active length, in.	44
Overall length of fuel element, in.	48
Core structural material	Stainless steel
Fuel-element data	Cylindrical, series-connected diodes, UO_2-Mo fuel, Mo alloy electrodes, ZrO_2 insulator, stainless-steel sheath
Sheath outside diameter, in.	0.620
Sheath thickness, in.	0.015
Insulator (ZrO_2) thickness, in.	0.100
Collector thickness, in.	0.020
Plasma (Cs) gap thickness, in.	0.010
Emitter (fuel-pellet cladding) thickness, in.	0.020
Fuel-pellet diameter, unclad, in.	0.290
U^{235} loading, core total, kg	117
UO_2 concentration in fuel pellets, g/cm^3	
Central zone	1.7
End zones	4.3
Burnable poison-element data, cylindrical zirconium boride-zirconium	
Diameter of rods, in.	0.43
Number of rods	129
Boron (natural) loading per rod, g	1.85
Total boron (natural) loading, g	240
Reflector control data	
Number of drums	18
Diameter of drums, in.	6
Drum composition	
Poison facing material	Ag-In-Cd
Drum body	BeO
Nuclear worth of control drum system, %	
Cold	2.0
Hot	2.5
Nuclear worth of control fuel-bundle system, %	3.0
Average thermal core flux, initial, nv	7×10^{12}
Control requirements, %	
Cold-hot	0.5
Equilibrium poisons	1.5
Maximum poisons	0.3
Lifetime	1.0
Core heat-transfer and hydraulic characteristics	
Heat flux, Btu/(hr)(sq ft)	
Average	66,400
Maximum	197,200
DNB ratio	6.4
Exit quality, %	
Average	15
Hot channel	30
Reactor flow rate, lb/hr	403,000
Mass flow rate, lb/(hr)(sq ft)	234,000
Thermionic characteristics	
Electrical power density, watts/cm^2	4.0
Diode efficiency, %	10
Emitter temperature	
Average, °C	1450
Average, °F	2642
Maximum, °C	1500
Maximum, °F	2732
Collector temperature	
Average, °C	650
Average, °F	1202

cycle, i.e., steam from the reactor coolant is sent directly to an air-steam condenser (part *b* of Fig. X-1). The relatively low steam pressure is chosen on the basis of overall practicability and transportability, inasmuch as high pressure is not required for thermodynamic reasons.

The solid moderator (zirconium hydride) is used to minimize the temperature defect of reactivity and to minimize the variation of the

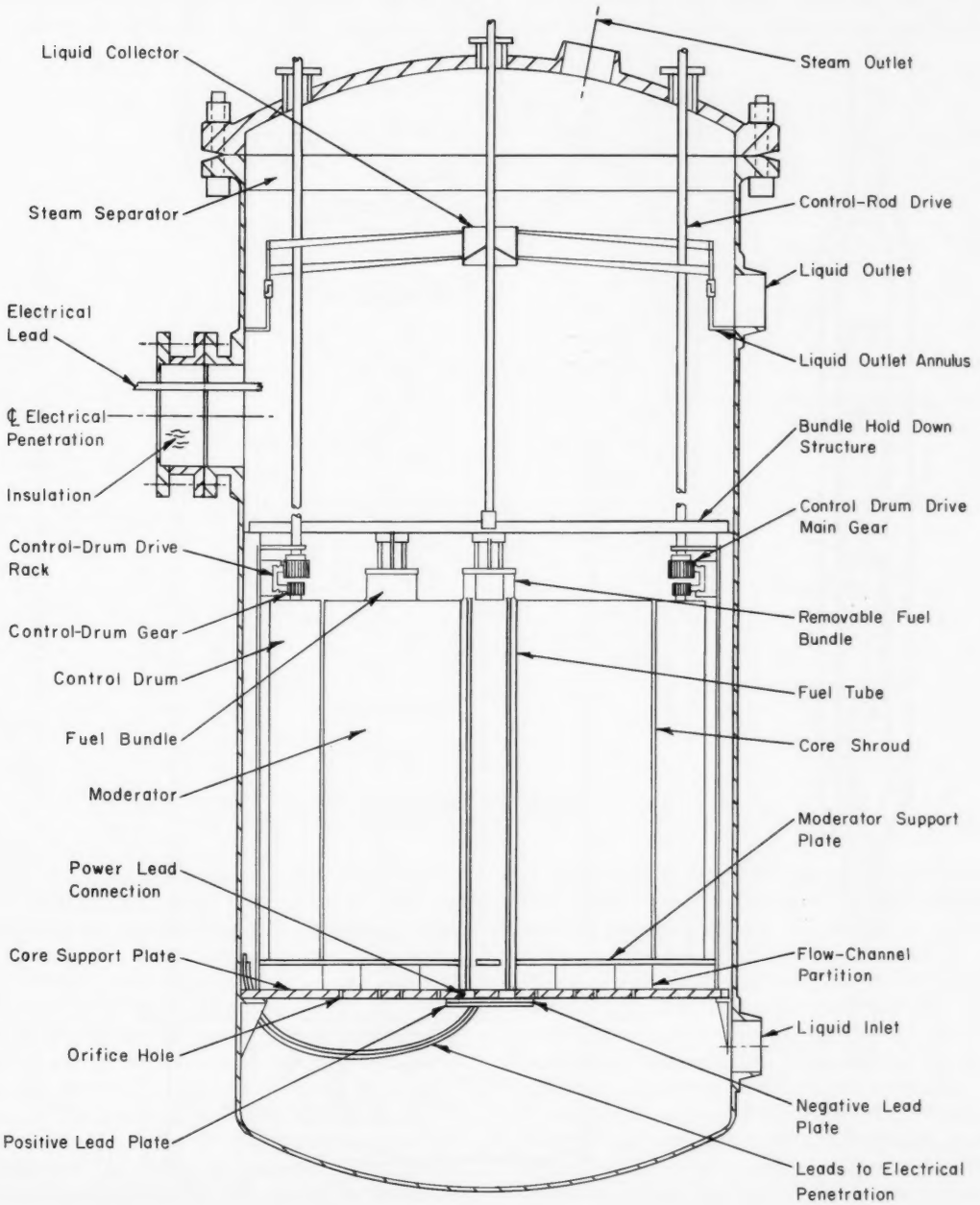

Fig. X-2 Pressure vessel and internals.[1]

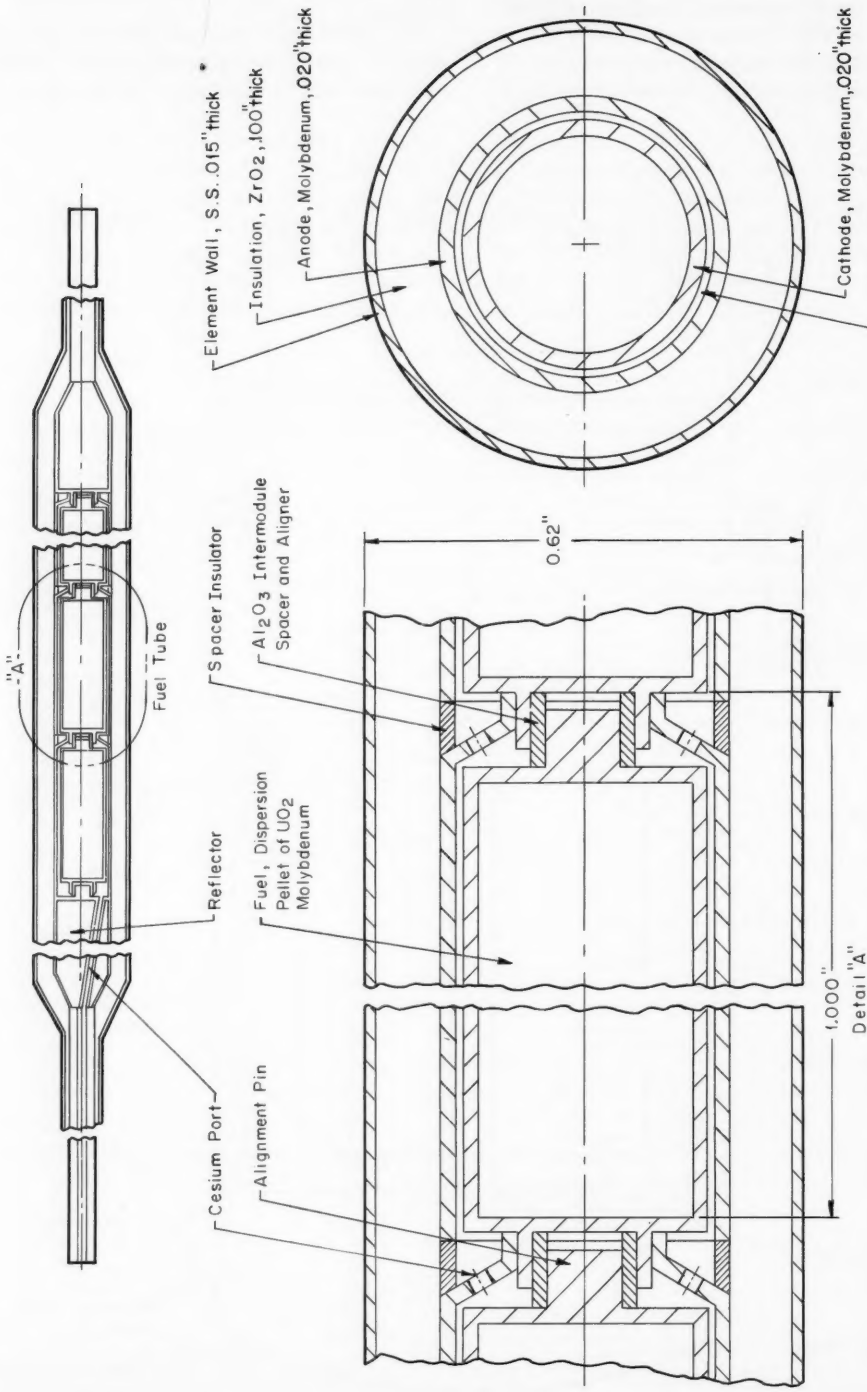

Fig. X-3 Fuel element for thermionic nuclear power plant.[1]

spatial power distribution with power level. A spatial power distribution that stays constant with time, particularly in the axial direction, is highly desirable in this reactor type to obtain the best performance from the in-core thermionic diodes. As indicated in later paragraphs, the diodes in a given fuel element are connected in series electrically. The fission-heated cathodes of the diodes depend on electron emission for cooling, and, at the same time, the electron emission current density depends on the cathode temperature. In the series-connected system, the cooler, lower-power cathodes can choke off the "coolant" flow of electrons to the hotter cathodes unless the areas of the several diodes, which are in series, are carefully proportioned to compensate for the effect. This can be done only if the power distribution among the diodes remains nearly constant. This consideration also influenced the choice of control system, which utilizes rotatable absorbing drums in the reflector (along with burnable poison) for operating control and movable fuel bundles for shutdown.

The core and associated components of the reactor are contained within the pressure vessel (see Fig. X-2). The control-drive mechanisms are attached directly to the pressure-vessel head. The basic internal structure is the core barrel, which locates and supports the core, moderator, reflector, and additional structure. Appended to the bottom of the core barrel is the core support plate that transmits the entire load to the core support brackets integral with the pressure vessel.

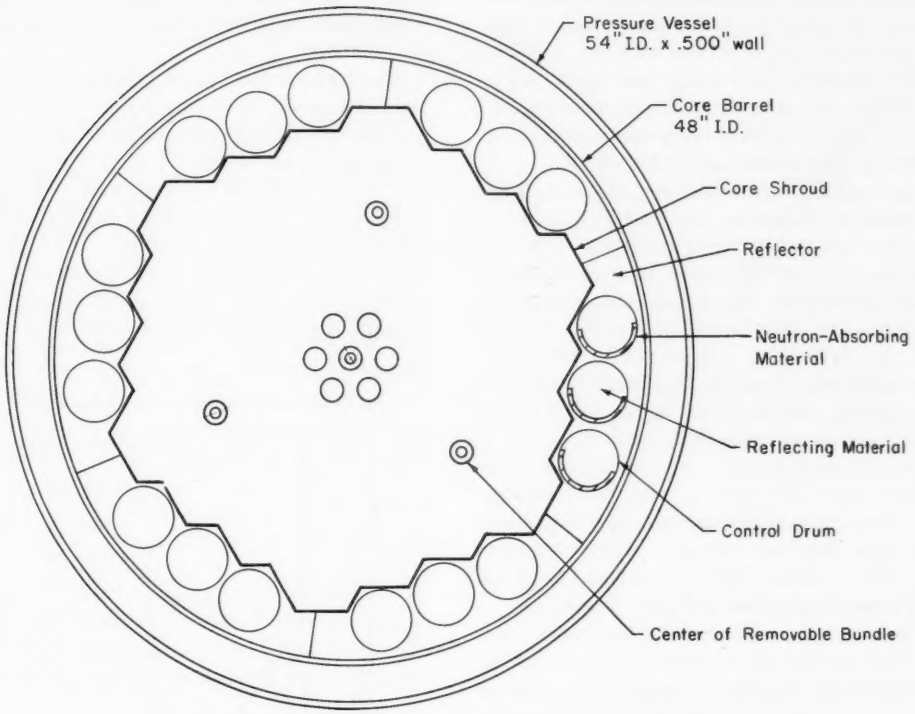

Fig. X-4 Cross-sectional view of pressure vessel and core.[1]

The construction of the fuel elements is shown in Fig. X-3. A dispersion pellet of UO_2-molybdenum serves as the fuel, and the molybdenum cladding serves as the emitter. A cesium gap separates the emitter from the molybdenum collector, which is electrically attached to the emitter of the adjacent fuel pellet. Outside the collector is a zirconium oxide sleeve enclosed by a stainless-steel tube. The zirconium oxide not only must isolate the collectors electrically from each other and the stainless-steel tube, but it must also provide a

medium for conducting the collector heat to the stainless-steel tube and thence to the coolant. The diode collectors are separated by Al_2O_3 spacers that serve as electrical insulators. At the end of each fuel element is a reflector section composed of beryllium oxide. The current-conducting loads from the ends are made of molybdenum.

The UO_2-molybdenum cermet was chosen because of the good compatibility of UO_2 and molybdenum. In addition, molybdenum has a moderate neutron-capture cross section (relative to other possible materials) and good high-temperature strength. UO_2 was chosen in preference to other uranium compounds because of its proven performance characteristics.

Six materials — molybdenum, niobium, iridium, rhenium, tungsten, and tantalum — were considered for the cathode material. The last four were rejected because of their large thermal and epithermal absorption cross sections that would have resulted in two or three times higher fuel inventory. Reference 1 also states that molybdenum at an 8- to 12-mil interelectrode spacing and niobium at a 2- to 4-mil spacing give comparable performance.

Since recrystallization sets a maximum temperature limit of 1550°C for molybdenum, 1450°C was chosen as a conservative design temperature for the cathode. The reference[1] states that a more detailed design program would probably allow for a higher value.

The fuel tubes are welded into the upper grid, which also serves as a cesium plenum and as an electrically insulated chamber for making interelement electrical connections between the power-producing fuel elements. The cesium reservoir, supported several inches above the upper grid by three support rods, contains the cesium supply required by the thermionic diodes, which is carried from the top of the reservoir down to the upper grid by a tube. Each cesium reservoir contains a thermocouple, an electric heater, and the required electrical connections needed for control of the cesium pressure.

The lower end of each fuel element is formed into an electrical receptacle that mates with a banana plug that projects from, but is electrically insulated from, the core support plate. Each banana plug is electrically connected to one of two (positive and negative) lead plates attached below the core support plate. Two fuel elements, serially connected, form individual circuits. Thus one of the two serially connected fuel elements connects to one lead plate, and the other element connects to the electrically opposite lead plate. The lower ends of the elements in one cluster are bound together by a tube structure for rigidity. A spacer tube is inserted in the center of the cluster to distribute the coolant flow around the elements. These tubes will contain solid moderator or burnable poison. All the elements are separated from the spacer tube and from each other by spirally wound wire spacers located along the length of the elements.

The fuel elements are grouped in clusters of five. Seven clusters are joined in a triangular pattern to a hexagonally shaped upper grid. This grouping forms a fuel bundle. No lower grids are used; therefore the clusters of each fuel bundle can be lowered into a pattern of holes in the solid moderator designed to accommodate them. An array of 32 such bundles, a 34-element bundle, and four control bundles, which contain six instead of seven fuel tube clusters,

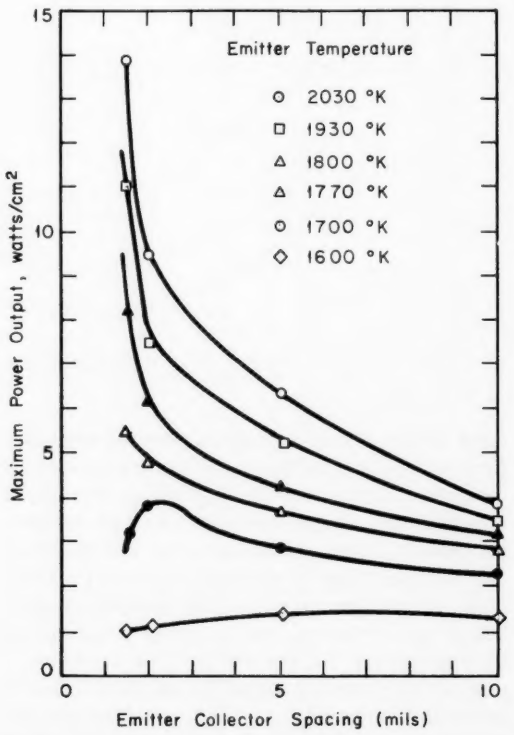

Fig. X-5 Optimum electric power density as a function of interelectrode spacing and emitter temperature.[2]

comprise the 1274-fuel-element core. The following is a summary of the fuel arrangement in the core.

Number of thermionic modules (diodes) per fuel element	44
Number of fuel elements per cluster	5
Number of seven-cluster fuel bundles (35 fuel elements)	32
Number of six-cluster fuel bundles (30 fuel elements)	4
Number of 34-fuel-element bundles	1
Total number of fuel elements	1274
Total number of fuel bundles	37

There is a positive and a negative lead plate for each fuel bundle. The 74 leads make a total of 37 individual circuits leaving the reactor, and each circuit nominally carries 1100 amp of direct current at 32 volts. The power leads from the lead plates are taken out along the bottom of the support plate to the pressure-vessel wall, and up the wall in a water-cooled aluminum bus that is located in the 2-in. annulus formed between the core barrel and the pressure-vessel wall, to the two insulated pressure-vessel penetrations. The water-cooled bus passes through the penetrations and terminates at the input terminals of the power converter. The latter is an acyclic motor–synchronous generator rated at 1350 kw (0.8 power factor) at 480 volts, 60 cycles.

Silicone rubber is used for a potting compound at the pressure-vessel electrical penetrations. It is expected to perform satisfactorily because of the low radiation level and low pressure.

Eighteen revolvable drums (see Fig. X-4) in the reflector provide control for operation and scram. These drums are ganged in sets of three so that one drive mechanism can control a set of three drums. The drums are made of either solid beryllium or cans of BeO, with a $\frac{1}{4}$- to $\frac{3}{8}$-in. thickness of Ag-Cd-In wrapped around 180° of the drum. The drums are located in reflector cutouts and are supported at the bottom by the moderator support plate and at the top by extensions from the core barrel.

General Thermionic Considerations

Reference 2 is a recent report on thermionic power generation which gives details of operating experience with practical thermionic converters as well as general principles. Figure X-5, from the reference, illustrates the sensitivity of the power output of a thermionic converter to the emitter-collector spacing, and Fig. X-6 illustrates comparisons between ideal converters and several thermionic converters developed to date. Above about 1800°K, for the case of a niobium emitter and a molybdenum

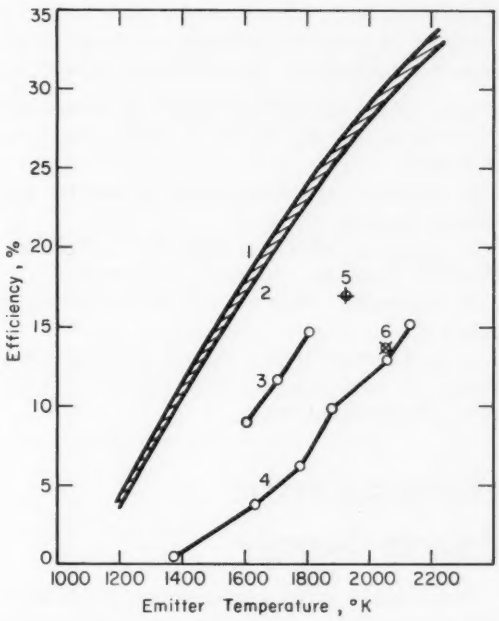

1. Efficiency of ideal converter including only radiation losses, emissivity 0.25
2. Efficiency of ideal converter including only radiation losses, emissivity 0.33
3. Calculated efficiency of molybdenum emitter converter, not including radiation from back of emitter — Thermo Electron Engineering Corp., private communication
4. Calculated efficiency of tungsten emitter converter, not including radiation from back of emitter — V. C. Wilson and J. Lawrence, General Electric Company Scientific Report No. 3, Contract AF 19-(694)-5472, August 1960
5. Measured efficiency of molybdenum emitter converter — N. S. Rasor, IAS Paper No. 61-72, January 1961
6. Measured efficiency of tantalum emitter converter — Thermo Electron Engineering Corp., private communication

Fig. X-6 Thermal efficiency of thermionic converters.[2]

collector, the maximum power output increases rapidly with decreasing interelectrode spacing (Fig. X-5), and the maintenance of small spacings has given rise to structural problems. The reference states that these problems currently limit the life of practical devices to about 1000 hr, but it expresses confidence that the structural problems will be solved after sufficient development work and that eventually the life of converters probably will be limited only by the corrosive effects of cesium and the evaporation of the emitter. The reference[2] also presents concepts of several thermionic nuclear reactors and discusses the following problems:

1. Diffusion of gaseous fission products into the cesium, and its effects on converter performance
2. Metallurgical compatibility of emitter and nuclear fuel materials
3. Extent and effects of distortion of emitter-clad fuel elements
4. Corrosive effect of cesium on electrode materials
5. Development of high-temperature electrical insulation metallurgically bondable to collector and structural materials

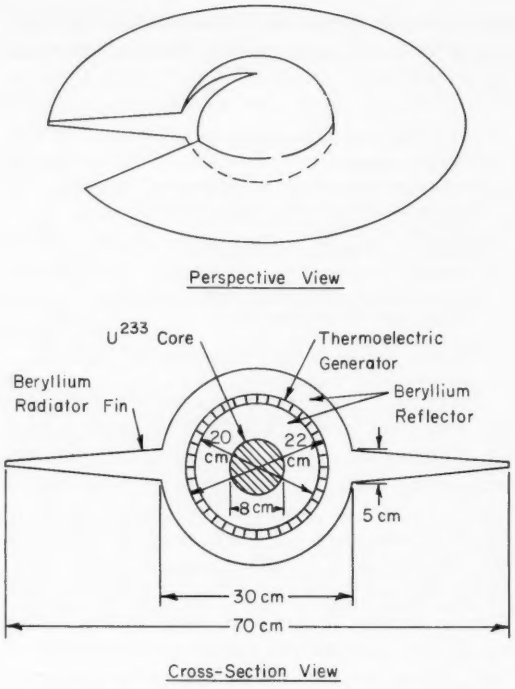

Fig. X-7 Conduction-cooled reactor system.[3]

Thermoelectric Power Supply

Reference 3 gives a conceptual design for a 200-watt reactor-powered thermoelectric power supply for space applications. It employs an unshielded reactor that consists of a split sphere of pure U^{233} metal reflected by beryllium metal (Fig. X-7). U^{233} was chosen over U^{235} because of its considerably lower critical mass (giving a lower total weight), and it was chosen over plutonium because of its higher melting point. The core, which transfers its heat to the beryllium reflector and cooling radiator by conduction, operates with a central temperature of 764°C and at a thermal power of 5 kw, as required by the generator efficiency of 4%. Reactivity is controlled by varying the separation of the uranium hemispheres by means of the cleft in the complete unit, which is indicated in Fig. X-7.

Lead telluride was chosen as the thermoelectric material because: "...there is, however, only one material, lead telluride, which is truly operational from the standpoint of having operated satisfactorily in power supplies and having fairly well-known operating limits and properties."[3] The reference concludes that the final feasibility of the device is dependent on the radiation-damage effects to the thermoelements. It also concludes that the upper limit for the power level of the particular reactor discussed is the thermal-stress limit of the thermoelements. If the allowable temperature gradients in the thermoelements could be doubled, the power output could be doubled by the addition of a larger radiator.

References

1. Martin-Marietta Corporation, Aerospace Division, Feasibility Study of Water-Cooled Thermionic Nuclear Power Plant, USAEC Report MND-2903 (Vol. 1), November 1962.
2. E. P. Gyftopoulos and G. N. Hatsopoulos, Thermionic Nuclear Reactors, *IEEE Trans. Commun. Electron.*, 65: 98-108 (March 1963).
3. D. R. MacFarlane, A 200-Watt Conduction-Cooled Reactor Power Supply for Space Application, USAEC Report ANL-6694, Argonne National Laboratory, March 1963.

NUCLEAR SCIENCE ABSTRACTS

The U. S. Atomic Energy Commission, Division of Technical Information, publishes *Nuclear Science Abstracts (NSA)*, a semimonthly journal containing abstracts of the literature of nuclear science and engineering.

NSA covers (1) research reports of the U. S. Atomic Energy Commission and its contractors; (2) research reports of government agencies, universities, and industrial research organizations on a world-wide basis; and (3) translations, patents, books, and articles appearing in technical and scientific journals.

Complete indexes covering subject, author, source, and report number are included in each issue. These are cumulated quarterly, semiannually, and annually providing a detailed and convenient key to the literature.

Availability of *NSA*

SALE *NSA* is available on subscription from the Superintendent of Documents, U. S. Government Printing Office, Washington, D. C., 20402, at $30.00 per year for the semimonthly abstract issues and $22.00 per year for the four cumulated-index issues. Subscriptions are postpaid within the United States, Canada, Mexico, and all Central and South American countries, except Argentina, Brazil, British and French Guiana, Surinam, and British Honduras. Subscribers in these Central and South American countries, and in all other countries throughout the world, should remit $37.00 per year for subscriptions to semimonthly abstract issues and $25.00 per year for the four cumulated-index issues.

EXCHANGE *NSA* is also available on an exchange basis to universities, research institutions, industrial firms, and publishers of scientific information. Inquiries should be directed to the Division of Technical Information Extension, U. S. Atomic Energy Commission, P. O. Box 62, Oak Ridge, Tennessee, 37831.

TECHNICAL PROGRESS REVIEWS may be purchased from Superintendent of Documents, U. S. Government Printing Office, Washington, D. C., 20402. *Isotopes and Radiation Technology* at $2.00 per year for each subscription or $0.55 per issue; the other four journals at $2.50 per year and $0.70 per issue. The use of the coupon below will facilitate the handling of your order.

POSTAGE AND REMITTANCE: Postpaid within the United States, Canada, Mexico, and all Central and South American countries except as hereinafter noted. Add $0.50 per year, or $0.15 per single issue for the *Isotopes and Radiation Technology* journal and $0.75 per year or $0.20 per single issue for the other four journals for postage to all other countries, including Argentina, Brazil, British and French Guiana, Surinam, and British Honduras. Payment should be by check, money order, or document coupons, and MUST accompany order. Remittances from foreign countries should be made by international money order, or draft on an American bank, payable to the Superintendent of Documents, or by UNESCO book coupons.

order form

SUPERINTENDENT OF DOCUMENTS
U. S. GOVERNMENT PRINTING OFFICE
WASHINGTON , D. C., 20402

Enclosed:
document coupons ☐ check ☐ money order ☐

Charge to Superintendent of Documents No._____

Please send a one-year subscription to

☐ NUCLEAR SAFETY

☐ POWER REACTOR TECHNOLOGY

☐ REACTOR FUEL PROCESSING

☐ REACTOR MATERIALS

(Each subscription $2.50 per year; $0.70 per issue.)

☐ ISOTOPES AND RADIATION TECHNOLOGY

(Each subscription $2.00 a year; $0.55 per issue.)

SUPERINTENDENT OF DOCUMENTS
U. S. GOVERNMENT PRINTING OFFICE
WASHINGTON, D. C., 20402

(Print clearly)

Name _____

Street _____

City _____ Zone ____ State _____